Aus dem

Institut für Prophylaxe und Epidemiologie der Kreislaufkrankheiten (IPEK) der
Ludwig-Maximilians-Universität München

Dissertation

zum Erwerb des Doctor of Philosophy (Ph.D.)
an der Medizinischen Fakultät
der Ludwig-Maximilians-Universität zu München

Role of the cannabinoid receptor CB1 in the regulation of bone marrow hematopoiesis

vorgelegt von
George Mories Anwar Shakir

aus:

Kairo / Ägypten

Jahr:

2025

Mit Genehmigung der Medizinischen Fakultät der
Ludwig-Maximilians-Universität München

Erstes Gutachten von:	Prof. Dr. Sabine Marten-Steffens
Zweites Gutachten von:	Prof. Dr. Hendrik Sager
Drittes Gutachten von:	Priv. Doz. Dr. Johanna Tischer
Viertes Gutachten:	Prof. Dr. Michael Albert

Dekan: **Prof. Dr. med. Thomas Gudermann**

Datum der Verteidigung:

15.05.2025

The results of this work were presented at the following conferences:

Oral presentations:

09/2022	IRTG 1123 Annual Retreat, Tutzing, Germany
09/2023	DZHK 2023 Retreat, Potsdam, Germany
09/2024	47th European Lipoprotein Club, Tutzing, Germany
10/2024	IRTG 1123 Annual Retreat, Tutzing, Germany

Poster presentations:

10/2021	IRTG1123 Annual Retreat, Venice, Italy
01/2023	Munich Heart Alliance Winter Meeting, Munich, Germany
06/2023	IRTG1123 Annual Retreat, Venice, Italy
07/2023	CRC1525 Summer School, Würzburg, Germany
11/2024	SFB1123 Annual Retreat, Grainau, Germany

Table of content

Table of content

Summary

Atherosclerosis is the major underlying cause of cardiovascular diseases, which are the leading cause of death worldwide. Endogenous lipid mediator signalling through cannabinoid receptors plays a causal role in atherosclerosis, and blocking the cannabinoid receptor 1 (CB1) has been shown to reduce atherosclerotic plaque burden and improve metabolic risk factors. To date, experimental studies have mainly focused on the effects of CB1 on vascular and myeloid cells in atherosclerosis. However, the role of CB1 signalling in *de novo* leukocyte production in the bone marrow, a process called hematopoiesis, is still largely unknown. Given that hypercholesterolemia leads to increased monocyte production in the bone marrow and thereby promotes atherosclerotic plaque formation, the aim of this thesis was to study the effect of global loss of CB1 signalling on hematopoiesis. Furthermore, mechanistic experiments were designed to clarify the specific contribution of the hematopoietic versus stromal cell CB1 in this process.

Deficiency of the CB1 encoding gene *Cnr1* had minimal effect during homeostasis on mature myeloid cells and hematopoietic stem and progenitor cells (HSPCs) during homeostasis. Under low-grade inflammation, achieved by backcrossing with mice on atherogenic apolipoprotein E deficiency (*Apoe*$^{-/-}$) background, *Cnr1* deficiency increased monocytes in blood and femur, reduced bone marrow stem cell factor (SCF) levels, increased C-X-C motif chemokine receptor 4 (CXCR4) expression on myeloid progenitors, and led to enhanced mobilization of HSPCs into the blood. This phenotype was predominantly observed in male animals, whereas females did not exhibit such a phenotype but rather displayed reduced neuronal innervation in the bone marrow niche. Upon Western diet (WD) feeding, both female and male *Cnr1* deficient mice developed monocytosis and larger atherosclerotic plaques compared to the corresponding controls. Besides, *Cnr1* deficiency affected the viability of HSPCs. Bone marrow transplantation experiments showed that stromal *Cnr1* expression is important for myeloid differentiation during chronic inflammation. In mice lacking *Cnr1*, G-CSF injection led to an accumulation of common myeloid progenitors, further highlighting the importance of CB1 in acute inflammatory responses. Additionally, an increase in common myeloid progenitors was also observed in *Ldlr*$^{-/-}$ mice upon peripheral CB1 antagonism. However, this phenotype was only observed in males. Finally, single cell RNA sequencing revealed that *Cnr1* deficiency in myeloid progenitors was associated with genes that play a role in apoptosis and oxidative stress, and that these genes are predicted to be regulated by transcription factors linked to myeloid differentiation (such as CEBPB and PU.1).

These data highlight a role for CB1 in regulating hematopoiesis during acute and chronic inflammation. More in-depth studies are needed to determine which specific cell types in the

hematopoietic niche are primarily regulated by CB1 and the underlying downstream mechanisms.

List of tables

List of figures

Abbreviations

2-AG	2-Arachidonoylglycerol
7AAD	7-Aminoactinomycin D
ABC	Adenosine triphosphate-binding cassette
ABCA1	ABC sub-family A member 1
ABCG1	ABC sub-family G member 1
AC	Adenylyl cyclase
ACEA	Arachidonyl-2'-chloroethylamide
ACK	Ammoniumchlorid-kalium
Adipoq	Adiponectin, C1Q and collagen domain containing
AEA	Arachidonyl-ethanolamide
AECs	Arteriolar endothelial cells
AM281	1-(2,4-dichlorophenyl)-5-(4-iodophenyl)-4-methyl-N-morpholin-4-ylpyrazole-3-carboxamide
ANGPT1	Angiopoietin 1
ANOVA	Analysis of variance
APC	Antigen-presenting cell
ATAC	Assay for transposase-accessible chromatin
ATLO	Artery tertiary lymphoid organ
BSA	Bovine serum albumin
BSL2	Bio-safety cabinets class 2
cAMP	3',5'-cyclic AMP
CANTOS	The Canakinumab antiinflammatory thrombosis outcome study
CAR cells	CXCL12-abundant reticular cells
CB1	Cannabinoid receptor 1
CB2	Cannabinoid receptor 2
CCL2	C-C motif chemokine ligand 2
CCR2	C-C motif chemokine receptor 2
CCR5	C-C motif chemokine receptor 5
CFU	Colony forming unit
CGRP-1	Calcitonin related polypeptide alpha
CH	Clonal hematopoiesis
CHEA3	ChIP-X enrichment analysis 3
CHIP	Clonal hematopoiesis of indeterminate potential
cKit	KIT proto-oncogene, receptor tyrosine kinase
CLP	Common lymphoid progenitor
CMO	Cell multiplexing oligo
CMP	Common myeloid progenitor
Cnr1	Cannabinoid receptor 1 encoding murine gene
CNS	Central nervous system
CVD	Cardiovascular disease
CX3CL1	C-X3-C motif chemokine ligand 1
CXCL12	C-X-C motif chemokine ligand 12
CXCR3	C-X-C motif chemokine receptor 3
CXCR4	C-X-C motif chemokine receptor 4
DAG	Diacylglycerol
DAGL	Diacylglycerol lipase
DAMPs	Damage-associated molecular pattern

DARC	Duffy antigen receptor for chemokines
DCs	Dendritic cells
DEG	Differentially expressed gene
DMEM	Dulbecco's modified eagle medium
DMSO	Dimethyl sulfoxide
DNA	Deoxyribonucleic acid
DNMT3	DNA (cytosine-5) methyltransferase 3 alpha
ECS	Endocannabinoid system
EDTA	Ethylenediaminetetraacetic acid
ELISA	Enzyme-linked immunosorbent assay
FAAH	Fatty acid amide hydrolase 1
FBS	Fetal bovine serum
FDR	False discovery rate
FITC	1.2 Fluorescein isothiocyanate
Gapdh	Glyceraldehyde 3-phosphate dehydrogenase
G-CSF	Granulocyte colony stimulating factor
GEM	Gel beads-in-emulsions
GM-CFU	Granulocyte-macrophage colony-stimulating factor
GMP	Granulocyte-monocyte progenitor
GPCR	G protein-coupled receptor
GSEA	Gene set enrichment analysis
HEPES	2-[4-(2-hydroxyethyl)piperazin-1-yl]ethane-1-sulfonic acid
Hprt	Hypoxanthine phosphoribosyltransferase 1
HSCs	Hematopoietic stem cell
HSPCs	Hematopoietic stem and progenitor cell
Icam1	Intercellular adhesion molecule 1
IEL	Internal elastic lamina
IFN	Interferon
IL-10	Interleukin 10
IL-1β	Interleukin 1 beta
IL-6	Interleukin 6
IL-7	Interleukin 7
JAG1	Jagged canonical Notch ligand 1
KO	Knockout
LDL	Low density lipoprotein
Ldlr	Low density lipoprotein receptor encoding mouse gene
Lepr	Leptin receptor encoding mouse gene
Lin	Lineage markers
LK	Lineage- cKit+
LSC	Leukemic stem cell
LSK	Lineage- cKit+ Sca1+
LT-HSC	Long term hematopoietic stem cell
MAGL	Monoacylglycerol lipase
MAPK	Mitogen-activated protein kinases
M-CSF	Macrophage colony-stimulating factor
MEP	Megakaryocyte–erythroid progenitor
MFI	Mean fluorescence intensity
MI	Myocardial infarction
MCP-1	Monocyte chemoattractant protein

MPPs	Multipotent progenitors
MSCs	Mesenchymal stem cells
NAPE	N-acyl phosphatidylethanolamine
NAPE-PLD	N-acyl phosphatidylethanolamine phospholipase D
NE	Norepinephrine
NETs	Neutrophil extracellular traps
NLRP3	NLR family pyrin domain containing 3
NO	Nitric oxide
OPN	Osteopontin
oxLDL	Oxidized low density lipoprotein
PAMP	Pathogen-associated molecular pattern
PBS	Phosphate-buffered saline
PCA	Principal component analysis
PE	Phycoerythrin
PEG3000	Polyethylenglycol 3000
PerCp	Peridinin chlorophyll protein
PI3K	Phosphoinositide 3-kinase
qPCR	Quantitative PCR
RBC	Red blood cell
RNA	Ribonucleic acid
ROS	Reactive oxygen species
ROUT	Robust regression and outlier removal
RT	Room temperature
SCF	Stem cell factor
SECs	Sinusoidal endothelial cells
SEM	Standard error of the mean
SLAM	Signaling lymphocytic activation molecule
SNAI	Snail family transcriptional repressor 1
SNS	Sympathetic nervous system
ST-HSC	Short term hematopoietic stem cells
TEAD1	TEA domain transcription factor 1
TEAD4	TEA domain transcription factor 4
TET2	Tet methylcytosine dioxygenase 2
TF	Transcription factor
TH	Tyrosine hydroxylase
THC	Tetrahydrocannabinol
TLR	Toll-like receptor
TMB	3,3´,5,5´-tetramethylbenzidine
TPO	Thyroid peroxidase
tSNE	t-distributed stochastic neighbour embedding
TSS	Transcription start site
TWIST2	Twist family BHLH transcription factor 2
UMAP	Uniform manifold approximation and projection
Vcam1	Vascular cell adhesion protein 1
VSMC	Vascular smooth muscle cell
WD	Western diet
WHO	World health organization
wks	Weeks

1 Introduction

1.1 Cardiovascular diseases

Cardiovascular diseases (CVDs) are the leading cause of death worldwide, with nearly 18 million deaths worldwide according to the WHO in 2019 [1]. CVDs comprise, among other, atherosclerosis that can lead to stroke or heart attack. The development of CVDs is associated with different risk factors that can be separated into modifiable and non-modifiable factors. Modifiable risk factors include hypertension, diabetes, unhealthy diet, dyslipidaemia, and smoking [2], whereas non-modifiable risk factors include ethnicity, sex, and age [3]. These factors promote vascular inflammation and oxidative stress, which affects the integrity of the blood vessels and cardiac homeostasis [4]. With the current increase in the mean age of individuals and poor lifestyle habits, it is of great importance to develop new therapies and diagnostic tools for CVDs. Current strategies used include therapeutic drugs and improved lifestyle management such as regular exercise, quitting smoking, and eating a healthy diet. Pharmacological treatment includes, among others, drugs to lower blood pressure and decrease cholesterol levels (including statins) and antiplatelet medication [5]. Despite the progress in understanding the mechanisms leading to CVDs, they remain the leading cause of mortality with atherosclerosis being the main cause of stroke and myocardial infarction (MI) [6].

1.2 Atherosclerosis

Atherosclerosis represents the most prevalent underlying cause of CVD. The formation of atherosclerotic plaques occurs in large or medium-sized arteries. Plaque development is a dynamic process that follows different stages and can eventually lead to blocking of the blood flow inside the vessel. The progression of a plaque occurs faster in vessel areas with low or oscillatory blood flow. The rupture or detachment of a plaque can lead to stroke or MI [7]. Plaque formation begins with a dysfunction of the endothelium. Healthy endothelial cells produce a variety of substances that perform various functions such as vasodilation (nitric oxide NO), antithrombotic (antithrombin and heparin) beside others. These factors regulate the vascular tone, maintain the vasculature healthy and hinder the formation of plaques inside vessels which protects the vascular system [4]. Endothelial dysfunction due to infection, stress, hypertension, or other factors can lead to increased permeability for blood-borne molecule that causes the accumulation of LDL and cholesterol particles within the intima. The persistence of stressors results in an increased infiltration of lipid molecules, which in turn activates endothelial cells [8]. Activated endothelial cells produce more cytokines and adhesion molecules, which enhances the recruitment, adhesion and extravasation of circulating leukocytes to the growing plaque. The majority of these leukocytes are recruited primarily from the bone marrow and the spleen [4], and include predominantly myeloid cells (such as

monocytes) but also lymphoid cells (such as T and B cells). Several chemokines including C-C motif chemokine receptor 2 (CCL2) recruit monocytes into the plaque [9]. Adhesion molecules such as vascular cell adhesion molecule 1 (VCAM-1), intercellular adhesion molecule 1 (ICAM-1) and selectins facilitate the adhesion and migration of monocytes into the intima [10]. With the accumulation of oxidized low density lipoproteins (oxLDL) into the intima, more monocytes infiltrate into the intima and differentiate into macrophages. These macrophages engulf the oxLDL and transform into foam cells [11]. At this stage, the early plaque is termed fatty streak. Foam cells produce cytokines and growth factors that affect the proliferation of vascular smooth muscle cells. The accumulating cells inside the growing plaque turn into apoptotic or necrotic cells, leading to the formation of a necrotic core that increases inflammation. The necrotic core is lipid-rich and usually covered by a fibrous cap that is composed of smooth muscle cells and collagen. The size of the necrotic core affects plaque stability: stable plaques have a small necrotic core and a thick fibrous cap with a high content of collagen, while rupture-prone plaques have a thin cap and accumulate more apoptotic and necrotic cells (Figure 1) [12]. Advanced plaques are characterized by necrotic core, accumulation of apoptotic cells, defective efferocytosis, and calcification [13].

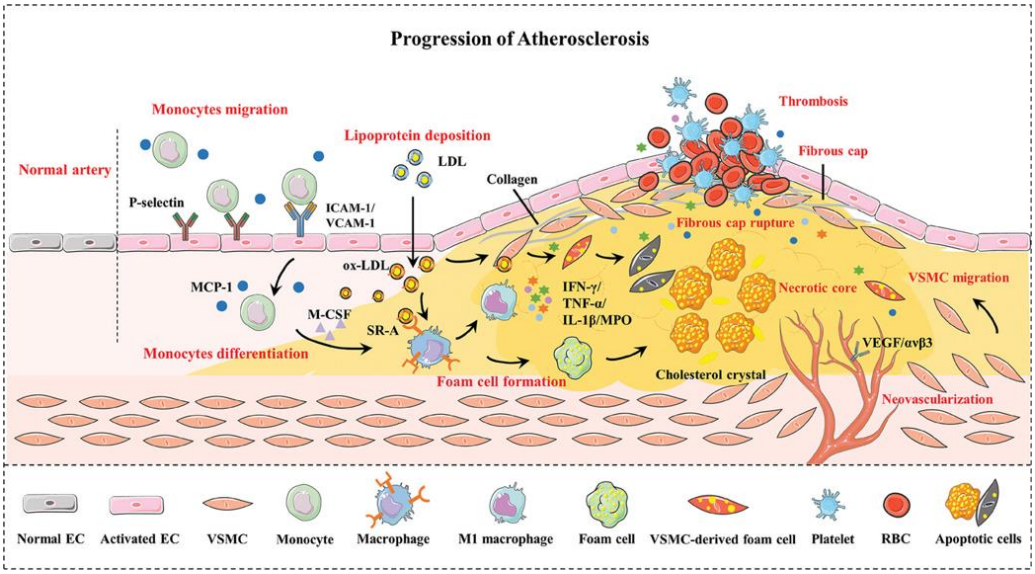

Figure 1. Schematic representation showing plaque formation in a blood vessel and the different stages with different cells/factors that drive this process. The formation of a plaque starts with endothelial cell activation that leads to the recruitment of monocytes by chemokines and attachment to the endothelium. Infiltration of more lipids and engulfment by monocytes lead to the formation of foam cells that by time form the necrotic core. In case of unstable plaques, rupture of the plaque can occur and leads to formation of a thrombus and blockage of the blood flow. ECs = endothelial cells, oxLDL = oxidized low-density lipoprotein, ICAM-1 = intercellular adhesion molecule-1, VCAM-1 = vascular cell adhesion molecule-1, MCP-1 = monocyte chemotactic protein-1, M-CSF = macrophage colony-stimulating factor, VSMCs = vascular smooth muscle cells, IFN-γ = interferon-γ, IL-1β = interleukin-1β, TNF-α = tumor necrosis factor-α, MPO = myeloperoxidase, VEGF = vascular endothelial growth factor (Adapted from Wang et al [14]).

1.3 Leukocytes in atherosclerosis

Leukocytes or white blood cells are the cells that form the immune system, which consist of innate and adaptive immune cells that can infiltrate and accumulate in the growing plaque [15]. Monocytes, which belong to innate immune system, are one of the first immune cells recruited to inflammatory sites. The recruitment of these cells is achieved through chemokines production by endothelial cells, which attract monocytes to the site of inflammation [16]. In this context, many studies have demonstrated the major role of chemokine receptors expressed by leukocytes and cognate ligands in this process, including chemokine receptors CCR2, CCR5 and CXCR3 [17]. In a study, Boring et al. it was shown that *Apoe*$^{-/-}$ *Ccr2*$^{-/-}$ mice have reduced atherosclerotic lesion area and less macrophage infiltration into the plaque, this phenotype was independent of lipid metabolism or cholesterol levels [18], which points to the importance of CCR2 for monocytes recruitment. In another study, Saederup et al. used a triple knock-out animal model *Cx3cl1*$^{-/-}$ *Ccr2*$^{-/-}$ *Apoe*$^{-/-}$ to study the effect of knocking out the chemokine ligand and the corresponding receptor at the same time. The data showed that targeting multiple chemokine ligands or receptors simultaneously led to an enhanced protective effect against atherosclerosis [19]. Monocytes recruited to inflammatory sites tether and adhere to the endothelium by binding to adhesion molecules and then extravasate into the tissue, where they subsequently transdifferentiate into macrophages [20]. Macrophages transform into foam cells when engulfing oxLDL particles via scavenger receptors that can recognize and bind to lipoprotein, phospholipids and cholesterol esters. Knocking out scavenger receptors leads to a reduction in foam cell formation. For example, knocking out CD36 which function as a scavenger receptor reduced the ability of macrophages to bind and engulf oxLDL compared to WT phenotype [21]. *In vivo* studies using CD36 KO mice on *Apoe*$^{-/-}$ background showed that CD36 KO develops smaller lesion areas. *In vitro*, macrophages derived from *Apoe*$^{-/-}$*CD36*$^{-/-}$ mice accumulated fewer oxLDL particles [22].

During plaque formation, neutrophils play a role through phagocytosis, degranulation and generation of neutrophil extracellular traps (NETs). Similar to monocytes, neutrophils are attracted by cytokines and chemokines [23] and can transmigrate through the dysfunctional endothelium by interaction between adhesion molecules and integrins. This transmigration can cause further damage to the endothelium. Moreover, neutrophils produce reactive oxygen species (ROS) and secrete several enzymes (such as elastases or myeloperoxidases) and chemokines that induce apoptosis and contribute to the progression of plaque [24]. Neutrophils can also promote the recruitment and adhesion of monocytes to the endothelium. Various lines of evidence show that activated endothelial cells can promote the deposition of NETs along the endothelium, thereby enhancing the attraction of monocytes to the lesion area [25].

Although most of the research focuses on the role of innate immune cells in atherosclerosis, there is growing evidence that adaptive immune cells play a role in atheroma progression. A strong relationship between adaptive immune cells and disease-specific antigens has been shown as adaptive immune cells can encounter disease specific antigen in the secondary lymphoid organs [26, 27]. In general, depletion of CD4+ T cells in mice attenuates atherosclerotic lesion development as T cells produce cytokines that can recruit more monocytes, differentiate vascular smooth muscle cells (VSMCs) or induce apoptosis [28]. Naïve T cells reside in secondary and tertiary lymphoid organs where they get activated through interaction with antigen-presenting cells (APCs) or dendritic cells (DCs) [29]. Activated CD4+ T cells differentiate into different helper T or regulatory T cell subsets. Regulatory T cells have atheroprotective characters, while helper T cell subsets have controversial roles depend on the cytokines mix produced [28, 29].

The other main adaptive immune cell type is the B cell, the contribution of B cells at the early plaque stage is minimal, while with the plaque progression they start to be located at artery tertiary lymphoid structures (ATLOs). Within draining lymph nodes and ATLOs, B cells produce distinct antibodies (called immunoglobulins) which are capable of recognizing specific antigens present within the plaque [30]. B cells can be atherogenic or atheroprotective depending on the subtype [31].

1.4 Hematopoiesis

Hematopoiesis is a lifelong process that meets the daily demand for blood cells, it also responds to different conditions that require compensation of lost blood cells like bleeding or infection. The hematopoietic system consists of different types of cells organized in a hierarchical system. The hematopoietic stem cells (HSCs) are the most primitive precursors and reside at the top of the hierarchy, while newly produced mature blood cells are at the end of the hematopoietic developmental tree. HSCs and multipotent progenitors (MPPs) can produce cells of two different lineages, lymphoid or myeloid lineage [32]. The common myeloid progenitors (CMPs) are responsible for myelopoiesis and common lymphoid progenitors (CLPs) are responsible for lymphopoiesis (Figure 2). Regulation of proliferation and differentiation of HSCs is controlled by intrinsic and extrinsic signals. Hematopoiesis takes place inside long bones like femurs and cage ribs where the bone microenvironment provides the HSCs with what is defined as "bone marrow niche". Different cells such as osteoblasts, mesenchymal stem cells and sympathetic neurons form this niche and interact with HSCs. This interaction occurs through different cues including secreted and adhesion molecules [33]. Under certain conditions, especially inflammation or infection, hematopoiesis can shift from bone marrow to extramedullary hematopoiesis in the spleen [34].

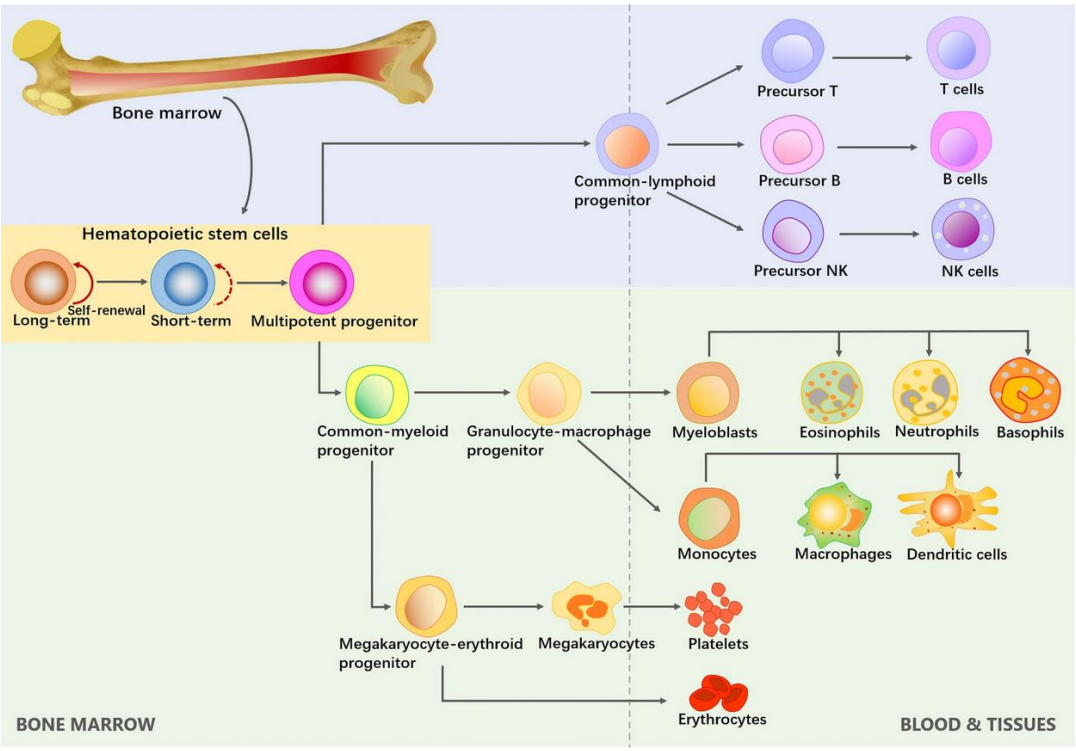

Figure 2. Classical model of hematopoiesis. Scheme depicting the hematopoietic stem cell system development and differentiation inside the bone marrow, where all the hematopoietic system progenitors and stem cells reside. (Adapted from Zhang et al. [35]).

1.5 Hematopoietic and progenitor stem cells

The production of mature blood cells begins with HSCs, which represent a rare and very small portion of the whole hematopoietic system. HSCs are able to reconstitute the whole hematopoietic system and are characterized by a high ability to self-renew. HSCs are quiescent most of the time and divide into two populations, long-term HSC (LT-HSC) and short-term HSC (ST-HSC). LT-HSCs are more dormant while ST-HSCs are active and ready to differentiate [36]. There are multiple different progenitors between HSCs and mature leukocytes. These progenitors are called multipotent progenitors (MPPs) or committed progenitors and are characterized by self-renewal and multi-potency. HSCs and MPPs are known to express high levels of stem cell antigen-1 (Sca-1) and stem cell factor receptor (cKit) while being negative for known maturation markers such as CD3, B220, CD11b, Gr1, and Ter119. HSCs and MMPs are also defined as LSK ($Lin^{-}Sca\text{-}1^{+}cKit^{+}$). Committed progenitors on the other hand express low levels of Sca-1, high levels of cKit and are also negative for any maturation marker, and are defined as LK ($Lin^{-}cKit^{+}Sca\text{-}1^{-/low}$).

LSK encompasses the population of multipotent hematopoietic stem cells which are HSCs and MPPs. After extensive research, it is now possible to split this pool of cells into different populations using distinct markers. In particular, the SLAM factors (SLAMF1 and SLAMF2 or CD150 and CD48 respectively) can be used to differentiate LSKs into four cell populations [37, 38]. These four populations are functionally distinct regarding hematopoietic system

reconstitution ability, transcriptomes and epigenetic modifications [39]. It is believed that under homeostasis, MPPs are derived from HSCs and are already biased to a certain lineage, with MPP2 being erythroid biased and MPP3 being myeloid biased [40]. LK identifies a population of more committed progenitors and can be divided into three main populations, CMPs, GMPs and MEPs (Figure 3) [41, 42].

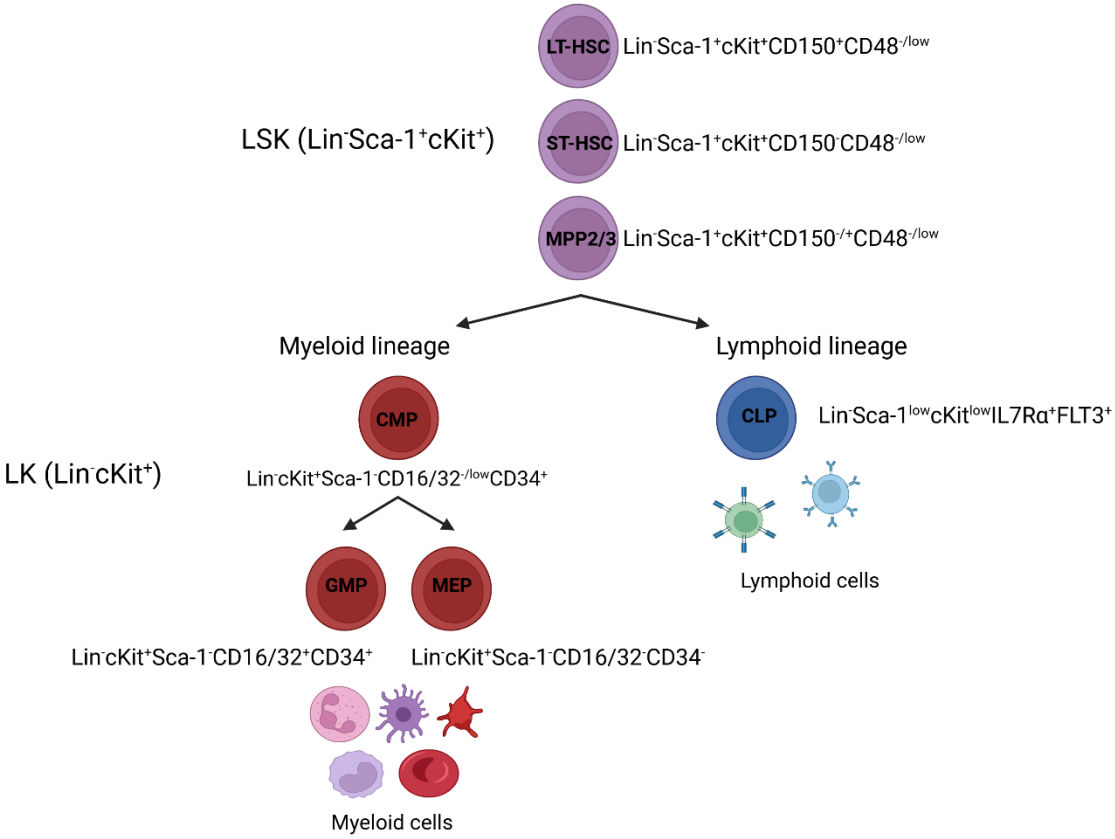

Figure 3. Identification markers for murine hematopoietic stem and progenitor cell populations. CD150 = signaling lymphocytic activation molecule family member 1; CD16/32 = FcγRIII/FcγRII; CD34 = hematopoietic progenitor cell antigen; CD48 = signaling lymphocytic activation molecule family member 2; cKit = KIT proto-oncogene, receptor tyrosine kinase; FLT3 = fms related receptor tyrosine kinase 3; IL7Rα = interleukin-7 receptor subunit alpha; Lin⁻= Lineage negative for maturation markers; Sca-1 = stem cell antigen. The Figure was generated using BioRender.

The classical hierarchy of hematopoiesis starts with the LT-HSCs as most primitive, followed by ST-HSCs that produce MPPs. The MPP population is heterogeneous and can be divided into at least two other progenitor populations (MPP2 and MPP3). The next step of differentiation gives rise to the committed progenitors that can be either myeloid-committed or lymphoid-committed. Lymphoid-biased progenitors are termed common lymphoid progenitors (CLPs), whereas myeloid-biased progenitors are termed common myeloid progenitors (CMPs). CMPs produce granulocyte/monocyte progenitors (GMPs) or megakaryocyte erythroid progenitors (MEPs). During homeostasis, there are two proposed models to explain how these cells differentiate. The discrete model and a continuous model: the discrete model

assumes that every population is well defined and the differentiation is a stepwise system. The continuous model proposes that differentiation happens with no definite stage but rather overlapping and heterogeneous populations. This latter model is receiving more support from recent research studies describing HSPCs as a continuum pool of cells [43].

1.6 The bone marrow niche

The definition of the hematopoietic stem cell niche developed over the last decades and the theory of having only one niche for all HSCs was proven wrong [44]. The bone marrow niche is a microenvironment that consists of different cell types and regulates HSC proliferation and division through direct and indirect contact. These niche stromal cells play important roles in HSC maintenance, quiescence, and homing by providing support during homeostasis and different stress conditions [45]. Mutations or failure in any niche cell type can lead to bone marrow hematopoiesis failure under homeostatic or physiological conditions. HSCs were found to be located in different sites within the bone marrow: the perivascular niche and endosteal niche [46]. Niche cells include non-hematopoietic cells namely mesenchymal stem cells (MSCs), osteoblasts, osteoclasts, adipocytes, endothelial cells, and perivascular stromal cells. Other niche cells comprise cells of hematopoietic origin including megakaryocytes, macrophages and lymphoid cells. The marrow space is also innervated with sympathetic nerves that are surrounded by Schwann cells (Figure 4) [47, 48].

Niche cells express adhesion molecules and secrete soluble factors in order to regulate HSPC proliferation, differentiation, homing, and retention. Regulatory surface markers include integrins, selectins, cadherins, and adhesion molecules such as ICAM1 and VCAM1 [49]. By using animal models deficient for adhesion molecules, it became clear that these molecules play a pivotal role in regulating homing, mobilization and retention of HSCs. Another mechanism for regulating HSCs is through growth factors secreted by distinct niche cells. These factors can be cell-specific or can be produced from different cells. The most studied factors are C-X-C motif chemokine ligand 12 (CXCL12) and stem cell factor (SCF), which bind to their cognate receptors C-X-C chemokine receptor type 4 (CXCR4) and receptor tyrosine kinase (cKit). CXCL12 and SCF are important for HSC maintenance and quiescence. In addition, the CXCL12/CXCR4 axis is very important for homing and egress of HSCs from the bone marrow into the circulation [50]. CXCL12 is mainly produced by perivascular stromal cells (LepR+, Nestin$^{low/high}$, referred to as CAR cells) and by osteoblasts. During homeostasis, CXCL12 levels within the bone marrow niche are regulated by sympathetic innervation through adrenergic signals following a circadian rhythm [51]. While most studies focus on the role of the sympathetic nervous system (SNS) innervation in the bone marrow niche, a recent study from Gao et al. found that nociceptive neurons also regulate the retention and mobilization of HSCs into the circulation [52]. SNS nerves are found along blood vessels that support the

marrow with nutrients and oxygen. These blood vessels are formed by a layer of endothelial cells which are an important source of SCF and the angiocrine factors Jagged-1 and Jagged-2. These Notch ligands play an important role, especially in the regeneration of the marrow after irradiation or a chemical insult [53-55]. Furthermore, both bone-forming cells (osteoblasts) and bone-absorbing cells (osteoclasts) are very important for the niche, as they create the endosteal niche, which is the niche for quiescent HSCs. This is also the site for lymphopoiesis and maturation of lymphoid-biased progenitors [56]. Osteoblasts express various factors that are important for the quiescence and maintenance of HSCs such as osteopontin (OPN), angiopoietin-1 (Ang-1) and thrombopoietin (TPO).

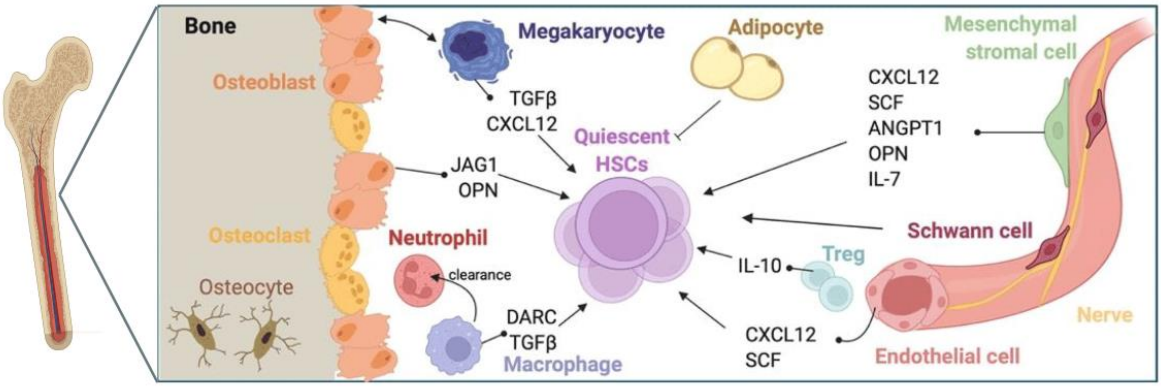

Figure 4. Schematic representation of the main different cell types forming the bone marrow niche. The scheme shows the bone marrow niche structure located inside the femur. The niche consists of different hematological and non-hematological cell types. These cells interact with HSCs through either direct interaction via adhesion molecules or by secreting chemokines, growth factors and interleukins. The niche cells interact with the HSCs to regulate quiescence, proliferation and lineage commitment. ANGPT1 = angiopoietin 1, CXCL12 = C-X-C motif chemokine ligand 12, DARC = atypical chemokine receptor 1, IL-7 = interleukin 7, IL-10 = interleukin 10, JAG1 = jagged canonical Notch ligand 1, OPN = osteopontin, SCF = KIT ligand, TGF-β = transforming growth factor beta. (Adapted from Aprile et al. [57]).

1.6.1 Neuronal regulation of hematopoiesis

The central nervous system (CNS) and neuronal innervation within the bone marrow niche are of great importance for HSCs during homeostasis and stress [58]. Neuronal nerve fibers surrounded by Schwann cells are found near blood vessels in the niche and are in contact with stromal cells and endothelial cells that form the vessels. During homeostasis, nerve fibres regulate CXCL12 levels in the niche following a circadian rhythm [59]. Neuronal noradrenaline production activates stromal cells to produce CXCL12, which leads to the mobilization of HSCs into the blood. The CNS also regulates the HSC response during cardiac injury, ageing, leukaemia and psychological stress [51]. Stress has been identified as a major challenge facing the human population in recent decades. During a normal stressful event, the CNS is activated and produces catecholamines and corticosteroids. These hormones induce physical and cellular changes to overcome the stress situation. Afterwards, their levels return to pre-stress concentrations as they get cleared from the body. However, continuous high levels of

stress can have severe side effects and promote the development of various diseases [60]. Persistent stress has been linked to an immune system dysregulation, digestive tract diseases [61], cancer [62], and CVDs [63]. In 2014, Nahrendorf et al. demonstrated that chronic stress increases circulating monocytes and neutrophils in humans. These results were obtained through experiments performed in mouse models subjected to chronic stress, which led to the development of monocytosis and an increase in proliferation of HSPCs. These effects were due to the increase in noradrenaline in the bone marrow and a reduction of CXCL12 [64]. McKim et al. showed that social stress promotes the migration of HSCs to the spleen, leading to extramedullary hematopoiesis that lasted for 24 days after stressor removal with a bias toward production of myeloid and erythroid cells [65].

1.6.2 Hematopoiesis and cardiovascular diseases

It is now well known that there is a tight relation between CVD, stress-induced inflammation and hematopoiesis. In addition, most of the common risk factors of CVDs lead to the activation of the hematopoietic system, which increases the production of leukocytes [66]. The increase in leukocytes is directly associated with the initiation of atherosclerosis that may later on cause stroke or MI. The chronic state of inflammation associated with risk factors like obesity aging or smoking activates HSPCs into a proliferative state that can lead to the progression of clonal hematopoiesis (CH). CH is associated with ageing as the continuous proliferation of HSCs over time accumulates somatic mutations, which do not always cause malignancies but rather produce clonal expansion. These clones can be detected in blood and are termed clonal hematopoiesis of indeterminate potential (CHIP) [67]. Both clinically and experimentally, CHIP has been associated with the accelerated development of atherosclerosis and other cardiac complications (Figure 5). In 2014, the association between CHIP and both coronary heart disease and ischemic stroke was reported for the first time. The study utilized whole exome sequencing from more than 17 thousand individuals and identified many mutations that lead to the development of CHIP. The study found that the most frequently affected genes are tet methylcytosine dioxygenase 2 (*TET2*) and DNA (cytosine-5) methyltransferase 3 alpha (*DNMT3A*) [68]. TET2 is an epigenetic modifier and plays a role in DNA methylation. Mutations in this gene accumulate with aging and are clinically associated with different forms of blood disorders [69]. In mouse models, *Tet2* loss of function leads to higher HSCs proliferation with a myeloid bias. Using *Ldlr*$^{-/-}$ deficient mice and bone marrow transplantation, it was shown that hematopoietic *Tet2* deficiency drives clonal expansion with increased atherosclerotic plaque formation. The molecular mechanism was associated with NLR family pyrin domain containing 3 (NLRP3) inflammasome activation in macrophages and production of interleukin-1β (IL-1β), while inhibition of NLRP3 showed an atheroprotective effect [70]. These findings support the hypothesis that CH drives atherosclerosis development. It is also possible that

atherosclerosis and the low-grade inflammation state associated with plaque formation can drive CH. In 2021, Heyde et al. have employed a mathematical model plus animal experiments to emphasize that atherosclerosis drives CH, as it induces proliferation which increases the rate of somatic mutations; results that were in line with patient data [71].

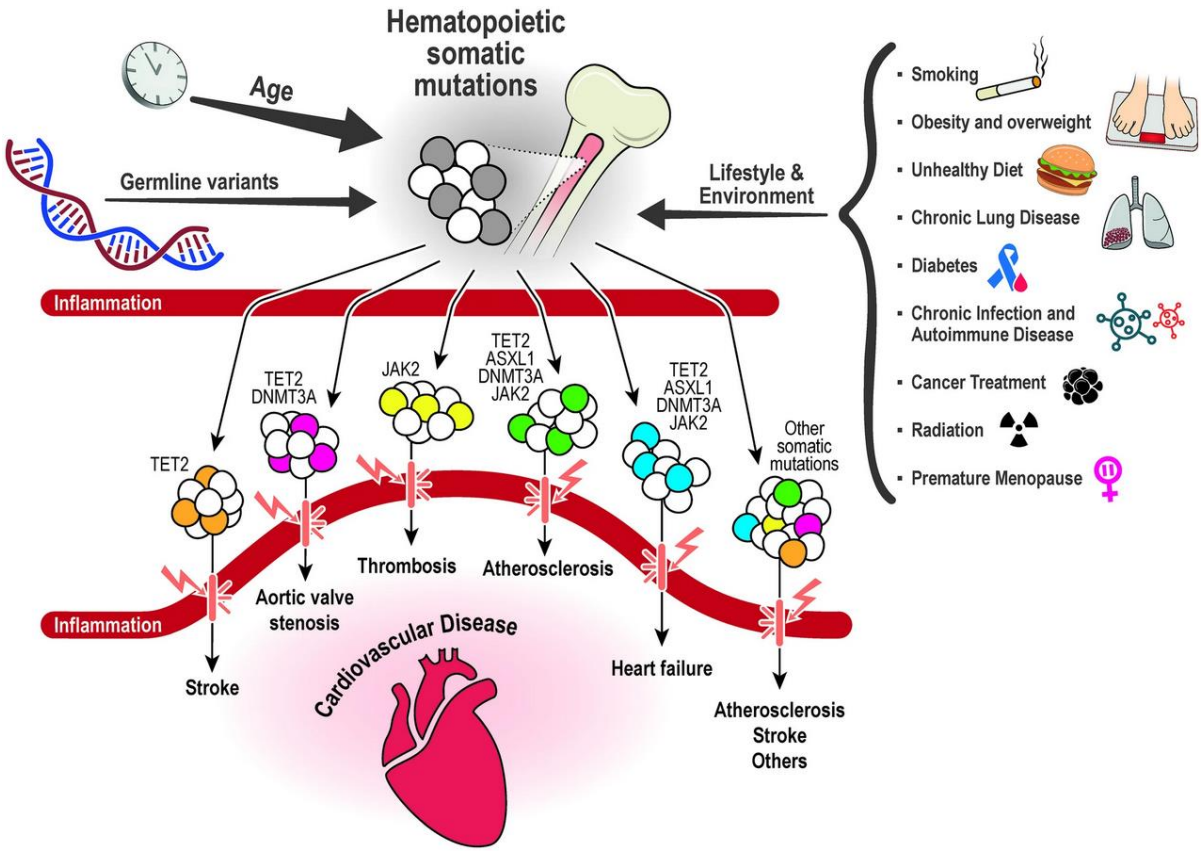

Figure 5. Multiple causes driving hematopoietic somatic mutations that increase the risk of cardiovascular complications. Different stressors can affect HSCs and their genome integrity. Somatic mutations increase with pathological conditions including aging, lifestyle and environmental factors such as smoking and radiation. These factors lead to a state of inflammation that favors the occurrence of somatic mutations, some of which can lead to clonal hematopoiesis. Several mutations have a strong association with the occurrence of cardiovascular diseases. (Adapted from Haring et al. [72]).

Further experimental studies have investigated the relationship between lifestyle-related HSC activation and atherosclerosis development. In 2019, McAlpine et al. demonstrated that sleep quality can affect the proliferation of HSCs. Mice subjected to sleep fragmentation developed monocytosis with worse atherosclerotic outcomes compared to the control group. The authors linked this effect to hypocretin, a neuropeptide that regulates myelopoiesis and is produced in the lateral hypothalamus [73]. In the same year, Nahrendorf et al. showed the importance of exercise in reducing inflammation and HSC proliferation. Using a voluntary running model in mice, it was shown that exercise reduces the number of circulating leukocytes and adipose tissue leptin production. The reduction in leptin levels by exercise led to an increase in the production of the quiescence factors CXCL12 and SCF by LepR+ stromal cells. These findings

were supported by human data from the CANTOS study, showing that individuals with exercise routines had fewer circulating leukocytes [74].

Currently, the correlation between immune metabolic diseases, the development of CVDs and the perturbation of hematopoiesis is widely accepted. In obesity, high levels of cholesterol or fatty acids lead to enhanced myelopoiesis which results in the development of leukocytosis. Cholesterol regulates cellular proliferation and hypercholesterolemia enhances proliferation of HSPCs. This regulation happens as lipid rafts within the plasma membrane act as a hub for cytokine receptors. The change in cholesterol levels and efflux leads to disturbance of these lipid rafts and dysregulates cytokine downstream signalling which affects HSPCs proliferation and activation [75]. Several studies have shown that HSPCs express cholesterol efflux transporters like adenosine triphosphate-binding cassette (ABC) transporters and that mice deficient for ABCA1 and ABCG1 develop leukocytosis with enhanced proliferation of HSPCs and myeloid bias [76]. Cholesterol efflux also plays a role in regulating HSC mobilization and affects extramedullary hematopoiesis, leading to myeloid skewing [77]. The occurrence of a cardiac complication can also lead to increased proliferation of HSPCs and myelopoiesis, which increases the risk of a secondary cardiac complication. In 2012, Dutta et al. demonstrated that MI increases the sympathetic nerve activity in the bone marrow, which in turn decreases the retention factors SCF and CXCL12. This disturbance of retention factors in the bone marrow leads to the migration of HSPCs to the spleen where they proliferate and produce more myeloid cells. All these findings were linked to an acceleration of atherosclerosis development in mice subjected to MI compared to non-infarcted controls [78].

CVD can also affect hematopoiesis through altering the bone marrow vascular niche. Rohde et al. showed that Western diet (WD) resulted in endothelial cell dysfunction within the bone marrow vascular niche, as *Apoe*$^{-/-}$ mice fed with WD had altered bone marrow angiogenesis and increased vascular leakage. Transcriptomic analysis showed that bone marrow endothelial cells acquire an inflammatory phenotype and increase the production of interleukin-6 (IL-6) due to WD [79].

1.6.3 Hematopoiesis and inflammation

The bone marrow provides a protected environment for HSCs from stressors and pathogens. This idea changed recently, as research has shown that HSCs directly respond to different stressors. These stressors can be physiological (e.g. ageing) or pathophysiological (e.g. diabetes) or in the form of an injury or tissue damage. In most cases, this leads to production of cytokines and inflammatory molecules such as interleukins, interferons and colony-stimulating factors, which also play an important role in basal hematopoiesis and maturation of the hematopoietic system. Elevated levels of these molecules can have adverse effects on

the hematopoietic system and promote myelopoiesis. HSCs can sense and respond to different types of inflammatory signals as they express different receptors for growth factors and inflammatory cytokines including IL-1β, IL-6, macrophage colony-stimulating factor (M-CSF), and type 1 and 2 interferons (IFN) [80]. In addition, HSCs can directly sense tissue damage in response to injury, as they express toll-like receptors (TLRs) that sense pathogen-associated molecular pattern molecules (PAMPs) or damage-associated molecular pattern molecules (DAMPs) [81]. HSCs respond to higher leukocyte demand by exiting the quiescent state and proliferating to provide new blood cells for immune defense. Afterwards, HSCs return to quiescence and homeostasis to avoid exhaustion.

Both acute and chronic inflammation affect and modulate the hematopoietic system [82, 83]. Acute inflammation can be the result of a viral or bacterial infection, chemical stressors, injuries, or allergic reactions. It usually lasts for a short time and induces HSC proliferation to adapt to the high demand for myeloid cells required for pathogen defense. This process of fast and high production of myeloid cells is called emergency myelopoiesis [84]. If inflammation persists for a prolonged period, it establishes a chronic inflammation condition which may be a result of ageing, smoking, pathologic inflammatory conditions such as diabetes, obesity, CVDs, or cancer. Each of these conditions affects HSPCs in different ways but in general a persistent state of inflammation leads to myeloid lineage skewing [85]. Chronic inflammation also causes CH that leads to bone marrow failure and development of malignancies (Figure 6) [80].

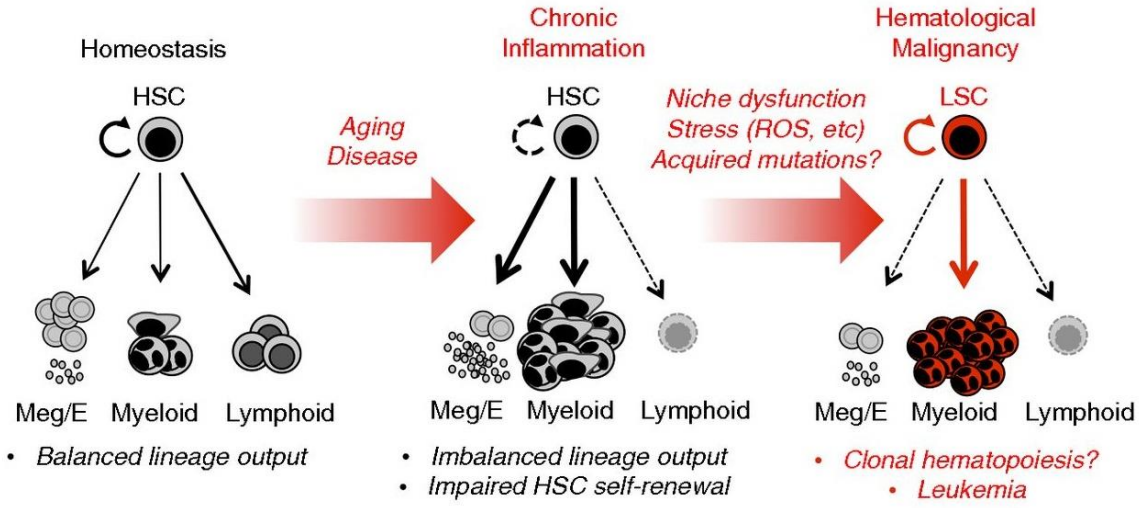

Figure 6. Chronic inflammation and the associated effect on the hematopoietic system. During homeostasis the proliferation and differentiation of hematopoietic stem cells is controlled and balanced to generate all blood cells on demand. The process of aging and certain diseases create a state of chronic inflammation that affects the normal state of HSCs, leading to increased proliferation and more bias toward myeloid differentiation. Chronic inflammation may change the niche homeostasis which can lead to niche dysfunction. Altogether, these events can trigger the development of hematological malignancies and clonal hematopoiesis at the level of HSCs and an increased number of mature myeloid cells. HSC = hematopoietic stem cell, Meg/E = megakaryocyte/erythrocyte, LSC = leukemic stem cell. (Adapted from Pietras [80]).

Several studies have shown how metabolic diseases such as obesity or diabetes can change steady-state hematopoiesis towards myeloid biased differentiation, leading to an increase in circulating monocytes and neutrophils [86]. As an example, obesity is associated with a chronic low grade of inflammation that can activate HSCs as mentioned before [87, 88]. Adipocytes in the bone marrow niche also play an important role in the regulation of HSC proliferation and differentiation, and an increase in adipocyte volume is associated with dysregulated hematopoiesis. More research is needed to understand the effect of metabolic disease on hematopoiesis, which is generally associated with increased myelopoiesis and myeloid progenitors in the bone marrow [89, 90].

1.7 The endocannabinoid system

In addition to cytokines and chemokines, lipid mediators also play a key role in the regulation of inflammation. A group of lipid mediators named endocannabinoids has been extensively investigated in homeostasis and in neuronal development. Furthermore, endocannabinoids have been studied in the context of atherosclerosis, coronary artery disease and myocardial infarction [91]. Endocannabinoids are part of the endocannabinoid system (ECS) which is highly conserved in mammals and regulates vital processes during different stages of development. The ECS consists of different components that are responsible for synthesis, degradation and signalling. Two G protein-coupled receptors (GPCRs) termed cannabinoid receptors 1 and 2 (CB1/CB2) have been identified, which both couple to $G_{i/0}$ proteins [92, 93]. Activation of CB1 and the coupled G protein αi subunit leads to Ca^{2+} decreases and K^{+} increases through ion channels. Downstream signalling includes the inhibition of adenylyl cyclase (AC) activity and subsequently the synthesis of cAMP. Further downstream pathways include mitogen-activated protein kinase (MAPK) and phosphatidylinositol-3-kinase (PI3K) (Figure 7) [94].

Cannabinoid receptors can be phosphorylated after activation, which recruits β-arrestin, leading to receptor desensitization and internalization, which can induce other signalling pathways [95]. There are two main endocannabinoid ligands, N-arachidonoyl-ethanolamine (AEA; anandamide) and 2-arachidonoylglycerol (2-AG). Both ligands are synthesised from arachidonic acid, which is located as a precursor at the cell membrane. AEA is produced from N-acyl-phosphatidylethanolamine (NAPE) by N-acyl phosphatidylethanolamine phospholipase D (NAPE-PLD) and is degraded by fatty acid amide hydrolase (FAAH), whereas 2-AG is synthesized from diacylglycerol (DAG) by DAG-lipase-α (DAGLα) or DAGLβ and is degraded by monoacylglycerol lipase (MAGL) [96].

In recent years, researchers have found that the ECS is not only involved in the maintenance of homeostatic functions but also plays a key function in pathological conditions. The system

is highly studied in the CNS and is relevant in neuronal development and plasticity [97, 98]. It controls diverse behavioural activities and is involved in neurological disorders [99, 100]. It is mainly expressed at synaptic terminals where it regulates neurotransmitter release and synaptic plasticity and plays an important role in the regulation of food intake by controlling hypothalamic nuclei and the limbic system [101]. Besides the relevance of endocannabinoid signalling in the CNS, the receptors are also expressed in peripheral organs (Figure 8) [94]. CB1 is expressed in the liver [102], pancreas, adipose tissue and gastrointestinal tract [103]. In these organs, it coordinates food intake, energy expenditure and metabolism [103-106].

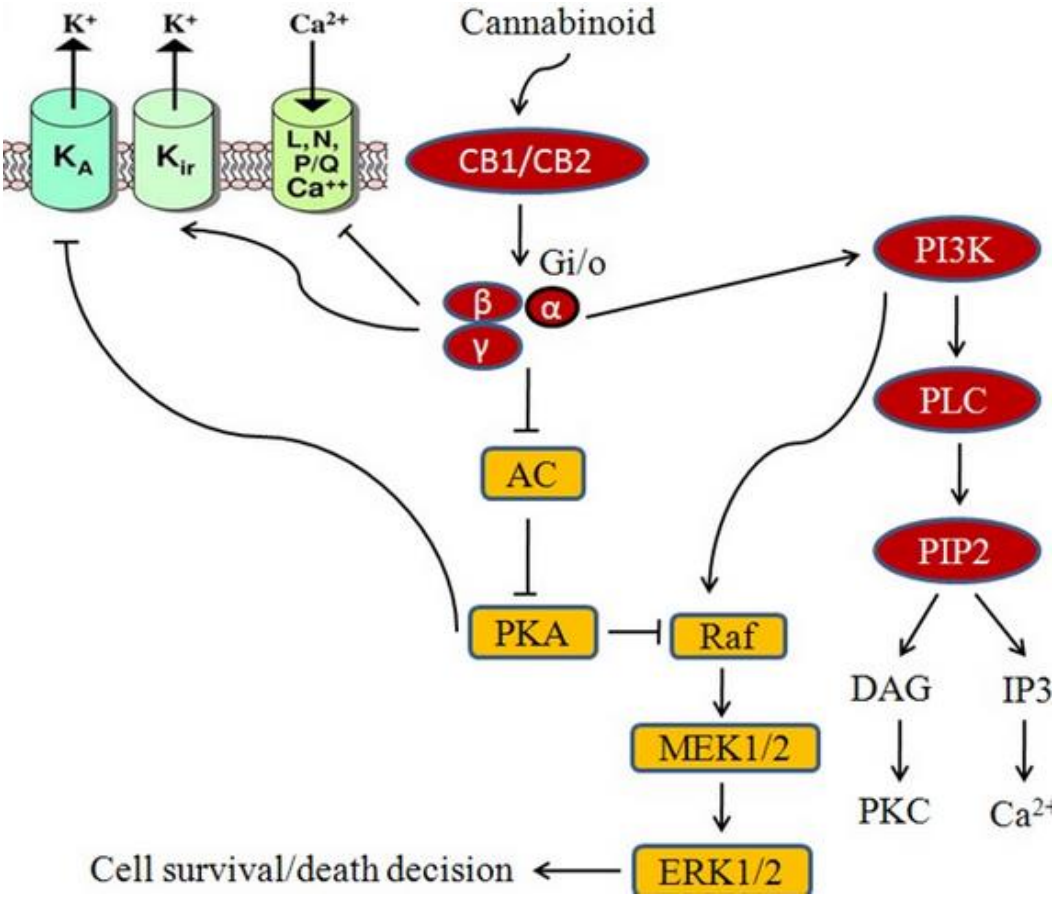

Figure 7. Cannabinoid receptor 1 downstream signalling pathways. The figure shows different pathways that are regulated/associated with cannabinoid receptors. Cannabinoid receptors couple to G protein subunit. Upon activation the signal is translated through different pathways. The G protein subunit regulates the concentration of Ca^{+2} and K^{+} ions through the ion channels. The signal can further be transmitted to affect cellular functions through PI3K (phosphoinositide 3-kinases) pathway and AC (adenyl cyclase). (Adapted from Chakravarti et al. [107]).

Pharmacological modulation of CB1 in rodents reduced food intake and body weight and hence improving metabolic parameters [108, 109]. CB1 is also expressed in different cardiovascular cells such as smooth muscle cells, myocardium and endothelial cells and many studies have shown that inhibiting CB1 has beneficial effects after MI or for reducing atherosclerosis progression [110]. The challenge with cannabinoid receptor modulation is to achieve organ specificity and specific cell type targeting, as the majority of pharmacological

compounds can affect the activity of the receptors in the CNS, which can lead to severe and unwanted side effects. Researchers are currently developing more specific molecules that can harness the beneficial effect of cannabinoid receptor targeting without having critical side effects [111].

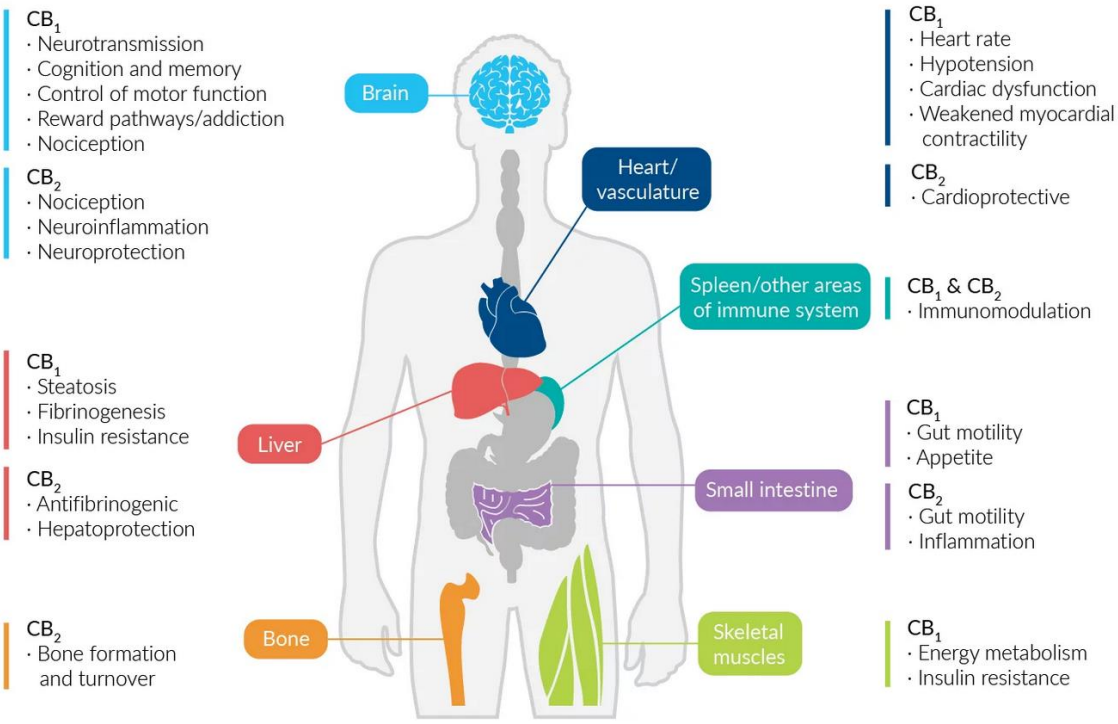

Figure 8. Expression of cannabinoid receptors in the human body. The endogenous cannabinoid system comprises of two receptors, CB1 and CB2. Both receptors are highly expressed in the central nervous system, where they regulate important neuronal processes, and play a role in neuronal development and synaptic transmission. In the periphery, both receptors are expressed in different organs to regulate organ-specific processes. In the heart, CB1 is associated with the regulation of heart rate and cardiac dysfunction. CB1 and CB2 are important for the immune system and are expressed on different immune cells, including monocytes and B cells (Adapted from https://www.caymanchem.com/news/cannabinoid-signaling-insights-to-future-pharmacotherapeutic-development last opened 19.11.2024).

Cannabis sativa is the source of phytocannabinoids, with tetrahydrocannabinol (THC) as the most abundant. In addition, synthetic ligands have been developed that are more specific to avoid off target effects [112]. Cannabinoids are used medically for the treatment of anxiety, depression or post-traumatic stress disorder, among other conditions [113]. In cardiovascular and inflammatory diseases, cannabinoids have shown therapeutic potential. In clinical studies, the CB1 antagonist rimonabant showed promising effects in cardiometabolic conditions [114]. In an experimental study, *Ldlr*$^{-/-}$ mice on a WD treated with rimonabant had a reduction in body weight, metabolic parameters and inhibition of atherosclerotic lesions [115]. Several following studies showed that endocannabinoid signalling is involved in atherosclerosis and that it regulates important pathophysiological aspects such as vascular inflammation and leukocyte recruitment [110, 116].

1.7.1 Cannabinoid receptor 1 and hematopoiesis

The relation between the endocannabinoid system and its potential involvement in regulating hematopoiesis is not well understood. Most of the research investigated the effect of ligands on mobilization and differentiation of the hematopoietic cells with a focus on CB2. CB2 was found to be important for recovery of the hematopoietic system after sub-lethal irradiation as activation of the receptor with a specific agonist increased HSCs survival after irradiation [117]. HSCs respond to endocannabinoids, especially 2-AG which acts as a chemoattractant [118]. Researchers have used single or multiple agonists to test the effect of activating CB1 and CB2 on HSCs. Hoggatt and Pelu found that treatment of LSKs with CP55940, a dual CB1 and CB2 agonist, led to a reduction in CXCR4 and VlA-4 (Integrin Subunit α 4) expression levels. Combined treatment with CP55940 and G-CSF (Granulocyte colony stimulating factor) enhanced the mobilization of HSCs into the blood, as confirmed by colony forming unit (CFU) assay as blood from mice injected with the combined treatment formed more Granulocyte/Monocyte-CFU compared to mice injected with G-CSF alone [119].

The ECS also plays an important role in bone homeostasis, remodelling and regeneration. Osteoblasts and osteoclasts are sources of endogenous ligands and express both cannabinoid receptors [120]. There is also a strong relationship between cannabinoid receptors, ageing and bone mass [121]. Osteoporosis is an age related disease in which the balance between bone resorption and bone formation is disturbed. Idris et al. found that CB1 has a protective effect against age-related osteoporosis and that CB1 is important in regulating the differentiation of stromal cells between adipocytes and osteoblasts which is important for bone homeostasis [122]. Bone homeostasis is important for HSCs as osteoblasts and osteoclasts are components of the bone marrow niche.

1.8 Animal models of hypercholesterolemia

Animal models that develop hypercholesterolemia and atherosclerosis in a similar mechanism as in humans are of great interest. Two widely used animal models are used in experimental studies, namely *Apoe*$^{-/-}$ and *Ldlr*$^{-/-}$ mice (Table 1).

Apoe$^{-/-}$ mice are widely used as a model for the formation of atherosclerotic plaques. Knocking out the *Apoe* gene disturbs the clearance of cholesterol and lipids from the plasma [123]. The *Apoe*$^{-/-}$ model is characterized by high levels of cholesterol-rich LDL particles in the blood which lead to the development of spontaneous atherosclerotic plaques. In this model different stages of plaque formation can be studied (from fatty streak to advanced necrotic plaques), allowing the study of biological mechanisms associated with plaque formation as well as therapeutic approaches. Besides that, *Apoe* deletion in these mice affects immune regulation and inflammatory responses [124, 125]. Different types of cells, including immune cells and

HSPCs express the *Apoe* gene. In HSPCs, *Apoe* deficiency leads to proliferation of HSPCs and affects normal hematopoiesis [126].

The *Ldlr*$^{-/-}$ animal model is another model that can be used to study atherosclerosis, based on genetic disruption of the *Ldlr* gene, which disrupts the endocytosis and uptake of LDL particles [127]. Upon WD feeding, the mice develop hypercholesterolemia. In humans, various mutations in the LDLR gene were related to hypercholesterolemia [128].

***Apoe*$^{-/-}$**	***Ldlr*$^{-/-}$**
The model was published in 1992	The model was published in 1993
APOE is a ligand for receptor-mediated uptake important for chylomicron and VLDL remnant clearance	LDLR is a cell-surface receptor that recognizes apoB100 and mediates endocytosis
A large increase in plasma apoB-containing lipoproteins, mainly in chylomicron remnant and VLDL fractions	A large increase in plasma apoB-containing lipoproteins, mainly in LDL fractions
Develops complex atherosclerosis lesions on a standard chow diet	Atherosclerosis development requires ≥ month of study periods unless a WD is administrated
More pronounced hypercholesterolemia and faster atherosclerosis development upon WD feeding	More pronounced hypercholesterolemia and large complex atherosclerosis plaques develop upon WD feeding
Severely hypercholesterolemic and has impaired immunoregulatory functions	Has less perturbed lipid metabolism and immune system
Three major human APOE alleles (E4, E3, E2) mediate different cardiovascular risks in humans	LDLR mutations are common monogenic trait In humans leading to familial hypercholesterolemia

Table 1. Comparison between *Apoe*$^{-/-}$ and *Ldlr*$^{-/-}$ as models for hypercholesterolemia. The table shows a comparison between the two most common animal models used to study hypercholesterolemia and atherosclerosis formation (adapted from Hansson et al. [124]).

1.9 Aim of this thesis

Development of CVDs is affected by risk factors that promote the development of atherosclerosis. There is a strong relationship between atherosclerosis risk factors and hematopoiesis. Enhanced hematopoiesis leads to overproduction of leukocytes and worsens atherosclerosis outcome due to accelerated development of plaques.

The aim of this thesis was to clarify the role of CB1 in regulating hematopoiesis in different biological states. For this purpose, animal models, molecular biology techniques, bone marrow transplant experiments, and single-cell sequencing were used to understand how CB1 affects hematopoietic stem and progenitor cells as well as bone marrow niche cells.

In particular, the following specific questions were addressed:

1. Does CB1 regulate hematopoiesis during homeostasis?
2. How does CB1 affect bone marrow niche factors important for HSPCs homeostasis?
3. What are the transcriptomic differences between wild type and *Cnr1*$^{-/-}$ HSPCs during homeostasis?
4. What is the effect of CB1 deficiency on hematopoiesis during chronic inflammation conditions induced by hypercholesterolemia?
5. What is the effect of CB1 deficiency on hematopoiesis in response to an acute inflammatory challenge?
6. What is the role of hematopoietic versus stromal cell CB1 in hematopoietic system reconstitution after irradiation?
7. What is the impact of pharmacological peripheral CB1 antagonism on hypercholesterolemia-driven myelopoiesis?

2 Materials and methods

2.1 Materials

2.1.1 Chemical and reagents

Chemicals/Reagents	Company
2-Methylbutane	Sigma-Aldrich Chemie GmbH, Munich, Germany
2-Propanol	Sigma-Aldrich Chemie GmbH, Munich, Germany
10X BD Perm/Wash	BD, Heidelberg, Germany
ACEA	Tocris, Wiesbaden-Nordenstadt, Germany
Acetic acid (glacial) 100% anhydrous	Merck KGaA, Darmstadt, Germany
Acetone	Sigma-Aldrich Chemie GmbH, Munich, Germany
BSA ≥ 98 %	Carl Roth GmbH + Co. KG, Karlsruhe, Germany
AM281	Tocris, Wiesbaden-Nordenstadt, Germany
AnnexinV binding buffer	Invitrogen, Karlsruhe, Germany
Antifade mounting medium	Vector Laboratories, Newark, United States
Citric acid	Merck KGaA, Darmstadt, Germany
CountBright absolute counting beads	Thermo Fisher Scientific, CA, USA
DMEM	Gibco, Bleiswijk, Netherlands
DMSO	Carl Roth GmbH + Co. KG, Karlsruhe, Germany
EDTA	Sigma-Aldrich Chemie GmbH, Munich, Germany
Embedding medium tissue-Tek OCT	Sakura Finetek, Torrance, USA
Eosin Y-solution	Sigma-Aldrich Chemie GmbH, Munich, Germany
Ethanol 99% (absolute)	VWR International, Radnor, USA
Fetal bovine serum	Sigma-Aldrich Chemie GmbH, Munich, Germany
Hanks buffered saline solution (HBSS)	Sigma, Merck, Darmstadt, Germany
Hematoxylin solution according to Mayer	Sigma-Aldrich Chemie GmbH, Munich, Germany
Hoechst 33342	Invitrogen, Karlsruhe, Germany
Hydrochloric acid	Merck KGaA, Darmstadt, Germany
Immu mount embedding medium	Thermo Fisher Scientific, CA, USA
Isopropanol	KMF Laborchemie, Lohmar, Germany
JD-5037	Hycultec GmbH, Beutelsbach, Germany
Ketamine	WDT eG, Garbsen, Germany
Methyl cellulose complete media	R & D, Wiesbaden-Nordenstadt, Germany
Neomycin sulfate	Gibco, Carlsbad, CA, USA

Oil red O	Sigma-Aldrich Chemie GmbH, Munich, Germany
Paraformaldehyde	Merck KgaA, Darmstadt, Germany
PBS (for cell culture)	Gibco, Bleiswijk, Netherlands
PBS powder	Biochrom AG, Berlin, Germany
Permeabilization buffer (10X)	Thermo Fisher Scientific, CA, USA
Polymyxin B -sulfat	Sigma-Aldrich Chemie GmbH, Munich, Germany
RapiClear 1.55	SUNJin lab, Hsinchu City, Taiwan
Red blood cell lysis/fixation solution (10x)	BioLegend, San Diego, USA
Recombinant Mouse G-CSF (carrier-free)	BioLegend, San Diego, USA
QIAzol lysis reagent	Qiagen, Venlo, The Netherlands
Roti-Histofix 4 %	Carl Roth GmbH + Co. KG, Karlsruhe, Germany
Sodium citrate tribasic dihydrate	Sigma-Aldrich Chemie GmbH, Munich, Germany
Sodium chloride 0.9%	B. Braun AG, Puchheim, Germany
Sodium chloride	Sigma, Merck, Darmstadt, Germany
Sucrose	Merck KgaA, Darmstadt, Germany
Tissue-Tek O.C.T	Sakura Finetek Germany GmbH, Staufen, Germany
TMB solution 1x	Thermo Fisher Scientific, CA, USA
Trypan blue dye	Bio-Rad, Hercules, USA
Tween 20	Sigma-Aldrich Chemie GmbH, Munich, Germany
Xylazine	WDT eG, Garbsen, Germany
Xylene	Sigma-Aldrich Chemie GmbH, Munich, Germany

Table 2. Chemicals and reagents

2.1.2 Buffers and solutions

Buffers and solutions	Composition
ACK lysis buffer	150 mM NH4Cl, 10 mM KHCO3, 0.1 mM Na_2EDTA, pH 7.4
Anesthesia	700 µl Ketamine (50 mg/ml), 500 µl Xylazine (20 mg/ml) in 4500 µl saline
Bone digestion cocktail	10mg/mL collagenase IV, 20 U/mL DNase I in DMEM (10%FBS)
ELISA reagent diluent	1.0 % BSA in PBS (pH 7.2-7.4)
ELISA substrate solution	1:1 mixture of Color Reagent A (H_2O_2) and Color Reagent B (Tetramethylbenzidine)

ELISA wash solution	10 mM phosphate buffer pH 7.4, 150 mM NaCl, 0.05% Tween 20
ELISA stop solution	2N H_2SO_4 in Milli-q H_2O
FACS buffer	0.5 % (w/v) albumin in PBS
ORO stock solution	0.5 % (w/v) ORO in 99 % 2-propanol
PBS solution 1X	9.55g PBS Dulbeccos in 1L ddH_2O (pH 7.4)

Table 3. Buffers and solutions

2.1.3 Kits

Kit	Company
peqGOLD Total RNA kit	Peqlab Biotechnologie GmbH, Erlangen, Germany
Single Cell RNA Purification Kit	NORGEN, Canada
PrimeScript RT Reagent Kit	Takara, Shiga, Japan
Probe qPCR master mix	Promega, Madison, USA
Qubit RNA High Sensitivity Assay Kits	Thermo Fisher Scientific, Eugene, USA
Qubit RNA IQ Assay Kits	Thermo Fisher Scientific, Eugene, USA
HS NGS Fragment kit (1-6000 bp)	Agilent, Santa Clara, USA
Chromium Next GEM Single cell 3' HT Kit v3.1, 8 rxns PN-1000370	10x Genomics, Leiden, The Netherlands
Chromium Next GEM Chip M Single Cell Kit, 16 rxns PN-1000371	10x Genomics, Leiden, The Netherlands
3' Feature Barcode Kit, 16 rxns PN-1000262	10x Genomics, Leiden, The Netherlands
3' CellPlex Kit Set A, 48 rxns PN-1000261	10x Genomics, Leiden, The Netherlands
Dual Index Kit TT Set A, 96 rxns PN-1000215	10x Genomics, Leiden, The Netherlands
Dual Index Kit NN Set A, 96 rxns PN-1000243	10x Genomics, Leiden, The Netherlands
Mouse CXCL12/SDF-1 DuoSet ELISA	R&D, Wiesbaden-Nordenstadt, Germany
Mouse SCF DuoSet ELISA	R&D, Wiesbaden-Nordenstadt, Germany
Mouse G-CSF DuoSet ELISA	R&D, Wiesbaden-Nordenstadt, Germany

Table 4. Kits

2.1.4 Primers

Murine gene	5'-3' primer sequence or Assay ID
Gapdh	Mm99999915_g1
Icam1	Mm00516023_m1
Vcam1	Mm01320970_m1
Cxcr4	Mm01292123_m1
Hprt	Fw GACCGGTCCCGTCATGC
	Rev TCATAACCTGGTTCATCATCGC
	Probe VIC-ACCCGCAGTCCCAGCGTCGTG-TAMRA

Table 5. Murine qPCR primers

MWG-Biotech AG provided the self-designed primers and probes for qPCR, while Life Technologies supplied the TaqMan Gene Expression Arrays.

2.1.5 Antibodies

Antigen	Conjugation	Dilution	Reference	Provider
7AAD	unconjugated	1:100	A1310	Invitrogen
Annexin V	BV395	1:100	564871	BD Bioscience
B220	PB	1:1000	103227	BioLegend
B220	BUV395	1:500	563793	BD Bioscience
c.Kit	PE-Cy7	1:1000	105814	BioLegend
CD101	PE	1:1000	2213785	Invitrogen
CD115	APC	1:500	17-1152-82	Invitrogen
CD11b	AF700	1:500	101222	BioLegend
CD11b	PE-Texas red	1:1000	101256	BioLegend
CD150	PerCp	1:500	115921	BioLegend
CD150	APC	1:500	115910	BioLegend
CD16/32	APC-Cy7	1:1000	101327	BioLegend
CD16/32	BV711	1:1000	101337	BioLegend
CD16/32 Fc block	unconjugated	1:1000	553142	BD Pharmingen
CD19	PE-Texas red	1:200	115554	BioLegend
CD45.1	PE	1:500	110707	BioLegend
CD45.2	PerCP	1:500	103131	BioLegend
CD45.2	BV711	1:200	109847	BioLegend
CD45.2	FITC	1:400	553772	BD Bioscience
CD45.2	APC-Cy7	1:500	109824	BioLegend

CD48	BV510	1:500	563536	BD Horizon
CXCR2	BV737	1:300	748680	BD Bioscience
Gr1	PB	1:1000	108429	BioLegend
Ki67	FITC	1:100	11-5698-82	Invitrogen
Ly6C	BV421	1:500	128031	BioLegend
Ly6C	AF700	1:500	128023	BioLegend
Ly6G	PE	1:500	551461	BD Pharmingen
Ly6G	BV395	1:1000	563978	BD Horizon
Ly6G	BV510	1:500	127633	BioLegend
m-SDF-1α (synthetic)	AF647	1:40	CAF-50_10ug	ALMAC
Sca1	BV605	1:500	108134	BioLegend
TER119	PB	1:200	116232	BioLegend

Table 6. Murine antibodies and fluorescent dyes for flow cytometry

Antigen	Type	Source	Dilution	Reference	Provider
Tyrosine hydroxylase	Primary	Rabbit	1:100	NB300-109	Novus
CGRP-I	Primary	Goat	1:1000	ab36001	Abcam
Anti-rabbit	Secondary	Donkey	1:400	711-605-152	JIR
Anti-goat	Secondary	Donkey	1:100	705-585-003	JIR

Table 7. Antibodies used for whole mount immunofluroscence staining

2.1.6 Enzymes

Enzyme	Final concentration	Company
Collagenase IV	0.125 U/µl	Worthington Biochemical Corp, Lakewood, USA
Deoxiribonuclease I	0.02 U/µl	Roche, Basel, Switzerland

Table 8. Enzymes used for tissue digestion

2.1.7 Consumables

Material	Company
40 um cell strainer blue	BD Falcon, Eysins, Switzerland
70 um cell strainer white/grey	BD Falcon, Eysins, Switzerland
Minicaps disposable capillary pipettes 10µL	Hirschmann, Eberstadt, Germany

Centrifuge tubes 15, 50 ml	Corning, Taufkirchen, Germany
Cover glass 10 mm	VWR, Ismaning, Munich, Germany
Cover slips 24x60 mm	Menzel-gläser, Braunschweig, Germany
Cryomold embedding dish 10 x 10x 5 mm	Sakura Finetek, Torrance, USA
Disposable pipettes 5 to 25 ml	Corning, Taufkirchen, Germany
ELISA 96-well-plate	Brand, Wertheim, Germany
FACS tubes (5ml Polystyrene round bottom)	BD Falcon, Eysins, Switzerland
FACS tubes + blue cell strainer	BD Falcon, Eysins, Switzerland
Filter pipette tips	Starlab, Hamburg, Germany
iSpacer 0.05mm 1.0mm	SUNJin lab, Hsinchu City, Taiwan
iSpacer 1.0mm	SUNJin lab, Hsinchu City, Taiwan
PCR tubes	Nippon Genetics, Düren, Germany
Microcentrifuge tube 0.5 to 5 ml	Starlab, Hamburg, Germany
Microlance needles 23G/16G/20G	BD Falcon, Eysins, Switzerland
Microscope slides 25x75x1mm	Menzel-gläser, Braunschweig, Germany
Multiwell cell culture plates flat, sterile 6,12, 24 well	Corning, Taufkirchen, Germany
Cell culture plate 35mm	Fisher Scientific GmbH, Schwerte, Germany
qPCR clear seal	Nippon Genetics, Düren, Germany
qPCR 96 well plates	Nippon Genetics, Düren, Germany
Sealing tape	Corning, Taufkirchen, Germany
Syringe sterile 1 to 10 ml	BD Falcon, Eysins, Switzerland
Tissue-tek	Sakura Finetek, Staufen, Germany

Table 9. List of consumable materials

2.1.8 Equipment

Equipment	Company
Autoclave LTA 400	Zirbus technology GmbH, Bad Grund, Germany
Balance SE 203 LR	VWR International, Radnor, USA
Chromium X	10x Genomics, Leiden, The Netherlands
Centrifuges Megafuge 1.0R	Heraeus, Hanau, Germany
Centrifuge 5418 R	Eppendorf AG, Hamburg, Germany
CO2 incubator CB 160	BINDER GmbH, Tuttlingen, Germany
FACSAria III Cell Sorter	BD Bioscience, San Jose, USA
FACSCanto II	BD Bioscience, San Jose, USA

Fragment analyzer 5200	Agilent, Santa Clara, USA
Hood HERAsafe	Heraeus, Hanau, Germany
Laboratory pH Meter 766	Knick GmbH, Berlin, Germany
Leica DMi8 Thunder system	Leica Biosystems, Wetzlar, Germany
Leica SP8 3X	Leica Biosystems, Wetzlar, Germany
Leica LMD7000 microscopes	Leica Biosystems, Wetzlar, Germany
Leica DM6000B microscopes	Leica Biosystems, Wetzlar, Germany
Leica CM 3050S cryostat	Leica Biosystems, Wetzlar, Germany
LSRFortessa X-20	BD Bioscience, San Jose, USA
Nanodrop ND1000 Peqlab	VWR International, Radnor, USA
PCR Plate Spinners	VWR International, Radnor, USA
PCR Thermocycler Biometra Tpersonal	Biometra GmbH, Göttingen, Germany
QuantStudio 6 Real-Time PCR Systems	Thermo Fisher Scientific, Eugene, USA
TC20 Automated Cell Counter	Bio-Rad Laboratories GmbH, Feldkirchen, Germany
Tecan F200 PRO microplate reader	Tecan Group, Maennedorf, Switzerland
Thermomixer F1.5	Eppendorf AG, Hamburg, Germany
TissueLyser LT	Qiagen, Hilden, Germany
Vortex Mixer TX4	VELP Scientifica, Usmate, Italy
Water bath type 1004	Memmert WB14 (Memmert GmbH + Co. KG)
Water Purification System Milli-Q	Merck Millipore, Billerica, USA

Table 10. List of equipments

2.1.9 Software

Software	Company
BD FACSDiva	BD Bioscience, San Jose, USA
FlowJo v10.3	Tree Star, Inc., OR, USA
GraphPad Prism 9.00	GraphPad Software Inc, USA
LAS V4.3	Leica Biosystems, Wetzlar, Germany
Image J software	National Institutes of Health, USA
10x Genomics Cell Ranger v7.1.0	10x Genomics, The Netherlands
IMARIS	Oxford instruments plc

Table 11. Software version and provider

2.2 Methods

2.2.1 Mouse model

Global CB1 deficient mice on C57BL/6J background (*Cnr1*$^{-/-}$ [129]) or on *Apoe*$^{-/-}$ background (*Apoe*$^{-/-}$*Cnr1*$^{-/-}$, for studies in atherogenic condition) were bred in-house and genotyped after weaning. *Cnr1*$^{+/+}$ or *Apoe*$^{-/-}$*Cnr1*$^{+/+}$, respectively, were used as corresponding controls. For experiments where WT mice were used as control, C57BL/6J from Janvier labs were used. For baseline analysis, male and female mice were euthanized at the age of 8 weeks. For atherosclerosis studies, mice were subjected to a WD (0.2% cholesterol, Ssniff, TD88137) for either 4 or 16 weeks. In a different set of experiments, *Ldlr*$^{-/-}$ mice were subjected to WD for 8 weeks. Afterwards, the mice were divided into two groups. One group received the peripheral CB1 antagonist JD5037 (3 mg/kg/day) for 8 weeks via i.p. injections (intraperitoneal injection) and the control group was injected with the vehicle mixture consisting of 10% DMSO, 40% PEG3000, 5% Tween-80, and 45% saline. During this period, both groups received continuous WD feeding. Mice were housed in ventilated cages, with 4 to 6 mice per cage. The housing environment was maintained at 23°C, 60% humidity and a 12-hour light-dark cycle. All animal experiments were approved by the local ethics committee (District Government of Upper Bavaria; License Number: 55.2-1-54-2532-111-13 and 55.2-2532.Vet_02-18-114) and conducted according to the institutional and national guidelines and following the ARRIVE guidelines [130].

2.2.1.1 Bone marrow transplantation

Donor and recipient mice 7 to 8 week old were used for transplantation. Recipients were irradiated two times with a 5G irradiation dose (Faxitron CP160) with at least 4 and maximum 6 hours between the two irradiations. Femurs and tibias were collected from donors and extraction of bone marrow cells was done in sterile conditions (using a cell culture biosafety BSL2 cabinet), In brief, bones were rinsed with 100% ethanol and cells were flushed from bones and pooled from at least two donor mice. Cells were counted using trypan blue and a TC20 automated cell counter (BioRad). Then, $2.5x10^6$ cells were transplanted through i.v injection (tail vein) into each recipient. To facilitate the recovery, recipients received mashed food (Chow food pellet soaked in water) for the first 10 days and water supplemented with antibiotics (Neomycin-sulfate 0.5g/L and Polymyxin B-sulfate 60000U/L) for one month. After 6 weeks of recovery, the diet was changed to WD for 4 weeks.

2.2.1.2 Granulocyte colony stimulating factor *in vivo* treatment

C57BL/6J or *Cnr1*$^{-/-}$ mice were injected i.p. on five consecutive days with 6.25. µg/animal/day of recombinant mouse G-CSF. G-CSF was diluted in PBS with 1% BSA and mice were injected always between 8:00-9:00 am and the end point harvest was 2 hours after the last injection

on the fifth day (harvest time 11.00 am). Control mice were injected with vehicle (1% BSA in PBS) following the same injection protocol.

2.2.2 Mouse dissection

At experimental end time points, mice were anaesthetized by i.p. injection of ketamine (80mg/kg) and xylazine (12mg/kg) using a 1 mL insulin syringe with a 30 G needle. Unless described otherwise, blood was collected via cardiac puncture using a 26 G micro-lance needle flushed with 0.5 M EDTA into an EDTA microtube. For intermediate blood sampling time points, blood was obtained via the tail vein using capillary pipettes. Blood samples were used for flow cytometry analysis or colony forming unit (CFU) assay. Mice were further perfused with 10 mL PBS, followed by collection of different organs, femurs and tibias. Plasma was collected from the blood by centrifugation at 3000xg for 10 minutes. Organs and plasma were snap-frozen in liquid nitrogen and stored at -80 °C. Heart tissues containing the aortic root area were snap-frozen in Tissue-Tek using liquid nitrogen pre-cooled isopentane and stored at -20°C. Femurs and a piece of spleen tissue were immersed in PBS and kept chilled on ice until further processing for flow cytometric analysis.

2.2.3 Colony forming unit (CFU) assay

Bone marrow mononuclear cells were isolated as described above. Cell number and viability were checked using trypan blue and an automated cell counter. Cells were resuspended in DMEM (2% FBS) and 10^4 cells per 35 mm cell culture dish were plated in mouse methylcellulose complete media. After 7-10 days, colonies were scored and counted according to their morphology, using a Leica microscope (Leica DM IL LED). For blood samples, 100 µL blood was lysed using 1X RBCs lysis buffer. Afterwards, cells were washed with sterile PBS and resuspended in 150 µL DMEM (2% FBS). Cells were plated as described above and colonies scored after 10 days.

2.2.4 Atherosclerotic lesion quantification

2.2.4.1 Oil Red O staining for aortic roots

Hearts were collected during organ harvest and kept on ice-cold PBS until further processing. Hearts were cut in half and embedded in OCT, and OCT blocks were kept at -20°C for storage. A cryotome CM3050S was used to cut aortic root sections with a thickness of 5 µm. Sections were collected from the onset of the aortic valves until they were no longer visible. Eight sections per heart (covering a total area of 400 µm) were used to quantify the aortic lesion. Sections were fixed with Roti-Histofix for 10 min and stored at RT till further processing. The first sections, showing the aortic root were incubated for 5 min PBS. After air drying, slides were incubated for 15 min in a working solution of Oil Red O (120 mL of the ORO stock solution

with 80 mL of ddH_2O). To remove excess stain, slides were dipped in 60% isopropanol. Further washing was done by rinsing in running tap water and then counterstaining using hematoxylin. Immu-Mount was used as the mounting media and images were taken by Leica DM6000B.

2.2.4.2 Hematoxylin-eosin staining for aortic roots

Hearts and further cutting of sections was done as mentioned in section 2.2.4.1. Eight sections per heart (covering a total area of 400 µm) were used to quantify the aortic lesion. Afterwards, Slides were exposed to PBS for 5 min then nuclei were exposed to Mayer's hematoxylin solution at RT for 1 min, followed by a 5 min rinse in running tap water. This was followed by incubation with Eosin Y solution for 2 minutes, then slides were washed in ddH_2O for 2 min. Slides were dehydrated through a series of 70% ethanol, 80% ethanol, 96% ethanol and 100% ethanol with each step lasting 20 sec. Finally, slides were exposed to xylene for 2 min. Slides were mounted with antifade mounting medium (Entellan, Merk). Images were captured using a Leica DM6000B fluorescence microscope, and lesion size measurements were performed using ImageJ software. Lesion size was assessed by calculating the ratio of cumulative lesion area to inner vessel perimeter.

2.2.5 Whole mount staining

For whole-mount imaging, the femur was isolated as previously described. For fixation, 2% paraformaldehyde solution was used for 8 hours at room temperature. Afterwards, 1X PBS was used for washing three times. The femurs were then incubated in 15% sucrose solution for 2 hours at 4°C, then in 30% sucrose solution overnight at the same temperature. Femurs were embedded in OCT and stored at -20 °C until further processing. For staining, OCT sections were trimmed using a cryotome until the marrow inside the femur was exposed. Femurs were removed from OCT and immersed into blocking buffer (1X PBS with 5% BSA and 0.5% TritonX) for 2 hours at room temperature. To stain for sympathetic and nociceptive nerves, tyrosine hydroxylase (TH) and calcitonin gene-related peptide (CGRP) were used as markers. Primary antibody staining was done using anti-TH (1:100) and anti-CGRP (1:1000) in 1 ml blocking buffer and incubation for 72 hours at 4°C. Femurs were then washed 3x with PBS and incubated with secondary antibodies for 72 hours at 4°C. Secondary antibodies were anti-rabbit AF647 (1:400) and anti–goat AF549 (1:100). HOCHSET was added for nuclear stain. Femurs were washed 3x with PBS, incubated overnight at room temperature with clearing solution (RapiClear 1.55), which also served as mounting media. The samples were imaged the following day using a confocal microscope (Leica LMD7000). To analyze the whole femur, 7 z-stack sections were captured as indicated by black arrows in the experimental scheme: 2 sections of the distal epiphysis, 1 section of the metaphysis, 1 section of the diaphysis, 1 section of the metaphysis, and 2 sections of the proximal epiphysis (Figure 9).

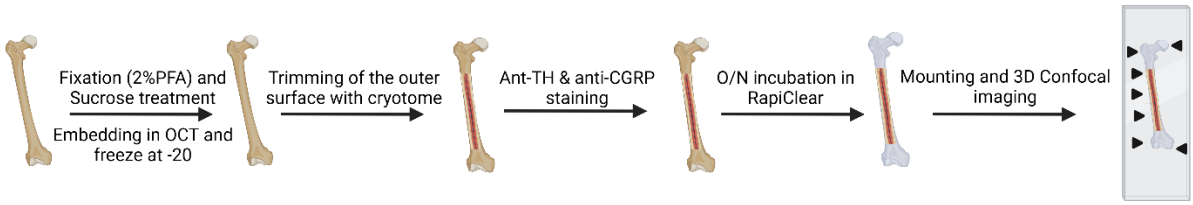

Figure 9. Preparation steps for whole mount imaging of femurs.

2.2.6 Enzyme-linked immunosorbent assay (ELISA)

Soluble bone marrow factors or plasma cytokines levels were measured using DuoSet ELISA kits (R&D Systems, Minneapolis, MN) following the manufacturer's instructions. To collect bone marrow lavage (supernatant), femurs were centrifuged for 2 minutes at 10000xg at 4°C, and then the pellet was suspended in 250 µL PBS per femur. Samples were centrifuged at 400xg for 5 min at 4°C, the supernatant was transferred into fresh tubes and stored at -20°C until further analysis. All ELISA incubation steps were at room temperature unless otherwise mentioned. A 96-well-plate was coated overnight with 100 µL of capture antibody working solution. Afterwards, the plate was washed three times with washing solution (0.05% Tween 20 in PBS, pH 7.2) and blocked for one hour using a blocking buffer (1% BSA in PBS, pH 7.2). The plate was washed as previously described and 100 µL of sample or standard per well was added and incubated for 2 hours. Standards were prepared by serial 2-fold dilutions of the stock. Afterwards, washing steps were repeated and 100 µL of capture antibody working solution was added to the plate for two hours. After washing, a 100 µL working solution of streptavidin-HRP was added and the plate was incubated for 20 minutes. Then, 100 µL of tetramethylbenzidine (TMB) substrate solution (Thermo Fisher Scientific) was added for 15-20 minutes. The reaction was stopped using 25 µL of 2N H_2SO_4. A Tecan Infinite F200 PRO microplate reader was used to measure the optical density at 450 nm with a reference wavelength of 550 nm. The sample values were then determined by interpolating with the standard curve, applying a fourth-order polynomial curve fitting mode with nonlinear regression (GraphPad Prism 9).

2.2.7 Flow cytometry – general overview

Flow cytometry was used to quantify immune cell populations in blood and tissues as well as to check for viability and cell cycle stage distribution. Depending on the tissue sample, different single-cell solution preparation steps were applied. Independent of the sample type, the protocol consists of major steps. The lysis step uses ACK buffer to remove red blood cells (RBCs), followed by filtration to remove debris and cell aggregates. To prevent unspecific binding, cells were incubated with 50 µL fluorescence-activated cell sorting (FACS) buffer solution, supplemented with anti-CD16/CD32 antibody. Subsequently, cells were stained with 100 µL staining mix. The incubation time with antibodies was between 30 and 45 min at 4°C

min unless otherwise mentioned. Afterwards, the cells were washed and suspended in 200 µL FACS buffer containing count bright absolute counting beads (Invitrogen). BD LSRFortessa X-20 Cell analyzer (BD Bioscience) or FACSCanto II were used to acquire the samples.

2.2.7.1 Flow cytometric analysis of leukocytes in blood, spleen and bone marrow

Blood samples were collected in an EDTA microtube. Consequently, RBCs lysis was performed by adding 1 mL of ACK buffer to 50 µL of blood and incubating it for 20 min at room temperature. Afterwards, a washing step was applied using FACS buffer. To obtain single cell suspension from bone marrow, femur bone was placed in a 1 mL pipette tip placed in a 2 mL tube and centrifuged for 2 min at 10000xg. Tips and bones were removed and ACK buffer was added to the collected cell pellet. A washing step was applied before finally suspending the cells in FACS buffer to proceed with staining protocol. To obtain splenic single-cell suspensions, part of the spleen was first mashed through a 70 µm cell strainer. The cell solution was centrifuged for 5 minutes at 4°C and ACK buffer was added to the cell pellet. This was followed by another filtration step through a 40 µm cell strainer. Then, the cells were resuspended in FACS buffer. After blocking non-specific binding with Fc block, spleen, blood and bone marrow cells were stained with antibodies. Myeloid cell were gated as live/singlets and $CD45^+CD11b^+$, then further gated as follows: $CD115^+Ly6G^-$ (monocytes) and $CD115^-Ly6G^+$ (neutrophils).

2.2.7.2 Hematopoietic and progenitor stem cells

To identify different HSPC populations in the bone marrow, spleen or circulating in the blood, the following antibody mix was used: lineage markers (CD3, B220, TER119, CD11B, GR-1), Sca-1 and cKit that allowed us to differentiate between HSCs (LSK - $Lin^-cKit^+Sca\text{-}1^+$) and committed progenitors (LK - $Lin^-cKit^+Sca\text{-}1^-$). Further gating of different populations of HSCs and multipotent progenitors (MPP) was based on SLAM factors CD150 and CD48. Committed myeloid progenitors and granulocyte monocyte progenitors were gated based on CD16/32 and CD34 expression. After gating live/single cells, different populations were defined according to table 12:

Cell population	Markers used for FACS gating
LT-HSC	$Lin^-cKit^+Sca\text{-}1^+CD150^+CD48^{-/low}$
ST-HSC	$Lin^-cKit^+Sca\text{-}1^+CD150^-CD48^{-/low}$
MPP2	$Lin^-cKit^+Sca\text{-}1^+CD150^+CD48^+$
MPP3	$Lin^-cKit^+Sca\text{-}1^+CD150^-CD48^+$
CMP	$Lin^-cKit^+Sca\text{-}1^-CD16/32^{-/low}CD34^+$

GMP	$Lin^-cKit^+Sca\text{-}1^-CD16/32^+CD34^+$
Pro1	$B220^-Ter119^-CD3^-CD115^-Ly6C^+Ly6G^-CXCR2^-CD11b^-ckit^+$
Pro2	$B220^-Ter119^-CD3^-CD115^-Ly6C^+Ly6G^-CXCR2^-CD11b^+ckit^{+/low}$
PreNeu	$B220^-Ter119^-CD3^-CD115^-Ly6G^{low}CD11b^+CXCR4^+CXCR2^-$
Immature neutrophils	$B220^-Ter119^-CD3^-CD115^-CD11b^+Ly6G^+CXCR4^+CXCR2^-$
Mature neutrophils	$B220^-Ter119^-CD3^-CD115^-CD11b^+Ly6G^+CD101^+CXCR2^+$

Table 12. Markers used in FACS gating for different cell populations.

To measure CXCR4 expression on different cell types, synthetic ligand that is fluorescently labelled was used (m-SDF-1α (CXCL12-AF647). For staining protocol, cells were first stained with 100 µL (CXCL12-AF647 (40nM) in PBS) and incubated for 30 min at 37°C, followed by washing one time with FACS buffer. Afterwards cells were stained as mentioned above.

2.2.7.3 Cell viability/apoptosis assay

AnnexinV and 7-AAD were used to determine the frequency of viable, apoptotic and dead cells. In brief, following the previously mentioned protocol to stain for different HSPC populations, cells were incubated for 10 min in Annexin V buffer (BioLegend) with Annexin V antibody at 4°C, followed by washing one time with Annexin V buffer. Cell pellets were suspended in 100 µL Annexin V buffer with 7AAD (1:100), and cells were incubated for at least 10 min before analysis.

2.2.7.4 Cell cycle analysis

To determine the distribution of HSPC populations in different cell cycle stages, Ki67 and 7AAD were used to differentiate between the G0, G1 and G2/S/M phases. After following the previously mentioned protocol for extracellular staining, cells were fixed using 4% Roti-Histofix for 20 min at 4°C. Cells were washed one-time using 1X BD perm/wash buffer, then incubated for 15 minutes with perm/wash buffer at 4°C. Cells were stained with Ki67 antibody in perm/wash buffer for 30 minutes at 4°C. Afterwards, cells were washed once with FACS buffer and resuspended in 100 µL FACS buffer containing 7AAD (1:100) then analysed with flow cytometry.

2.2.8 Gene expression analysis

2.2.8.1 RNA isolation from tissues

Total RNA was extracted from frozen bone marrow pellets. For each frozen pellet, 800 µL QIAzol lysis reagent (Qiagen, Netherlands) and Qiagen tissue lyser steel beads were added. Samples were homogenised using TissueLyser for 2 minutes at a frequency of 50 Hz. Afterwards, the lysate was transferred to a fresh tube and 120 µL chloroform was added.

Samples were vortexed for 30 seconds to mix both solutions. To separate the aqueous phase from the organic phase, samples were centrifuged at 12000xg for 15 minutes at 4 °C. Samples were separated into three distinct layers, and 400 µL of the aqueous was transferred to a new tube. RNA isolation was performed using the peqGOLD total RNA kit from Peqlab (VWR). All centrifugation steps were done at room temperature and a speed of 10000xg unless otherwise indicated. The aqueous phase was transferred to the RNA homogenizer column and centrifuged for 1 minute. An equal volume of 70% ethanol was added to the flow through and mixed 10 times by pipetting. Afterwards, 700 µL of the mix was added to the RNA mini-column and centrifuged for 1 minute. Columns were washed with 250 µL RNA wash buffer. To remove genomic DNA, columns were treated with 75 µL DNAse mixture (1.5 µL DNAse and 73.5 µL DNAse buffer) (DNase I Digest Kit). Columns were incubated for 15 minutes at room temperature. Afterwards, 250 µL RNA buffer was added to the columns, incubated for 2 minutes then centrifuged at 10000xg for 1 minute. This washing step was repeated two times. For the final elution step, 20-30 µL nuclease-free water was used. A Nanodrop 100 instrument was used to measure RNA concentration and purity.

2.2.8.2 RNA isolation from sorted cells

Single cell RNA purification kit (NORGEN) was used to isolate total RNA from sorted cells according to the manufacturer protocol. In brief, cells of interest were already sorted in 100 µL buffer RL (component of the used kit). Cells were mixed by pipetting and an equal volume of 70% ethanol was added to the cell lysate. Lysate was filtered through the RNA binding column by centrifugation for 1 min at 3500xg. The column was washed three times with 400 µL Wash Solution A and centrifuge for 1 min at 14000xg. Lastly, the column was dried by centrifugation for 2 minutes at 14000xg and RNA was eluted in 10 µL of elution solution A.

2.2.8.3 Reverse transcription

The primeScript RT reagent kit (TaKaRa) was used to generate complementary DNA (cDNA). Reaction components and volumes are indicated below.

Reagents	**Volume**
5x PrimeScript buffer	4 µL
PrimeScript RT enzyme mix	1 µL
Oligo dt Primer (50 µM)	1 µL
Random 6-mers (100 µM)	4 µL
RNA sample	Input up to 2 µg (depend on RNA conc.)
RNase free water	Complete till 20 µL

A reverse transcription reaction was done in a thermal cycler according to the thermal profile indicated below. Afterwards, samples were diluted using RNase-free water to achieve a concentration of 5ng cDNA/µL.

Temperature	Time
37°C	15 minutes
85°C	5 seconds
4°C	∞

2.2.8.4 Quantitative polymerase chain reaction (qPCR)

Gene expression quantification was performed using TaqMan probes and QuantStudio 6 Pro Real-Time PCR system (ThermoFisher). TaqMan probes were ordered from Life technologies. Each reaction was performed in 20 µL total volume with 25ng cDNA as input, using GoTaq probe qPCR master mix (Promega). Reaction components and volumes are indicated below.

Reagent	Volume
2x Master mix	10 µL
Primer probe stock	0.5 µL
cDNA (5ng/µL)	5 µL
RNase free water	4.5 µL

No template control (NTC) and no reverse transcriptase control (NRT) reactions were included. Each gene was pipetted into duplicates in a semi skirted 96-well qPCR plate. Fast program thermal profile is indicated below.

Temperature	Time	
Step 1: 95 °C	2 minutes	
Step 2: 95 °C	20 seconds	X39 cycle
Step 3: 95 °C	1 seconds	
Step 4: 60°C	20 seconds	

The ΔΔCt method was used to calculate fold changes relative to a calibrator (control group), using the housekeeping gene Hprt or Gapdh. The following formula was used for calculations.

ΔCt=Ct (gene of interest)-Ct (housekeeping gene)

ΔΔCt=ΔCt (sample) - average ΔCt (calibrator)

Fold change=$2^{-\Delta\Delta Ct}$

2.2.9 *In vitro* treatment with CB1 ligands

To test the effect of CB1 receptor activation or antagonism on HSPCs *in vitro*, bone marrow cells were isolated from C57BL/6J male mice as described. Cells isolated from one femur were resuspended in 1mL StemSpan SFEM medium (STEMCELL) and distributed equally into 3 wells. AM281 was added at a concentration of 1µM. Cells were incubated at 37°C for 30 min, 4 hours or 8 hours, and the percentage of cell cycle stage distribution of LSK and LK cells was subsequently checked by flow cytometry as previously described.

2.2.10 Single-cell RNA sequencing sample and library preparation

Single-cell RNA sequencing (scRNA-seq) of the bone marrow collected from male 9 week old *Cnr1*$^{-/-}$ and *Cnr1*$^{+/+}$ littermates (3 mice per group) was performed. Bone marrow HSPCs were collected from femurs and tibias by centrifugation for 2 min at 10000xg. ACK lysis buffer was added to the cell pellet and cells were subsequently washed two times with FACS buffer. For each animal, 2x10^6 cells were labelled with cell multiplexing oligos (CMO; 3' CellPlex Kit Set A PN-1000261; 10x genomics) according to the user guide, 6 different CMO were used representing one CMO for each mouse. In brief, the cells were incubated for 5 mins at room temperature with CMO. Afterwards, cells were washed two times with PBS (1% BSA), stained with an antibody cocktail against Lin markers, cKit and Zombie Green viability dye and sorted as live/ lineage$^-$cKit$^+$ cells using FACSAria III.

To isolate bone marrow niche cells, flushed bones were cut into small pieces with scissors and enzymatically digested in digestion cocktail (DMEM with 10% FBS, 10 mg of Collagenase IV and 20 U DNAse) in a shaking thermal block for 1 h at 37°C. The cell suspension was subsequently filtered through 70µm strainers. Cell multiplexing oligos were used as described above to label 2x10^6 cells per mouse, 6 different CMO were used representing one CMO for each mouse. Cells were washed two times with PBS containing 1% BSA, stained with an antibody cocktail against Lin markers, CD45 and Zombie Green viability dye and sorted as live/ lineage$^-$CD45$^-$ cells using FACSAria III.

The number of sorted HSPCs (Lin$^-$cKit$^{+/-}$) from each animal was 341–467*10^3 and stromal cells 49–128*10^3. All cells from WT animals were mixed together with 35000 HSPCs and 1650 stromal cells from each animals. Two cell mixes were used to generate sequencing libraries, each mix represent a genotype.

Chromium next GEM single cell 3' HT reagent kits v3.1 (Dual Index) with feature barcode technology for cell multiplexing were used to generate the libraries according to the 10x user guide (CG000419-Rev D). Chromium X device was used to generate the Gel Beads-in-emulsion (GEM). Library sequencing parameters were according to the same user guide. S2

flow cell (20028316, Illumina) was used to sequence the libraries on Novaseq 6000 (20012850, Illumina) with a sequencing depth of at least $25*10^3$ reads per cell.

2.2.11 scRNA-seq data pre-processing and clustering

Using the Ubuntu 20.04.3 LTS operating system, Cellranger multi (version 7.1.0) was used for alignment with refdata-gex-mm10-2020-A, demultiplex the 3‘ GEX with cell multiplexing according to CMO tags, filtering, barcode counting, and UMI counting. Cellranger aggr (version 7.1.0) was used to integrate separate multiple samples [131]. In R version 4.3.0 (2023-04-21) environment, Seurat (version 4.9.9.9044) [132] was used for filtering feature-barcodes-matrix with following exclusion criteria: genes expressed in less than 3 cells, cells with less than 200 or more than 7000 genes, and mitochondrial content of more than 25%. The SCTransform method was used to normalize the matrix, and data scaling was also done by Seurat. PCA, tSNE and UMAP methods were used to reduce dimensions and visualize cell profiles.

2.2.12 Annotation and post analysis

For annotation of clusters, published annotated data sets (accession numbers GSE106973 and GSE107727) were used as a reference [133]. Integration of individual samples was performed using a standard Seurat workflow by identifying integration anchors followed by using these anchors to integrate the two datasets with the “IntegrateData” function. For cells isolated from digested bones, annotation was performed according to the expression of known markers for the whole stromal cells fraction (*Cxcl12*, *LepR*, *Cdh5*, and *Pecam1*). A similar strategy was used to sub cluster the stromal cell fraction based on the expression of the following markers (*Cxcl12*, *LepR*, *Cdh5*, *Pecam1*, *Alpl* and *Spp1*). The “FindMarkers” function (Seurat package) was used to find differentially expressed genes (DEGs) with more than 0.25 Log_2FC between the two groups.

The Gene Ontology (GO) online database was used to perform enrichment analysis for DEGs. Analysis was performed with significant DEGs of minimum ± Log_2FC. Significant pathways (p-value less than 0.05 and false discovery rate (FDR) below 0.05) and relevant to the project were presented in the results. The ChIP-X Enrichment Analysis Version 3 (CHEA3) web server was used to predict the top 15 transcription factors (TFs) regulating significant DEGs. Gene Set Enrichment Analysis (GSEA) was performed using GSEA software (version 4.3.2), which was tailored for the Windows operating system. The analysis utilized different gene sets sourced from mouse collections. Pathways were considered significant according to predefined criteria, encompassing a normalized enrichment score below -1 or above 1, a false discovery rate below 0.25, and a nominal p-value less than 0.05.

2.2.13 Statistical analyses

Statistical analyses were conducted using Graphpad Prism version 10.2.3 (except for the RNA-seq and ATAC-seq data analysis, which was performed as described above). In all graphs data are presented as mean ± standard error of the mean (s.e.m) or as box plots showing medians with 25th and 75th percentiles and whiskers indicating the range. Normality and outliers test was done by using Shapiro-Wilk normality test and ROUT method, respectively. To test for significance between two data sets, student's unpaired t-test was used for data showing a Gaussian distribution, while the Mann-Whitney U test was used when data were not normally distributed. To compare more than two groups, one way or two way analysis of variance (ANOVA) was used. Correction for multiple comparison was done using Tukey or Bonferroni post-hoc test. P-values less than 0.05 were considered statistically significant.

3 Results

3.1 Effect of *Cnr1* deficiency on homeostatic hematopoiesis

To study the role of CB1 in hematopoiesis under homeostatic conditions, we used global *Cnr1* deficient mice on C57BL/6J background (*Cnr1*$^{-/-}$) and corresponding WT controls. Mice were 8 week old and sex-matched. We first analyzed the mature myeloid cells in blood and femurs using flow cytometry. In male mice, *Cnr1* deficiency was associated with significantly lower blood monocyte counts, while bone marrow monocytes were not affected. Neutrophil counts were similar between both genotypes in blood and femur (Figure 10. A, B). In female mice, *Cnr1* deficiency was associated with significantly higher blood neutrophils, while bone marrow neutrophils were not affected. Monocyte counts were similar between both groups in blood and femur (Figure 10. C, D). According to these results, deficiency of *Cnr1* had only minor effect on the mature hematopoietic system in global *Cnr1* KO mice in homeostatic condition.

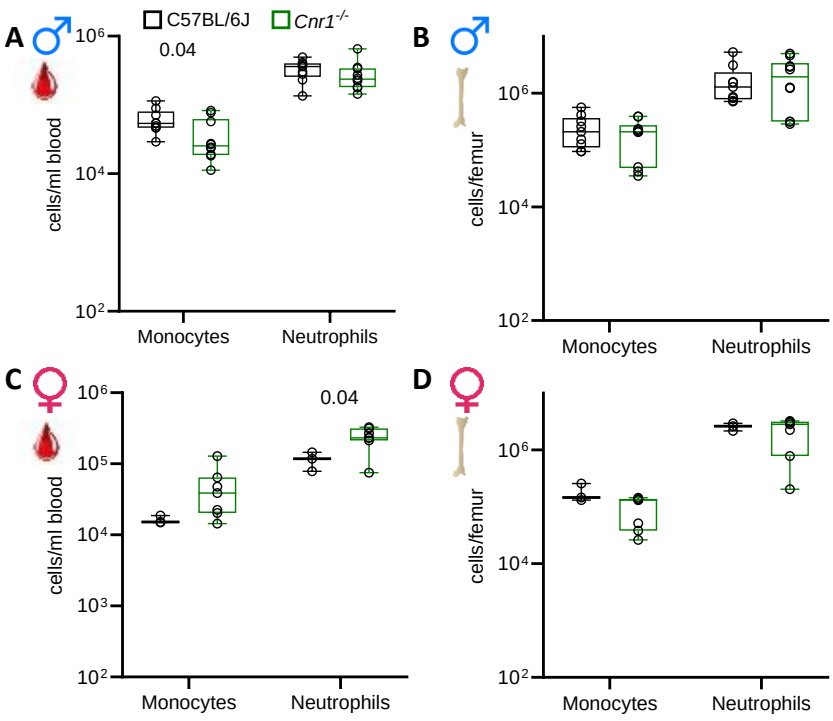

Figure 10. Circulating monocytes and neutrophils in sex-matched *Cnr1*$^{-/-}$ and WT mice. (**A, B**) Flow cytometric quantification of monocytes and neutrophils in blood (**A**) and bone marrow (**B**) of male mice. (**C, D**) Flow cytometric quantification of monocytes and neutrophils in blood (**C**) and bone marrow (**D**) of female mice. Each dot represents one mouse. Box plots show medians with 25th and 75th percentiles as boundaries and whiskers indicate the range. Shapiro-Wilk normality test and ROUT method for outlier testing was performed. Student's unpaired t-test was used for graph **C** while the Mann-Whitney U test was used for graph **A**, **B**, **D**. The exact p-values are shown in the graph.

Next, we compared the hematopoietic stem and progenitor populations in the bone marrow by flow cytometry (Figure 11. A). In male mice, *Cnr1* global deficiency tended to increase the LSK population in the bone marrow compared to WT mice (Figure 11. B), with no significant difference in any of the other HSPC populations (Figure 11. C-E). In female mice, no difference between the two groups in any of the cell types (Figure 11. B, C, F, G).

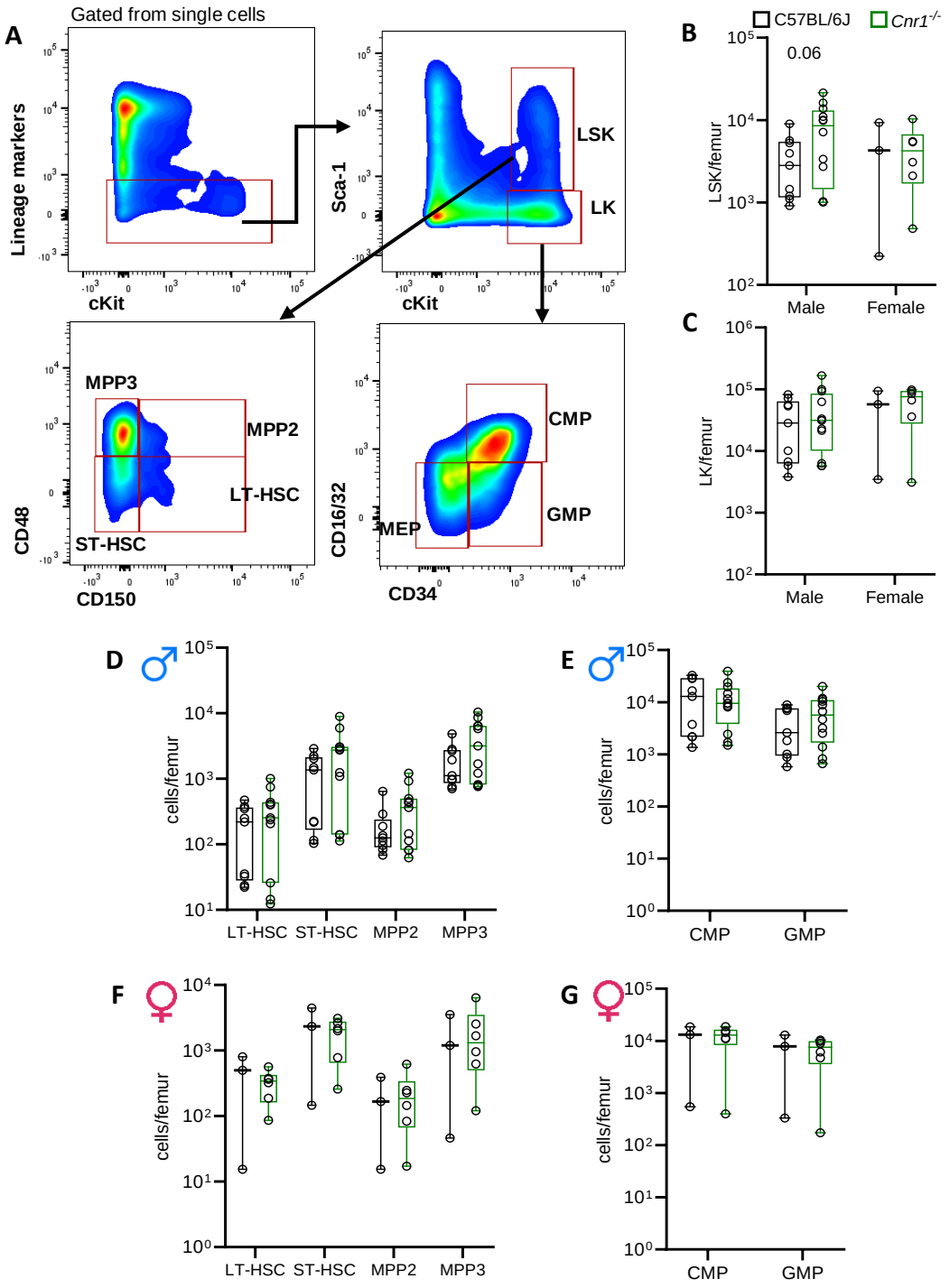

Figure 11. Effect of *Cnr1* deficiency on hematopoietic bone marrow progenitors. (**A**) Gating strategy used to identify primitive progenitors ($Lin^-Sca\text{-}1^+cKit^+$; LSK) and committed progenitors (Lin^-cKit^+; LK). LSKs were further differentiated with SLAM factors CD150 and CD48, while LKs were further differentiated with CD16/32 and CD34, as shown in panel A. All analyses were performed on 8 week-old mice and data were calculated per femur. (**B**, **C**) LSKs and LKs in male and female mice. (**D**, **E**) HSPC subsets in male mice or (**F**, **G**) in female mice, respectively. Each dot represents one mouse. Box plots show medians with 25th and 75th percentiles as boundaries and whiskers indicate the range. Shapiro-Wilk normality test and ROUT method for outlier testing was performed. Student's unpaired t-test was used for graphs **B**, **E**, **F**, **G**, while the Mann-Whitney U test was used for graphs **C**, **D**. The exact p-values are shown in the graph.

We next assessed the number of HSPCs in the blood of WT and *Cnr1* KO mice using flow cytometry and CFU assay (Figure 12). *Cnr1* deficiency in male mice resulted in a significantly increased number of circulating LSKs in the blood compared to the WT group, while there was no difference in LK numbers (Figure 12. A, B). There was no difference in the number of circulating LSKs or LKs in female mice (Figure 12. A, B). Despite comparable numbers of progenitor counts, blood cells from *Cnr1*$^{-/-}$ female mice formed fewer colonies in the CFU assay compared to the corresponding WT group. This raises the question if *Cnr1* deficiency affects the functionality of circulating HSPCs rather than their number in female mice (Figure 12. C, D).

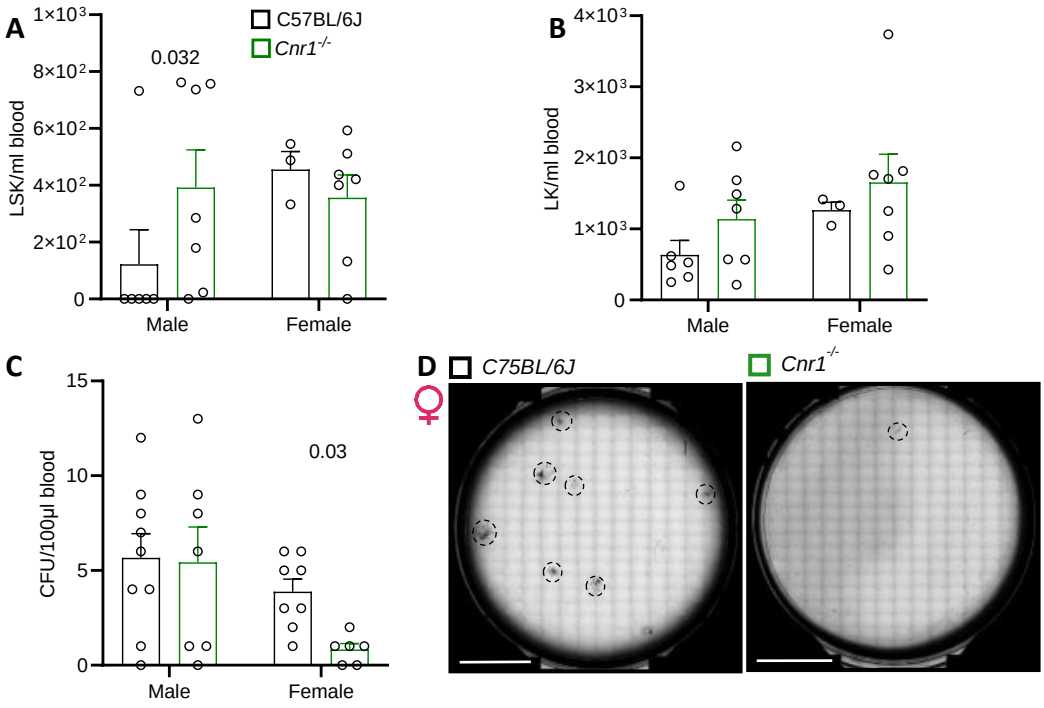

Figure 12. Effect of *Cnr1* deficiency on circulating hematopoietic progenitor cells. (**A**, **B**) Flow cytometric quantification of circulating LSKs and LKs in male and female mice of *Cnr1*$^{-/-}$ and WT mice. (**C**) Number of colonies formed per 100µl of blood. (**D**) Representative picture of a 35 mm culture plate with colonies marked by a circle, scale bar = 1cm. Each dot represents one mouse and all data are expressed as mean + s.e.m. Shapiro-Wilk normality test and ROUT method for outlier testing was performed. Student's unpaired t-test was used for graph **C** while the Mann-Whitney U test was used for graph **A**, **B**. The exact p-values are shown in the graph.

3.2 Effect of *Cnr1* deficiency on hematopoiesis in atherosclerosis-prone mice under normal diet condition

Our results so far indicate that *Cnr1* deficiency has minor effects on mature hematopoietic and HSPCs in homeostatic condition. The next aim was to study the impact of *Cnr1* deficiency in atherosclerosis-prone *Apoe*$^{-/-}$ mice with elevated plasma cholesterol levels due to impaired hepatic clearance [123], starting with a baseline characterisation under normal diet. For this purpose, *Apoe*$^{-/-}$ and *Apoe*$^{-/-}$*Cnr1*$^{-/-}$ mice at the age of 8 weeks were used. Male *Apoe*$^{-/-}$*Cnr1*$^{-/-}$ mice showed a moderate, non-significant increase in the number of circulating monocytes and

significantly reduced circulating neutrophils, while there was no difference in the number of bone marrow monocytes and neutrophils (Figure 13. A, B). In female mice, there was a significant increase in the bone marrow monocyte counts, while there was no difference in neutrophils and circulating cells in the blood compared to the sex-matched *Apoe*$^{-/-}$ control group (Figure 13. C, D).

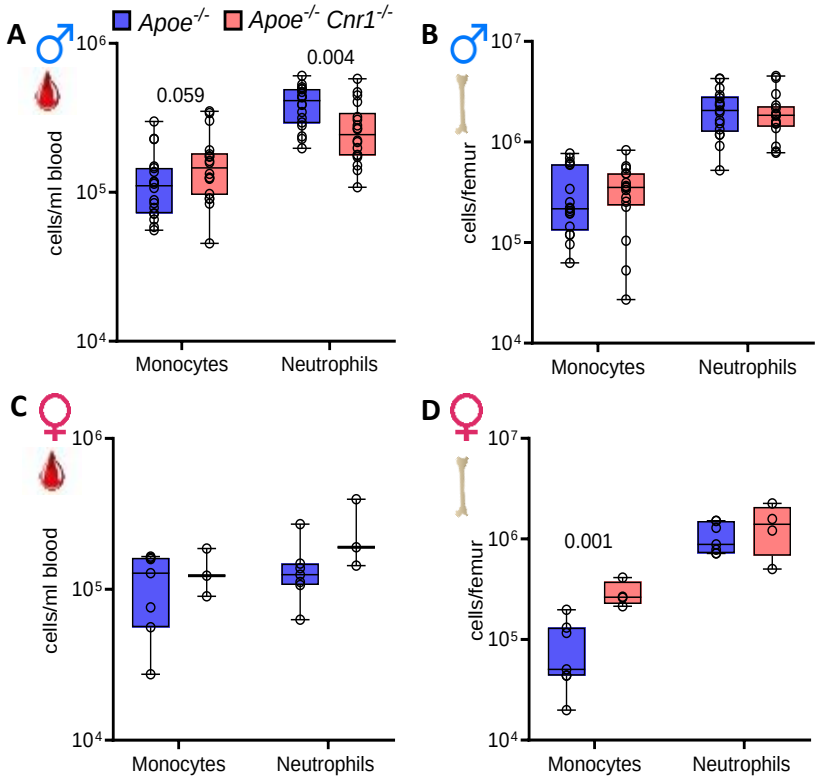

Figure 13. Circulating and femoral monocyte and neutrophil counts in sex-matched *Apoe*$^{-/-}$*Cnr1*$^{-/-}$ and *Apoe*$^{-/-}$ mice. (**A**, **B**) Flow cytometric quantification of monocytes and neutrophils in blood (**A**) and bone marrow (**B**) of male mice. (**C**, **D**) Flow cytometric quantification of monocytes and neutrophils in blood (**C**) and bone marrow (**D**) of female mice. Each dot represents one mouse. Box plots show medians with 25th and 75th percentiles as boundaries and whiskers indicate the range. Shapiro-Wilk normality test and ROUT method for outlier testing was performed. Student's unpaired t-test was used for graph **C**, **D** while the Mann-Whitney U test was used for graph **A**, **B**. The exact p-values are shown in the graph.

In addition, there was no difference in the numbers of LSKs or LKs between *Apoe*$^{-/-}$*Cnr1*$^{-/-}$ mice and *Apoe*$^{-/-}$ in the two sex groups (Figure 14. A, B). However, the more detailed analysis of the progenitor subpopulations (Figure 14. C - F) revealed a significant increase in CMPs in *Apoe*$^{-/-}$*Cnr1*$^{-/-}$ male mice (Figure 14. D). In female mice, there was a reduction in LT-HSCs compared to the *Apoe*$^{-/-}$ control group (Figure 14 E) , while there was no difference in committed progenitors (Figure 14. F).

To clarify potential effects of *Cnr1* deficiency on cell viability, apoptosis and cell cycle phases, bone marrow and blood cells were stained with 7AAD, Annexin V and Ki67. In the bone marrow, no significant differences in viability or cell cycle distribution were found between *Apoe*$^{-/-}$*Cnr1*$^{-/-}$ and *Apoe*$^{-/-}$ mice in either sex group (Figure 15). Similar to *Cnr1* global KO mice without *Apoe*$^{-/-}$ background, male *Apoe*$^{-/-}$*Cnr1*$^{-/-}$ mice showed a tendency for increased numbers of circulating LKs compared to *Apoe*$^{-/-}$ controls, although not significant (Figure 16. B). Consistent with this, blood cells from *Apoe*$^{-/-}$*Cnr1*$^{-/-}$ formed more colonies than the control

group (Figure 16. C, D). Female mice did not show any significant differences in the number of circulating LSKs or LKs or colonies formed (Figure 16. A-C).

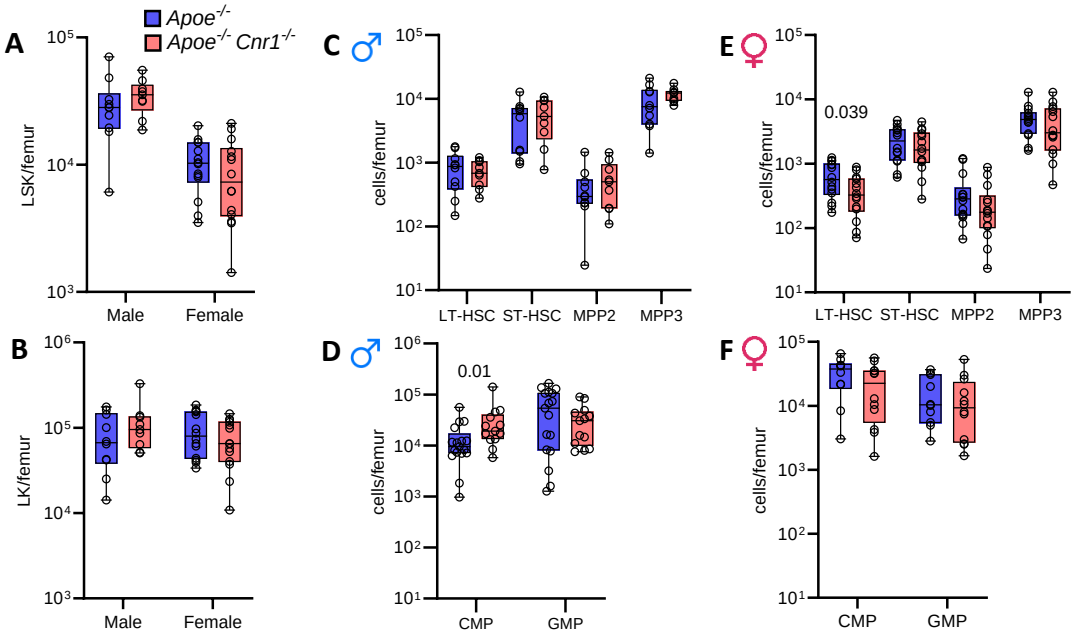

Figure 14. Femoral hematopoietic progenitors in sex-matched *Apoe*$^{-/-}$*Cnr1*$^{-/-}$ and *Apoe*$^{-/-}$ mice. (**A**-**F**) Flow cytometric quantification of HSPCs in femurs of *Apoe*$^{-/-}$ and *Apoe*$^{-/-}$*Cnr1*$^{-/-}$ mice. (**A**, **B**) Quantification of LSKs and LKs. (**C**-**F**) Primitive hematopoietic stem cells (LSK) and committed progenitors (LK) in male (**C**, **D**) and female mice (**E**, **F**). Each dot represents a mouse. Box plots show medians with 25th and 75th percentiles as boundaries and whiskers indicate the range. Shapiro-Wilk normality test and ROUT method for outlier testing was performed. Student's unpaired t-test was used for graph **A** while the Mann-Whitney U test was used for graph **B**-**F**. The exact p-values are shown in the graph.

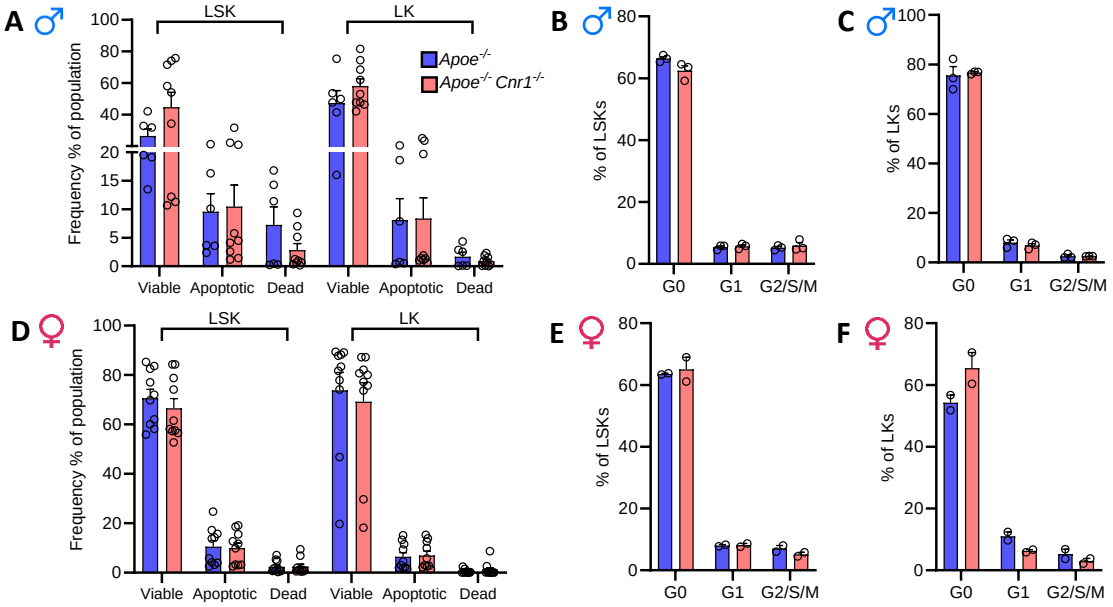

Figure 15. Viability and cell cycle distribution of femoral LSKs and LKs in sex-matched *Apoe*$^{-/-}$*Cnr1*$^{-/-}$ and *Apoe*$^{-/-}$ mice. (**A**-**F**) Frequency of viable, dead and apoptotic cells and frequency of cell cycle distribution (G0, G1, or G2/S/M phase) in male mice (**A**-**C**) and female mice (**D**-**F**). Each dot represents one mouse and all data are expressed as mean + s.e.m. Shapiro-Wilk normality test and

ROUT method for outlier testing was performed. Student's unpaired t-test was used for graph **C** while the Mann-Whitney U test was used for graph **A**, **B**, **D**. Statistical analysis was not applied to data shown in **F**, **E** due to insufficient sample size. No significant differences.

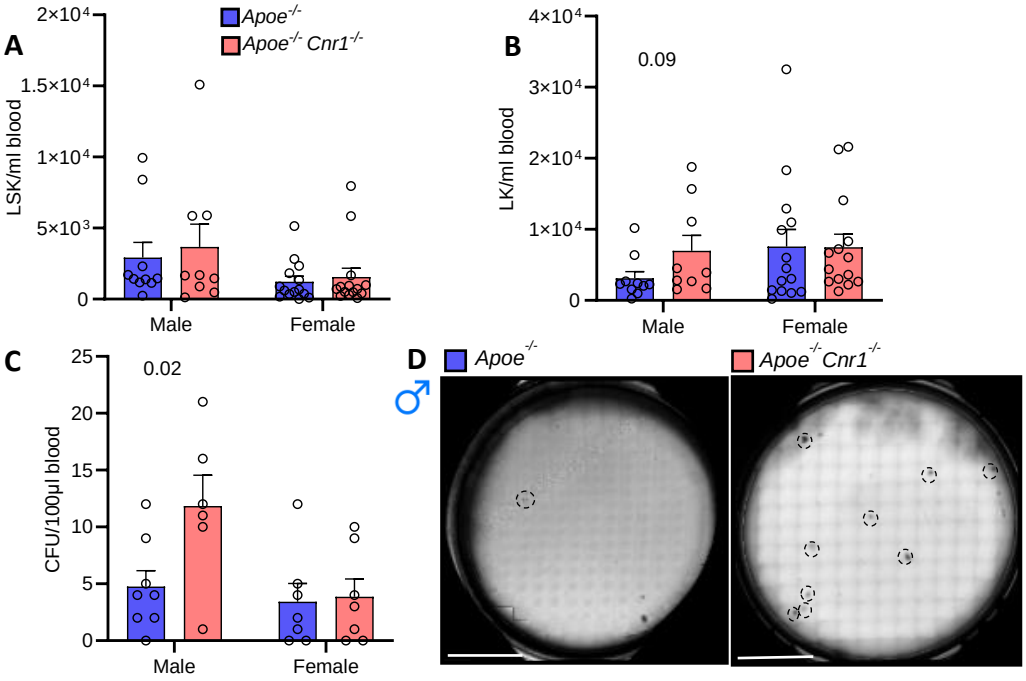

Figure 16. Circulating hematopoietic progenitors in sex-matched *Apoe*$^{-/-}$*Cnr1*$^{-/-}$ and *Apoe*$^{-/-}$ mice. (**A**, **B**) Flow cytometric quantification of circulating LSKs and LKs. (**C**) Quantification of colonies per 100µl of blood. (**D**) Representative picture of a 35 mm culture plate with colonies marked by a circle, scale bar = 1cm. Each dot represents one mouse and all data are expressed as mean + s.e.m. Shapiro-Wilk normality test and ROUT method for outlier testing was performed. Student's unpaired t-test was used for graph **C** while the Mann-Whitney U test was used for graph **A**, **B**. The exact p-values are shown in the graph.

3.3 Effect of *Cnr1* deficiency on bone marrow niche factors in atherosclerosis-prone mice under normal diet

Two of the most important stromal niche factors that regulate HSPCs are SCF and CXCL12. *Apoe*$^{-/-}$*Cnr1*$^{-/-}$ male mice had significantly lower bone marrow SCF levels compared to *Apoe*$^{-/-}$ controls, while no genotype-dependent difference was observed in female mice (Figure 17). Next, we used qPCR to measure the gene expression of chemokine receptors and adhesion molecules, in particular C-X-C chemokine receptor type 4 (*Cxcr4*) which binds CXCL12, intercellular adhesion molecule 1 (*Icam1*), and vascular cell adhesion molecule 1 (*Vcam1;* Figure 18. A, C). We also measured the gene expression levels of the leptin receptor (*Lepr*) as a marker for MSCs and adiponectin (*Adipoq*) as a marker for adipocytes (Figure 18. B, D). In male mice, *Cnr1* deficiency significantly increased the gene expression level of *Cxcr4* compared to *Apoe*$^{-/-}$ controls whereas the decrease in *Icam1* did not reach significance (Figure 18. A). No difference in *Adipoq* and *Lepr* expression was observed in males (Figure 18. B). In female mice, *Cnr1* deficiency tended to decrease the expression of *Icam1, Adipoq* and *Lepr* compared to the control group (Figure 18. C, D). To confirm the increase in CXCR4 surface

receptor expression on HSPCs cells in male mice, we used a fluorescently labelled recombinant mouse SDF-1α as a readout for detecting the receptor through functional ligand binding (CXCL12-AF647; Figure 19).

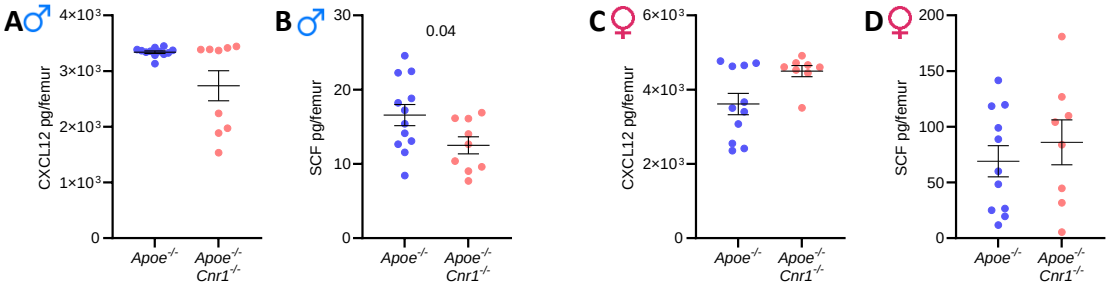

Figure 17. CXCL12 and SCF bone marrow levels in sex-matched *Apoe*$^{-/-}$*Cnr1*$^{-/-}$ and *Apoe*$^{-/-}$ mice under normal diet condition. ELISA quantification of CXCL12 (**A**, **C**) and SCF (**B**, **D**) in bone marrow lavage of 8-weeks-old mice fed with normal chow diet. Each dot represents one mouse and all data are expressed as mean + s.e.m. Shapiro-Wilk normality test and ROUT method for outlier testing was performed. Student's unpaired t-test was used for graph **B**, **D** while the Mann-Whitney U test was used for graph **A**, **C**. The exact p-values are shown in the graph.

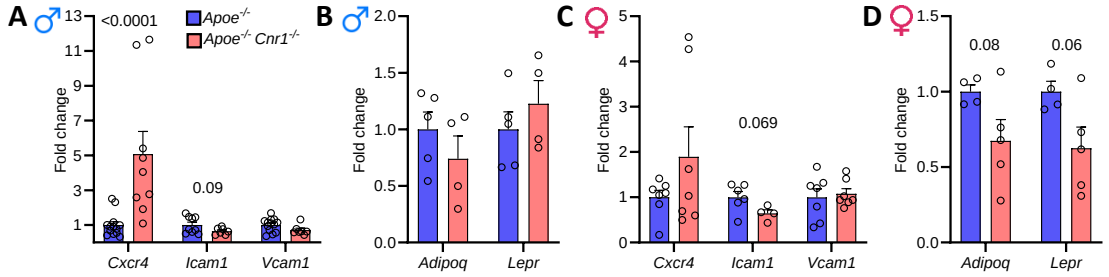

Figure 18. Gene expression of key bone marrow niche factors of sex-matched *Apoe*$^{-/-}$ and *Apoe*$^{-/-}$*Cnr1*$^{-/-}$ mice. Gene expression in bone marrow cells collected from (**A**, **B**) male or (**C**, **D**) female 8 week old mice fed with normal chow diet. Each dot represents one mouse and all data are expressed as mean + s.e.m. Shapiro-Wilk normality test and ROUT method for outlier testing was performed. Student's unpaired t-test was used for graph **B**, **C**, **D** while the Mann-Whitney U test was used for graph **A**. The exact p-values are shown in the graph.

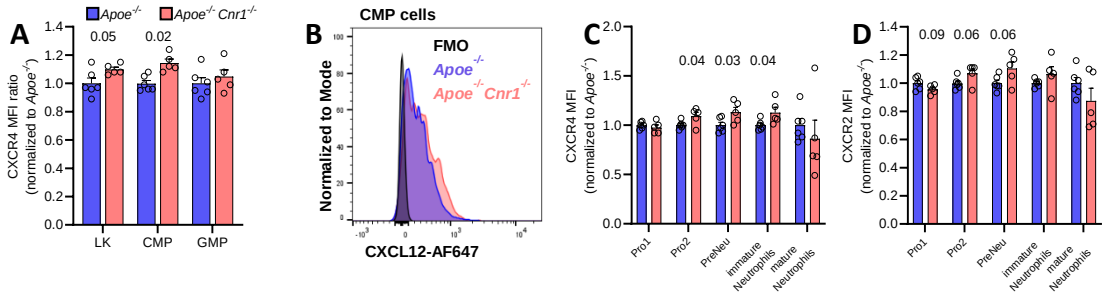

Figure 19. CXCR4 and CXCR2 expression levels on hematopoietic progenitors in male *Apoe*$^{-/-}$ and *Apoe*$^{-/-}$*Cnr1*$^{-/-}$ mice. Bone marrow cell from femurs of 8 week old male mice fed with normal chow diet were used for analysis. (**A**) Relative CXCR4 mean fluorescence intensity (MFI) on LK cells, common myeloid progenitors (CMP) and granulocyte-macrophage progenitor (GMP) normalized to the average of the *Apoe*$^{-/-}$ controls. (**B**) Representative histogram of flow cytometric quantification of CXCR4 expression on CMPs. FMO is the fluorescent minus one control, which represents the entire antibody panel without the CXCL12-AF647. (**C**, **D**) CXCR4 and CXCR2 MFI on neutrophil progenitors at different developmental stages, with Pro1 representing the most primitive neutrophil progenitor. Shapiro-Wilk normality test and ROUT method for outlier testing was performed. Student's unpaired t-test was used for graph **A**, **C** while the Mann-Whitney U test was used for graph **D**. The exact p-values are shown in the graph.

Cnr1 deficiency was associated with a significant increase in CXCR4 surface levels on LKs and CMPs (Figure 19. A). Neutrophil progenitors (Pro2, PreNeu and immature) also had significantly increased protein levels of CXCR4 compared to the control group, and also tended to have increased CXCR2 expression (Figure 19. C, D).

3.4 Effect of *Cnr1* deficiency in atherosclerosis-prone mice on bone marrow neuronal innervation under normal diet

The central nervous system is connected to the bone marrow and regulates hematopoiesis through neuronal signals. The bone marrow is innervated by sympathetic nerves that express tyrosine hydroxylase (TH), but also nociceptive nerves which are responsible for the sensation of pain and express calcitonin gene-related peptide (CGRP).

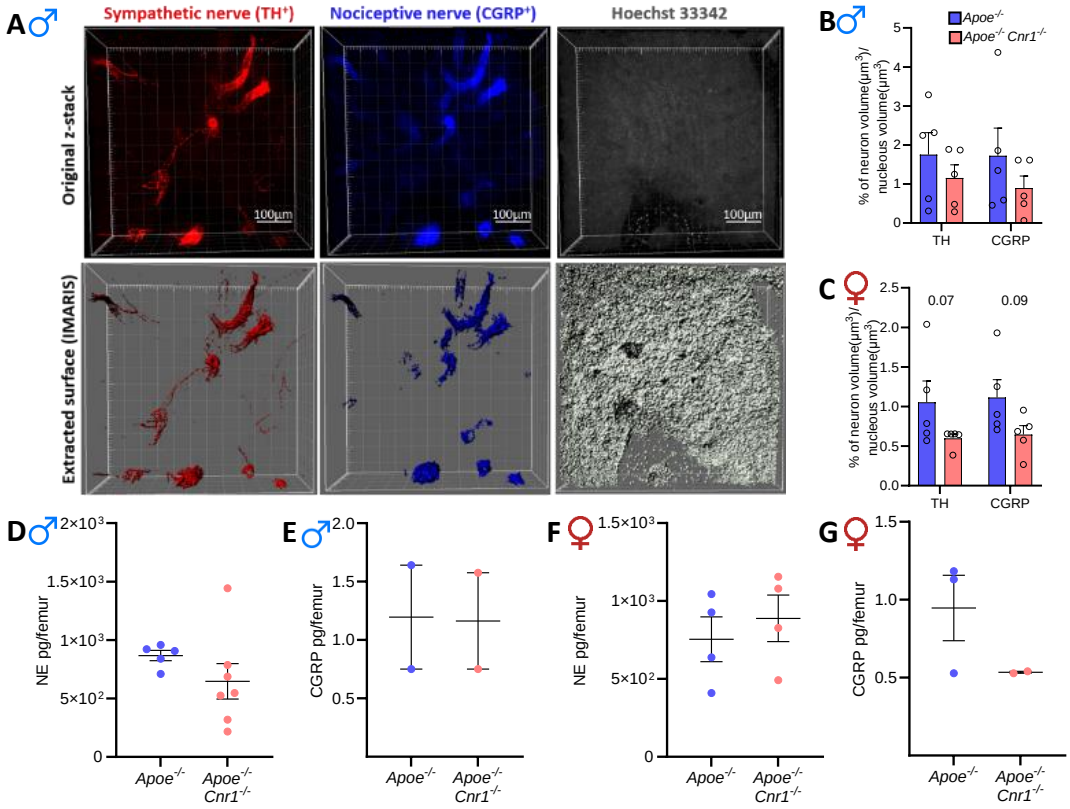

Figure 20. Quantification of TH$^+$ and CGRP$^+$ neuronal innervation in bone marrow of 8 week old sex-matched *Apoe*$^{-/-}$ and *Apoe*$^{-/-}$*Cnr1*$^{-/-}$ mice. (**A**) Representative images of z-stack sections of whole mount femurs stained against TH and CGRP. (**B**, **C**) Quantification of TH$^+$ or CGRP$^+$ nerve fibres showing the percentage of neuron volume corrected according to the volume of the whole z stack represented by nuclei volume. Each dot represents one femur from one animal and each dot is the sum of 7 z stacks covering different areas of the femur. (**D**-**G**) ELISA quantification of norepinephrine (NE) and calcitonin gene-related peptide (CGRP) in bone marrow lavage. Each dot represents one mouse and all data are expressed as mean + s.e.m. Shapiro-Wilk normality test and ROUT method for outlier testing was performed. Student's unpaired t-test was used for all graphs. The exact p-values are shown in the graph. Statistical analysis was not applied to data shown in **E**, **G** due to insufficient sample size.

The immunofluorescence analysis of the bone marrow did not reveal significant differences in neuronal densities between *Apoe*$^{-/-}$ and *Apoe*$^{-/-}$*Cnr1*$^{-/-}$ male and female mice, possibly due to the high variability of the data points (Figure 20. B, C). The analysis of neurotransmitter levels

in the bone marrow lavage did not reveal any difference in NE and CGRP levels between the genotypes. However, the small sample size and variability render these results inconclusive (Figure 20. D-G).

3.5 Effect of *Cnr1* deficiency on atherosclerosis and circulating myeloid cells under atherogenic diet

To subsequently investigate the impact of hypercholesterolemia on hematopoiesis, circulating leukocyte counts and atherosclerotic plaque development, *Apoe*$^{-/-}$*Cnr1*$^{-/-}$ and *Apoe*$^{-/-}$ mice were fed with WD for 4 or 16 weeks (Figure 21. A). After 4 weeks, *Cnr1* deficiency in male mice was associated with significant increase in the plaque size compared to the *Apoe*$^{-/-}$ control group (Figure 21. B, C). After 16 weeks, female mice with *Cnr1* deficiency had significantly larger plaques compared to the sex-matched *Apoe*$^{-/-}$ control group, while the difference in males was no longer significant (Figure 21. B, D).

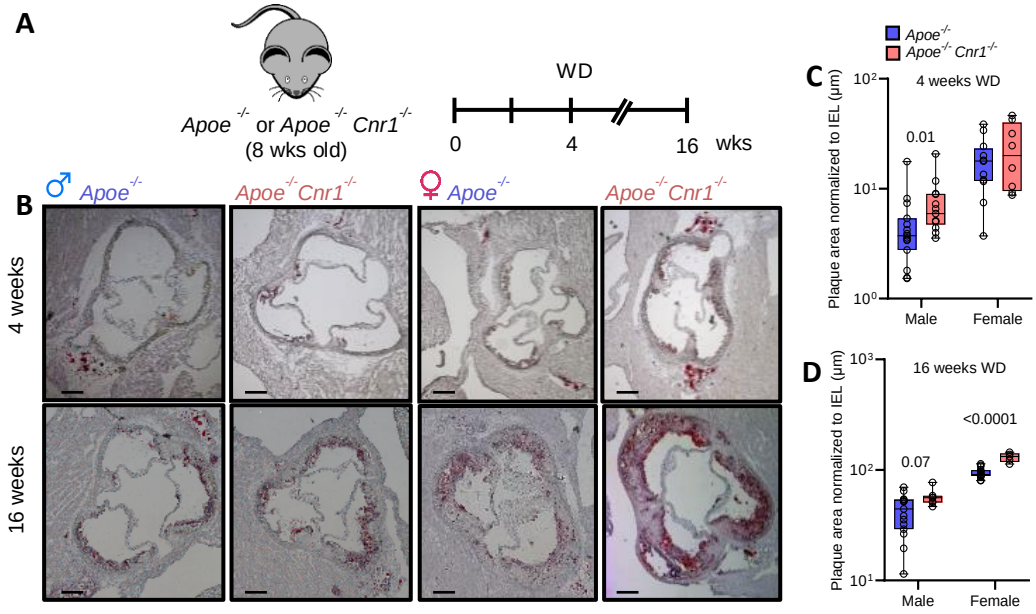

Figure 21. Atherosclerosis development in sex-matched *Apoe*$^{-/-}$*Cnr1*$^{-/-}$ and *Apoe*$^{-/-}$ mice. (**A**) Experimental design. (**B**) Representative pictures of aortic root sections stained with oil red O to quantify the plaque area. (**C**, **D**) Quantification of the lesion area normalized to the internal elastic lamina (IEL) after 4 and 16 weeks of WD. Scale bar = 200µm. Each dot represents one mouse. Box plots show medians with 25th and 75th percentiles as boundaries and whiskers indicate the range. Shapiro-Wilk normality test and ROUT method for outlier testing was performed. Student's unpaired t-test was used for graph **D** while the Mann-Whitney U test was used for graph **C**. The exact p-values are shown in the graph.

Male *Apoe*$^{-/-}$*Cnr1*$^{-/-}$ developed monocytosis and significant increase in circulating neutrophils after 16 weeks of the WD (Figure 22. A, B) while in the bone marrow, there was no difference in monocyte and neutrophil counts (Figure 22. C, D). In male spleens, a significant increase in monocyte counts after 4 weeks of WD was observed (Figure 22. E, F). Female mice developed blood monocytosis at an earlier time point (4 weeks WD), while there was no difference in

blood neutrophil counts at any of the time points (Figure 22. A, B). Monocyte numbers in bone marrow and spleen of females were significantly increased after 16 weeks (Figure 22. C, E), while no differences in femoral and splenic neutrophil counts were observed (Figure 22. D, F).

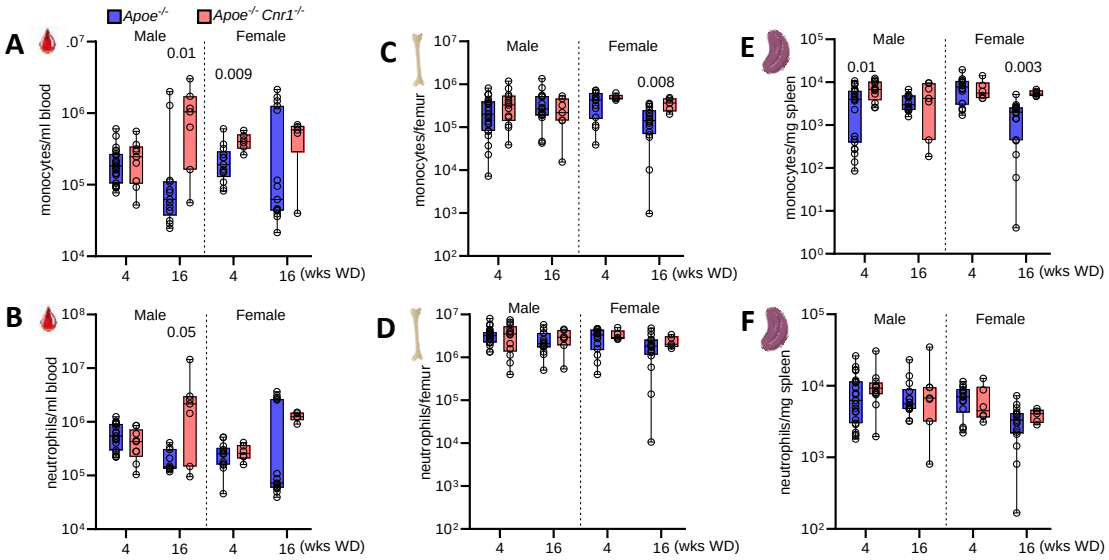

Figure 22. Blood and lymphoid organ myeloid cell counts in sex-matched *Apoe*$^{-/-}$*Cnr1*$^{-/-}$ and *Apoe*$^{-/-}$ mice under atherogenic diet. Flow cytometric quantification of monocytes and neutrophils in blood (**A**, **B**), bone marrow (**C**, **D**) and spleen (**E**, **F**) after 4 or 16 weeks of WD. Each dot represents one mouse. Box plots show medians with 25th and 75th percentiles as boundaries and whiskers indicate the range. Shapiro-Wilk normality test and ROUT method for outlier testing was performed. Mann-Whitney U test was used for all graphs. The exact p-values are shown in the graph.

3.6 Effect of *Cnr1* deficiency on hematopoiesis under atherogenic diet

The increase in mature myeloid cells under atherogenic diet was associated with an increase in hematopoietic stem and progenitor cell numbers in the bone marrow (Figure 23). *Cnr1* deficiency in male mice on *Apoe*$^{-/-}$ background was associated with a significant increase in LKs and LSKs after 16 weeks of WD. In female mice, however, *Cnr1* deficiency did not affect LK and LSK cell counts (Figure 23. A, B). CMPs were lower in male *Apoe*$^{-/-}$*Cnr1*$^{-/-}$ mice after 4 weeks WD, while GMPs in *Apoe*$^{-/-}$*Cnr1*$^{-/-}$ were significantly higher after 16 weeks of WD. No significant differences were found in female mice (Figure 23. C, D).

In addition to affecting the number of mature and progenitor hematopoietic cells, *Cnr1* deficiency reduced the viability and increased the apoptosis rate of LSK and LK cells in male mice after 4 weeks of WD, while female mice did not show any difference (Figure 24. A-B).

3.7 Effect of *Cnr1* deficiency in atherosclerosis-prone mice on bone marrow niche factors under atherogenic diet

So far, our results showed that *Cnr1* deficiency in the *Apoe*$^{-/-}$ model disturbs the hematopoietic stem and progenitor system, and that the phenotype is characterized by an increase in monocytes and CMPs in the bone marrow. This increase in the number of CMPs was not associated with a change in cell cycle distribution or cell viability. For the bone marrow niche

factors, *Cnr1* deficiency reduced SCF levels only in male mice, while there was no change in female mice.

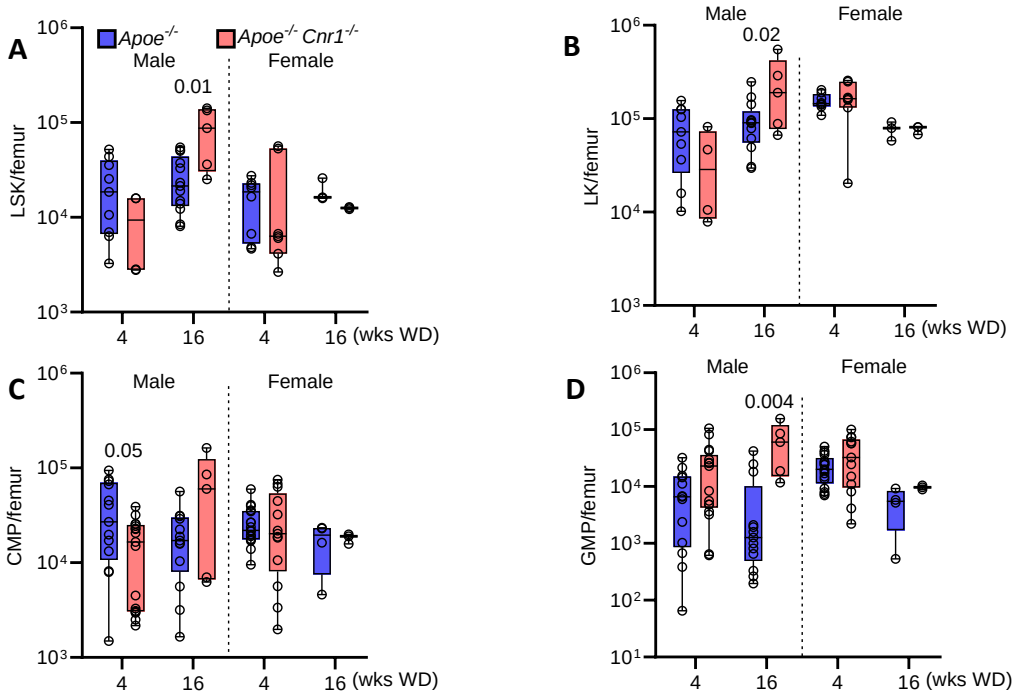

Figure 23. Hematopoietic stem and progenitor populations in sex-matched *Apoe*$^{-/-}$*Cnr1*$^{-/-}$ and *Apoe*$^{-/-}$ mice in hypercholesterolemia. (**A**-**D**) Flow cytometric quantification of LSKs (**A**), LK (**B**), CMPs (**C**), and GMPs (**D**). Each dot represents one mouse. Box plots show medians with 25th and 75th percentiles as boundaries and whiskers indicate the range. Shapiro-Wilk normality test and ROUT method for outlier testing was performed. Student's unpaired t-test was used for graph **B** while the Mann-Whitney U test was used for graph **A**, **C**, and **D**. The exact p-values are shown in the graph.

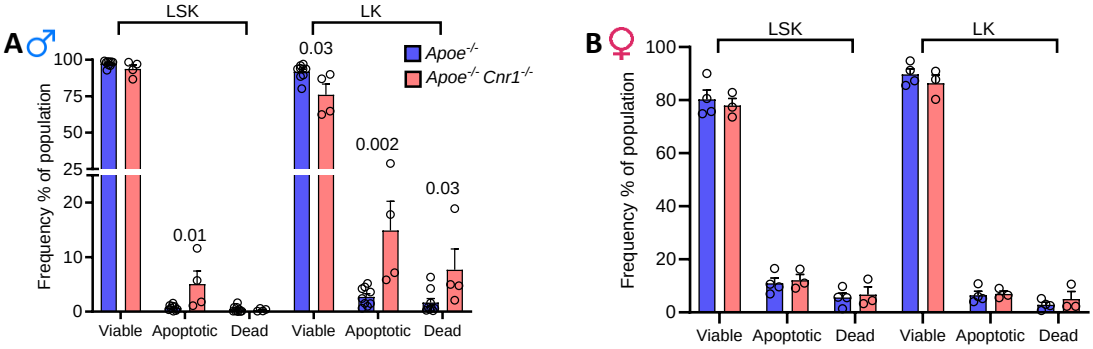

Figure 24. Cell viability of LSK and LK in sex-matched *Apoe*$^{-/-}$*Cnr1*$^{-/-}$ and *Apoe*$^{-/-}$ mice after 4 weeks WD. Relative frequencies of viable, dead and apoptotic cells among gated LSKs (**A**) and LKs (**B**) were assessed by flow cytometry. Each dot represents one mouse and all data are expressed as mean + s.e.m. Shapiro-Wilk normality test and ROUT method for outlier testing was performed. Mann-Whitney U test was used for all graphs. The exact p-values are shown in the graph.

Following up on the change in SCF under homeostatic conditions, we quantified protein levels of CXCL12 and SCF after 4 and 16 weeks of WD (Figure 25). No difference was detected in CXCL12 levels between the two genotypes (Figure 25. A, E). After 4 weeks of the WD, a lower SCF level was evident in male *Apoe*$^{-/-}$*Cnr1*$^{-/-}$ mice compared to control, comparable to the changes observed in normal diet condition (Figure 21. B), while the reduction in female *Apoe*$^{-}$

-/-Cnr1-/- mice was not significant (Figure 25. F). After 16 weeks, there was no significant difference, but the sample size was too small to be conclusive (Figure 25. C, D, E, F).

Cnr1 deficiency in male mice significantly increased *Icam-1* expression after 4 weeks WD (Figure 26. A), while there was no difference in *Lepr* or *Adipoq* (Figure 26. B). In female mice, there was a significant reduction in *Lepr* expression compared to the control (Figure 26. D), while other genes were comparable to the control group (Figure.26 C).

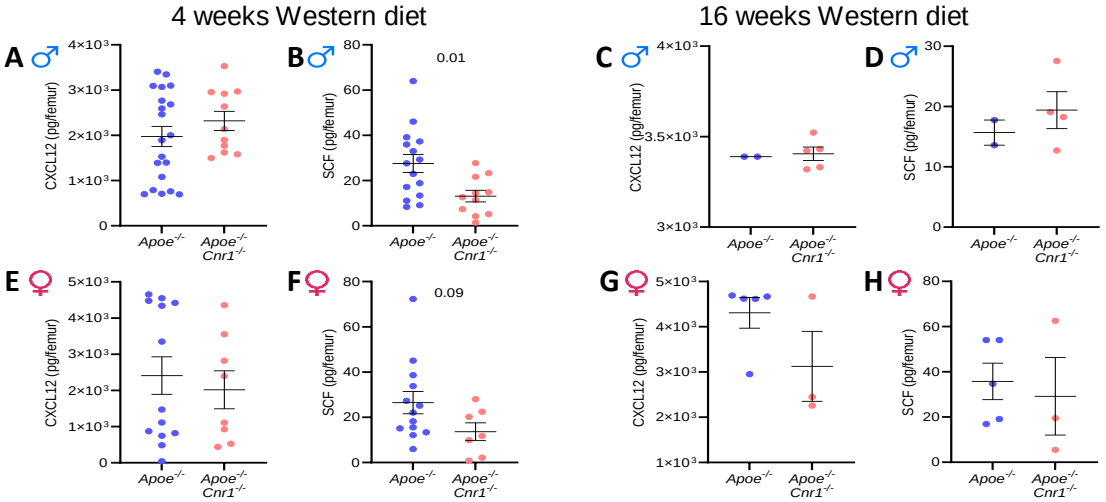

Figure 25. CXCL12 and SCF bone marrow concentrations in sex-matched *Apoe-/-* and *Apoe-/-Cnr1-/-* mice in hypercholesterolemia. ELISA quantification of CXCL12 and SCF concentration in male (**A**-**D**) and female (**E**-**H**) mice. Each dot represents one mouse and all data are expressed as mean + s.e.m. Shapiro-Wilk normality test and ROUT method for outlier testing was performed. Student's unpaired t-test was used for graph **B**, **F**, **H** while the Mann-Whitney U test was used for graph **A**, **E**, **G**. The exact p-values are shown in the graph. Statistical analysis was not applied to data shown in **C**, **D** due to insufficient sample size.

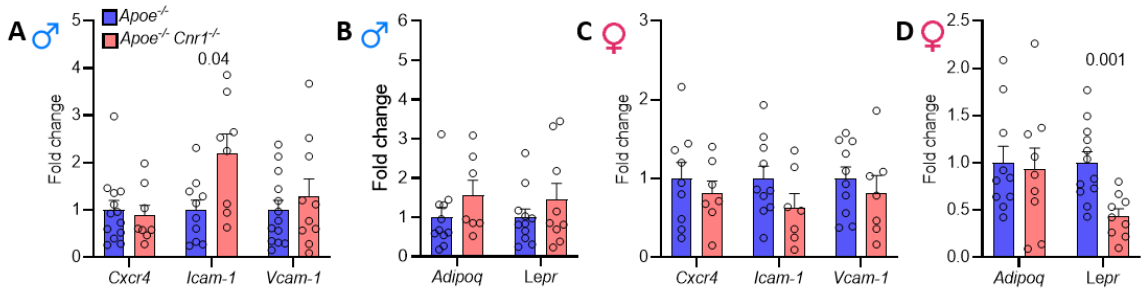

Figure 26. Gene expression of key bone marrow niche factors of sex-matched *Apoe-/-* and *Apoe-/-Cnr1-/-* mice in hypercholesterolemia. Gene expression in bone marrow cells collected from male (**A**, **B**) or female (**C**, **D**) 8 week old mice fed with 4 weeks WD. Each dot represents one mouse and all data are expressed as mean + s.e.m. Shapiro-Wilk normality test and ROUT method for outlier testing was performed. Student's unpaired t-test was used for graph **C** and **D** while the Mann-Whitney U test was used for graph **A** and **B**. The exact p-values are shown in the graph.

3.8 Effects of hematopoietic *Cnr1* deficiency on atherosclerosis and circulating myeloid cells under atherogenic diet

To dissect the impact of *Cnr1* deficiency in hematopoietic versus stromal cell populations, different bone marrow transplantation experiments were conducted. First, the role of

hematopoietic *Cnr1* deficiency on atherosclerosis development was investigated by transplanting *Cnr1* deficient bone marrow into lethally irradiated *Apoe*$^{-/-}$ recipients. The experimental design and duration of the experiment is shown in Figure 27 A.

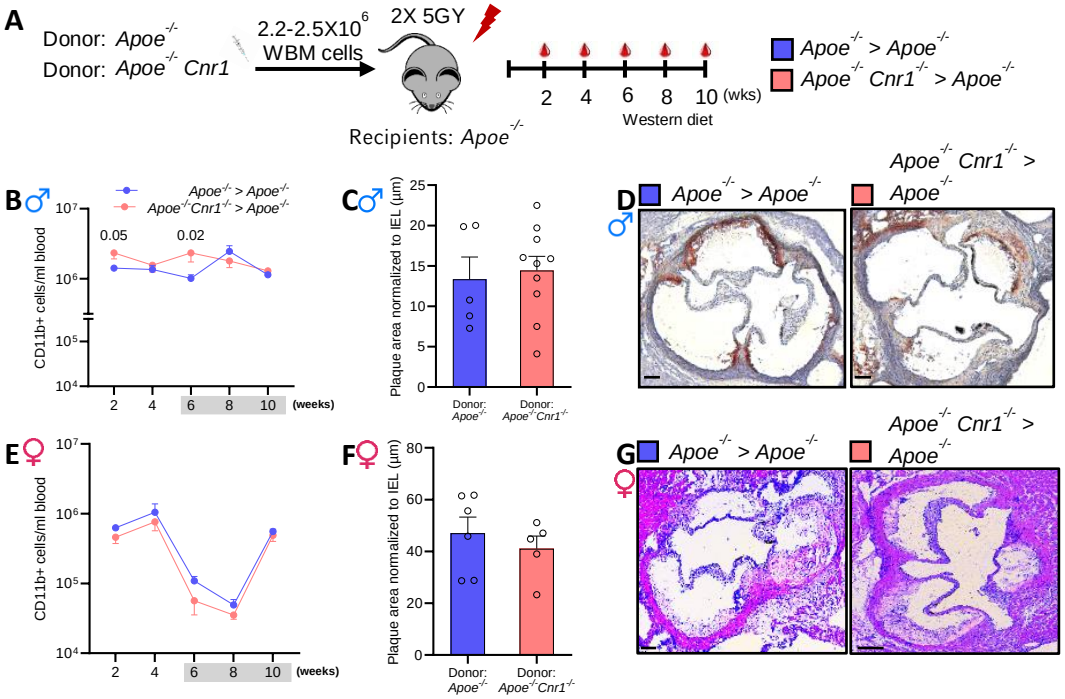

Figure 27. Impact of hematopoietic *Cnr1* deficiency on atherosclerosis development in sex-matched bone marrow chimeras. (**A**) Experimental design. (**B**-**D**) Data of male recipients showing flow cytometric analysis of myeloid blood counts at indicated time points (n = 8-11 per group) (**B**), quantification of the lesion area normalized to internal elastic lamina (IEL) after 4 weeks WD (**C**), representative pictures of aortic root sections stained with oil red O for plaque lipid staining (**D**). (**E**-**G**) Data of female recipients showing flow cytometric analysis of myeloid blood counts at indicated time points (n = 5-6 per group) (**E**), quantification of the lesion area normalized to internal elastic lamina (IEL) after 4 weeks WD (**F**), representative pictures of aortic root sections stained with hematoxylin and eosin (**G**). Scale bar = 100µm. Each dot represents one mouse and all data are expressed as mean + s.e.m. Shapiro-Wilk normality test and ROUT method for outlier testing was performed. Student's unpaired t-test was used for graph **B**, **C**, **E**, **G**. In graph **B**, **E**, statistical comparisons were applied between datasets of the same time point. The exact p-values are shown in the graph.

Male *Apoe*$^{-/-}$ mice receiving *Apoe*$^{-/-}$*Cnr1*$^{-/-}$ bone marrow had higher blood myeloid counts 2 and 6 weeks after reconstitution compared to sex-matched *Apoe*$^{-/-}$ bone marrow recipients. During the following 4 weeks of WD feeding, myeloid blood counts were comparable between the two groups (Figure 27. B). The aortic root plaque size was also comparable between both groups (Figure 27. C, D). In female mice, there were no significant differences in myeloid cell counts and plaque size (Figure 27. E-G).

At the experimental end point (10 weeks after transplantation), flow cytometry was used to quantify the numbers of circulating monocytes and neutrophils in the blood, bone marrow and spleen. In male mice, there was no difference in blood and spleen monocyte and neutrophil numbers between recipients of *Apoe*$^{-/-}$*Cnr1*$^{-/-}$ or *Apoe*$^{-/-}$ bone marrow (Figure 28. A, C). However, *Apoe*$^{-/-}$*Cnr1*$^{-/-}$ bone marrow recipients had fewer femoral monocyte and neutrophil

counts than the control group (Figure 28. B). In female mice, no differences in monocyte or neutrophil counts were found in either compartment (Figure 28. D-F).

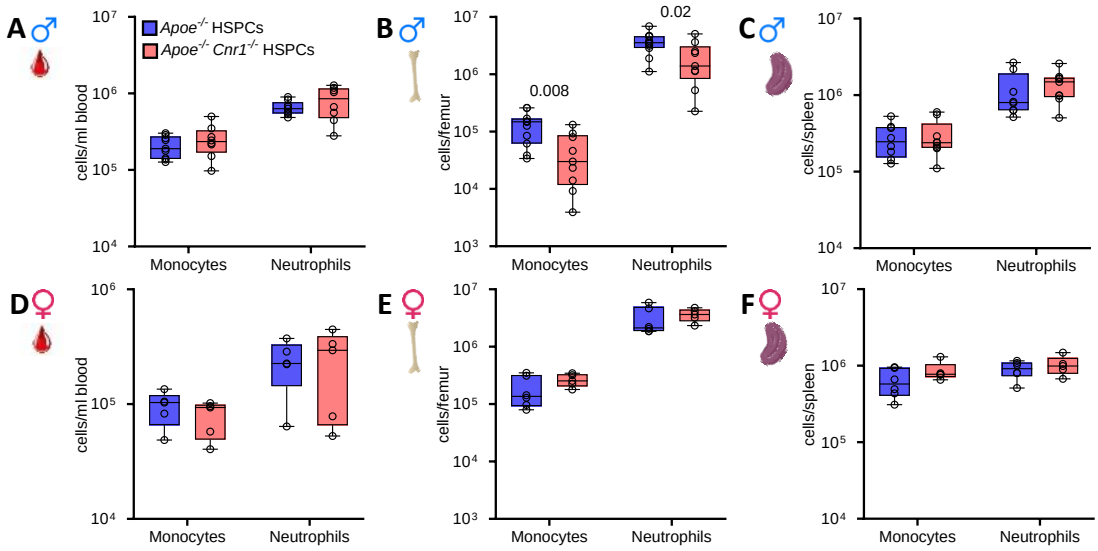

Figure 28. Monocyte and neutrophil counts in *Apoe*$^{-/-}$ recipients reconstituted with either *Apoe*$^{-/-}$ *Cnr1*$^{-/-}$ or *Apoe*$^{-/-}$ bone marrow.. (**A**-**C**) Monocyte and neutrophil counts in blood, femur and spleen of male chimeric mice. (**D**-**F**) Monocyte and neutrophil counts in blood, femur and spleen of female chimeric mice. All analyses were performed at the study end point, after 4 weeks of WD. Each dot represents one mouse. Box plots show medians with 25th and 75th percentiles as boundaries and whiskers indicate the range. Shapiro-Wilk normality test and ROUT method for outlier testing was performed. Student's unpaired t-test was used for graph **A**, **B**, **D** while the Mann-Whitney U test was used for graph **C**, **E**, **F**. The exact p-values are shown in the graph.

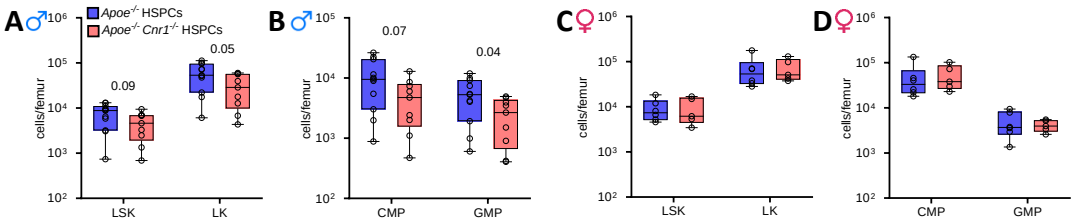

Figure 29. Hematopoietic progenitor cells in *Apoe*$^{-/-}$ recipients reconstituted with either *Apoe*$^{-/-}$ *Cnr1*$^{-/-}$ or *Apoe*$^{-/-}$ bone marrow. LSK and LK (**A**) or CMP and GMP counts per femur in male chimeric mice (**B**). LSK and LK (**C**) or CMP and GMP counts per femur in female chimeric mice (**D**). All analyses were performed at the study end point, after 4 weeks of WD. Each dot represents one mouse. Box plots show medians with 25th and 75th percentiles as boundaries and whiskers indicate the range. Shapiro-Wilk normality test and ROUT method for outlier testing was performed. Student's unpaired t-test was used for graph **A**, **B** while the Mann-Whitney U test was used for graph **C**, **D**. The exact p-values are shown in the graph.

Furthermore, there was tendency toward a reduction in the number of LSKs and a significant reduction in LKs in male recipients of *Apoe*$^{-/-}$*Cnr1*$^{-/-}$ bone marrow, a non-significant reduction in CMPs and a significantly lower number of GMPs. These findings suggest that lack of *Cnr1* in hematopoietic cells leads to reduced hypercholesterolemia-driven myelopoiesis in male mice (Figure 29. A, B). In female mice, no differences in the number of HSPCs were observed between the two groups (Figure 29. C, D).

3.9 Effects of stromal cell *Cnr1* deficiency on atherosclerosis and circulating myeloid cells under atherogenic diet

Next, we investigated the impact of stromal *Cnr1* deficiency on the development of atherosclerosis by transplanting *Apoe*$^{-/-}$ bone marrow cells into lethally irradiated *Apoe*$^{-/-}$ or *Apoe*$^{-/-}$*Cnr1*$^{-/-}$ recipients. The experimental design and the total duration of the experiment is shown in Figure 30 A.

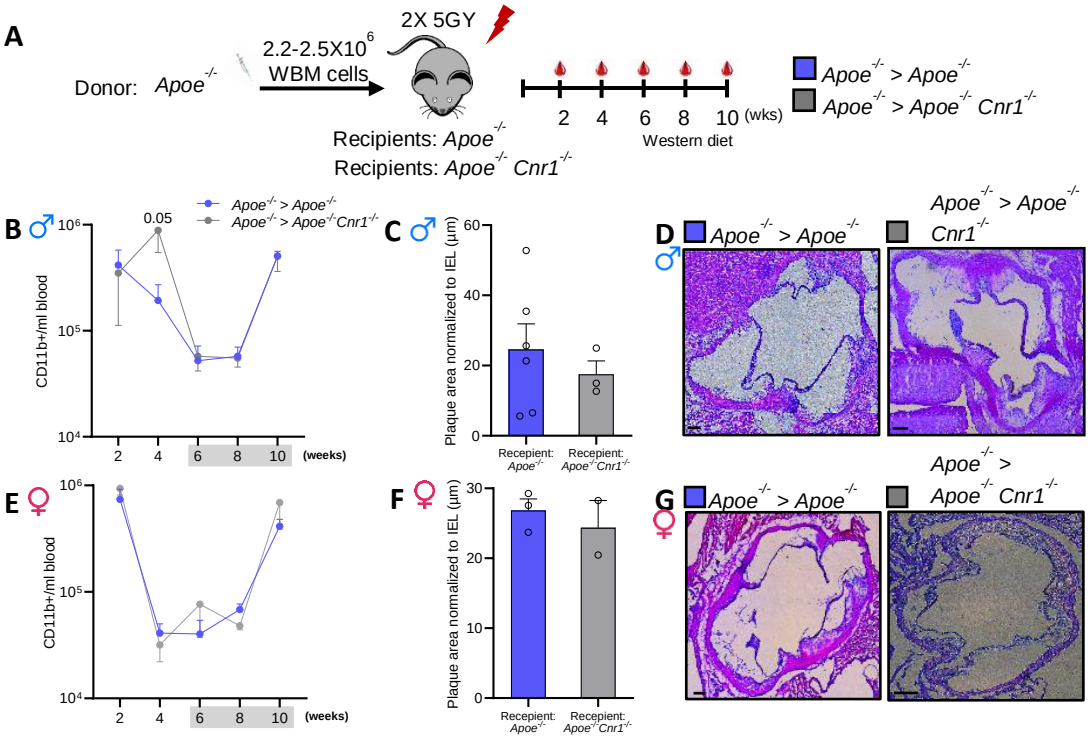

Figure 30. Impact of stromal *Cnr1* deficiency on atherosclerosis development. (**A**) Experimental design. (**B**-**D**) Data of male recipients showing flow cytometric analysis of myeloid blood counts at indicated time points (n = 4-6 per group) (**B**), quantification of the lesion area normalized to internal elastic lamina (IEL) after 4 weeks WD (**C**), representative pictures of aortic root sections stained with hematoylin and eosin (**D**). (**E**-**G**) Data of female recipients showing flow cytometric analysis of myeloid blood counts at indicated time points (n = 2-3 per group) (**E**), quantification of the lesion area normalized to internal elastic lamina (IEL) after 4 weeks WD (**F**), representative pictures of aortic root sections stained with hematoylin and eosin (**G**). Scale bar = 100µm. Each dot represents one mouse and all data are expressed as mean + s.e.m. Shapiro-Wilk normality test and ROUT method for outlier testing was performed. Student's unpaired t-test was used for graph **B**, **C**, while the Mann-Whitney U test was used for graph **E**. In graph **B**, **E**, statistical comparisons were applied between datasets of the same time point. Statistical analysis was not applied to data shown in **F** due to insufficient sample size. The exact p-values are shown in the graph.

In male mice, deficiency of *Cnr1* in the bone marrow niche did not affect the reconstitution efficiency after bone marrow transplantation, although a transient effect on myeloid cells was observed after 4 weeks (Figure 30. B). Likewise, there was no difference in the aortic root plaque size (Figure 30. C, D). In female mice, there was no genotype-dependent difference in myeloid cell counts or plaque size (Figure 30 E-G). However, the sample size for plaque analysis in some of the experimental groups was too small to yield meaningful results.

At the experimental end point (10 weeks after transplantation), flow cytometry was used to quantify the numbers of circulating monocytes and neutrophils in the blood, bone marrow and spleen (Figure 31). In both male and female mice, there was no difference in blood and spleen monocyte or neutrophil numbers between *Apoe*$^{-/-}$*Cnr1*$^{-/-}$ and *Apoe*$^{-/-}$ recipients (Figure 31. A, C-D, F). However, bone marrow monocyte and neutrophil counts were significantly higher in *Apoe*$^{-/-}$*Cnr1*$^{-/-}$ recipients compared to the control group, which was observed in both males and females (Figure 31 B, E).

In line with this finding, male *Apoe*$^{-/-}$*Cnr1*$^{-/-}$ recipients had higher numbers of LKs, CMPs and GMPs in (Figure 32. A, B). No differences were found in females, but the sample size was too small to be conclusive (Figure 32. C, D).

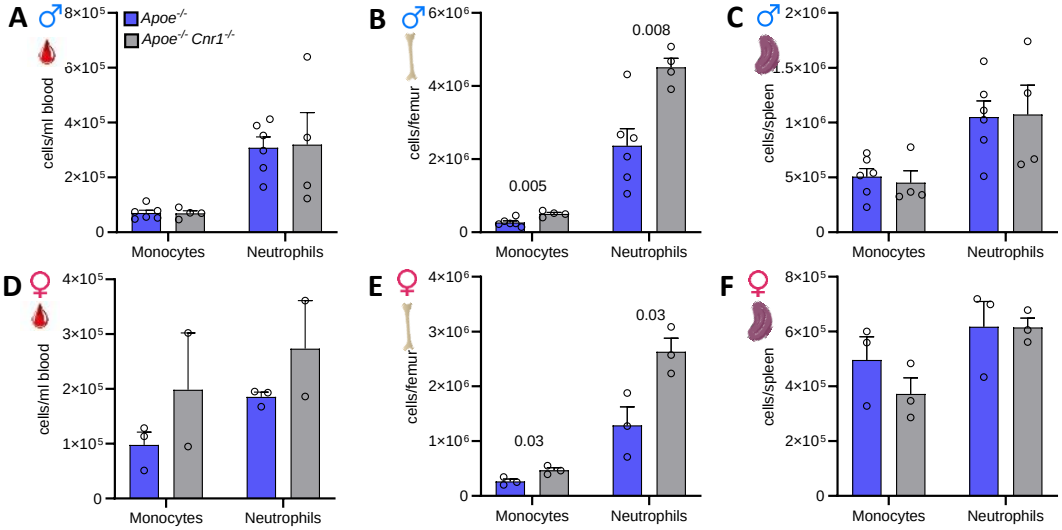

Figure 31. Monocyte and neutrophil counts in blood and lymphoid organs of *Apoe*$^{-/-}$ or *Apoe*$^{-/-}$ *Cnr1*$^{-/-}$ recipients reconstituted with *Apoe*$^{-/-}$ bone marrow.. (**A**-**C**) Monocyte and neutrophil counts in blood, femur and spleen of male chimeric mice. (**D**-**F**) Monocyte and neutrophil counts in blood, femur and spleen of female chimeric mice. All analyses were performed at the study end point, after 4 weeks of WD. Each dot represents one mouse and all data are expressed as mean + s.e.m. Shapiro-Wilk normality test and ROUT method for outlier testing was performed. Student's unpaired t-test was used for graph **A**, **B**, **D**, **E**, **F** while the Mann-Whitney U test was used for graph **C**. The exact p-values are shown in the graph.

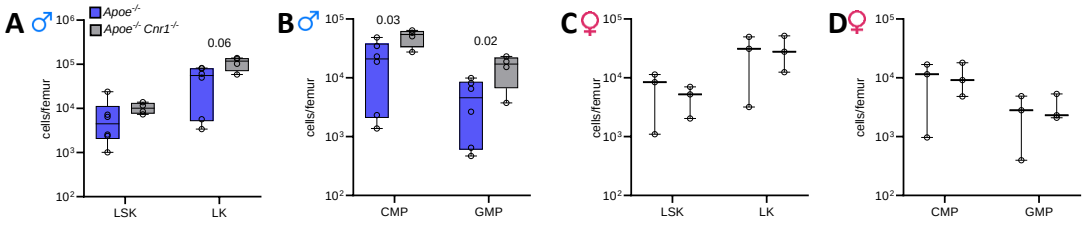

Figure 32. Hematopoietic bone marrow progenitors in *Apoe*$^{-/-}$*Cnr1*$^{-/-}$ or *Apoe*$^{-/-}$ recipients reconstituted with *Apoe*$^{-/-}$ bone marrow.. LSK and LK numbers per femurs (**A**), CMP and GMP in male chimeric mice (**B**). LSK and LK numbers per femur (**C**), CMP and GMP in female chimeric mice (**D**). All analyses were performed at the study end point, after 4 weeks of WD. Each dot represents one mouse. Box plots show medians with 25th and 75th percentiles as boundaries and whiskers indicate the

range. Shapiro-Wilk normality test and ROUT method for outlier testing was performed. Student's unpaired t-test was used for graph **B**, **C**, **D** while the Mann-Whitney U test was used for graph **A**. The exact p-values are shown in the graph.

To assess whether the increase in LK numbers in *Apoe*$^{-/-}$*Cnr1*$^{-/-}$ male recipients was due to an increased proliferation rate and possibly niche signals, cell cycle analysis and Ki67 staining was performed. No differences were observed between the two groups, but due to the high variability of the data points a larger sample size may be required to draw conclusions (Figure 33. A-C).

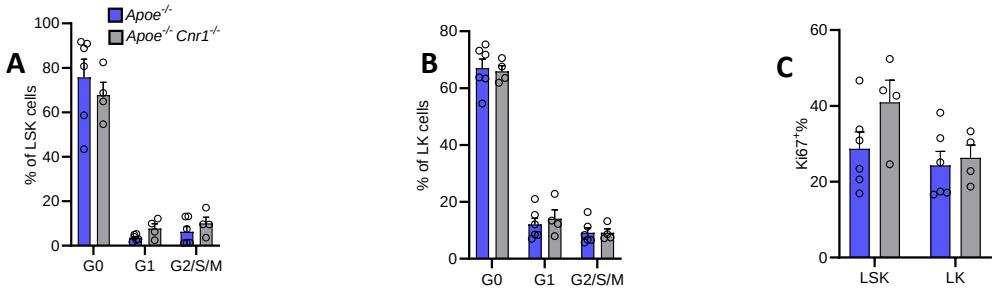

Figure 33. HSPC cell cycle distribution in male *Apoe*$^{-/-}$*Cnr1*$^{-/-}$ or *Apoe*$^{-/-}$ recipients reconstituted with *Apoe*$^{-/-}$ bone marrow. (**A**-**B**) Cell cycle analysis in LSK cells (**A**) and LK cells (**B**). Percentage of LSK or LK cells stained with Ki67 proliferation marker (**C**). Each dot represents one mouse and all data are expressed as mean + s.e.m. Shapiro-Wilk normality test and ROUT method for outlier testing was performed. Student's unpaired t-test was used for graph **B**, **C** while the Mann-Whitney U test was used for graph **A**. No significant differences.

3.10 Competitive reconstitution efficiency of *Cnr1* deficient versus WT bone marrow in atherosclerosis-prone mice

To further understand how *Cnr1* deficiency affects hematopoietic lineage differentiation after bone marrow reconstitution, a competitive transplantation experiment was performed. For this purpose, *Cnr1* deficient bone marrow was mixed with a *Cnr1* WT reference in equal proportions and subsequently transplanted into irradiated animals. In particular, bone marrow from mice expressing distinct CD45.1 and CD45.2 pan-leukocyte markers was used to track the chimerism in the recipients. Two different donors were used as competitors, either *Apoe*$^{-/-}$ CD45.2 (control group) or *Apoe*$^{-/-}$*Cnr1*$^{-/-}$ CD45.2 (KO group). These cells were mixed with *Apoe*$^{-/-}$ CD45.1 (reference) cells and transplanted into *Apoe*$^{-/-}$ CD45.1 recipients [134]. Blood myeloid cell counts were then monitored for 6 weeks (Figure 34. A).

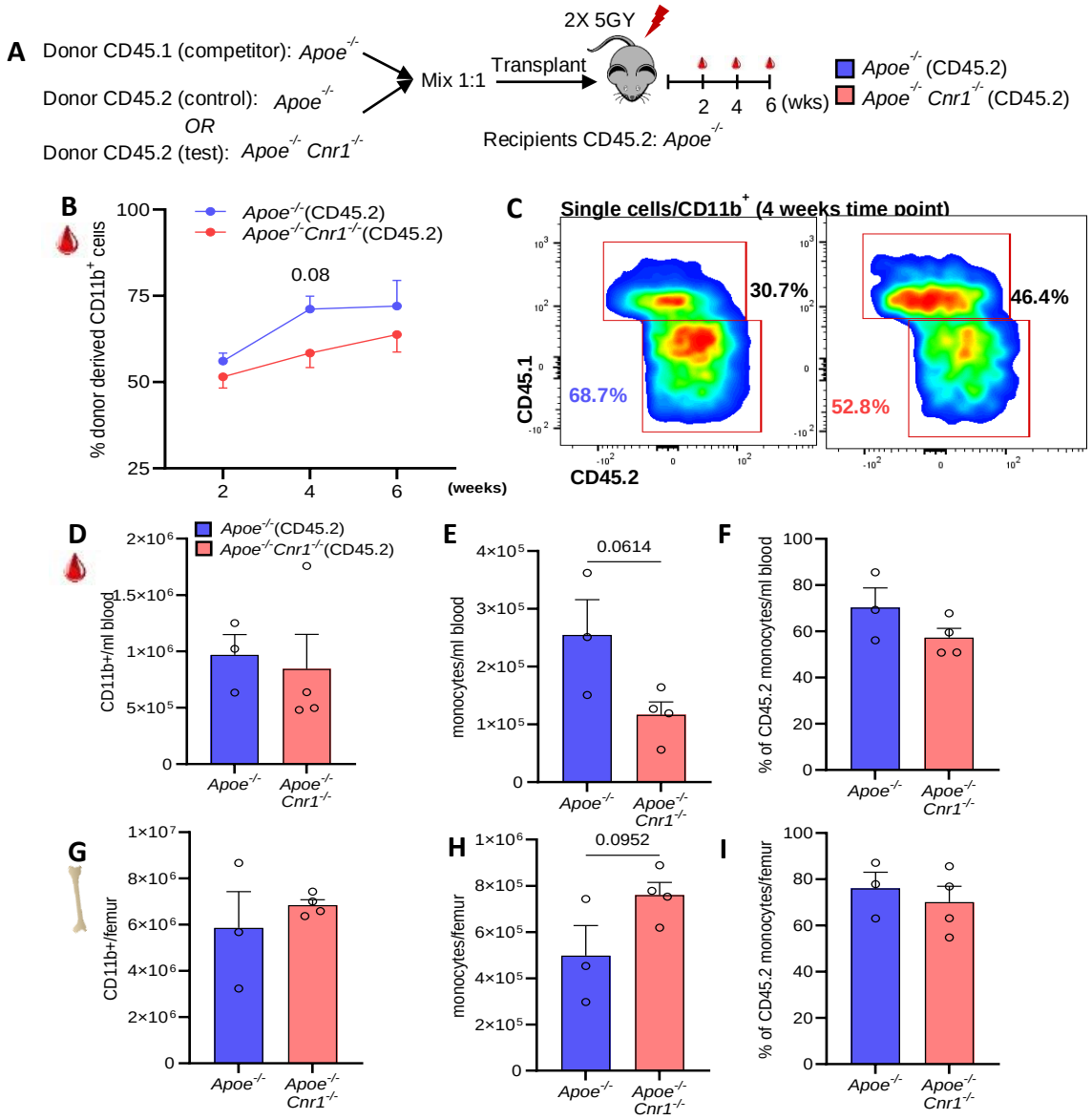

Figure 34. . Competitive reconstitution in mixed *Cnr1* deficient or *Cnr1* WT bone marrow chimeras (**A**) Experimental design: mixed [*Apoe*$^{-/-}$ (CD45.1) and *Apoe*$^{-/-}$*Cnr1*$^{-/-}$ (CD45.2)] or [*Apoe*$^{-/-}$ (CD45.1) and *Apoe*$^{-/-}$ (CD45.2)] bone marrow was transplanted into male *Apoe*$^{-/-}$ (CD45.1) recipients. (**B**) Proportion of CD11b+ (CD45.2+) cells of total CD45+ cells at indicated time points (n = 2-3). (**C**) Representative flow cytometry graphs showing the gating of CD11b+CD45.2 cells. (**D**-**E**) Flow cytometric quantification of circulating CD11b+ cells and monocytes. (**F**) Proportion of CD45.2+ monocytes out of total CD45+ monocytes in the blood after 6 weeks of transplantation. (**G**-**H**) Flow cytometric quantification of bone marrow CD11b+ cells and monocytes. (**I**) Proportion of CD45.2+ monocytes out of total CD45+ monocytes in the femur after 6 weeks of transplantation. Each dot represents one mouse and all data are expressed as mean + s.e.m. Shapiro-Wilk normality test and ROUT method for outlier testing was performed. Student's unpaired t-test was used for graph **B**, **E**, **F**, **G**, **H**, **I** while the Mann-Whitney U test was used for graph **D**. In graph B statistical comparisons were applied between datasets of the same time point. The exact p-values are shown in the graph.

Cnr1 deficient bone marrow cells tended to have a competitive disadvantage to reconstitute CD11b+ blood cells, as evident after 4 weeks post-transplantation (Figure 34. B, C). However, conclusive results were not possible due to the small sample size. *Cnr1* deficiency did not affect the number of circulating CD11b+ cells but tended to decrease the number of circulating

monocytes, while there was no change in chimerism after 6 weeks (Figure 34. D-F). In the femurs, no significant differences were observed (Figure 34. G-I). Recipients of *Cnr1* deficient bone marrow cells tended to have more LK cells with more cells in G1 phase compared to the control group (Figure 35. A, B). Bone marrow chimerism inside the bone marrow was not affected but the recipients of *Cnr1*$^{-/-}$ deficient cells had more CMPs and GMPs (Figure 35. C, D).

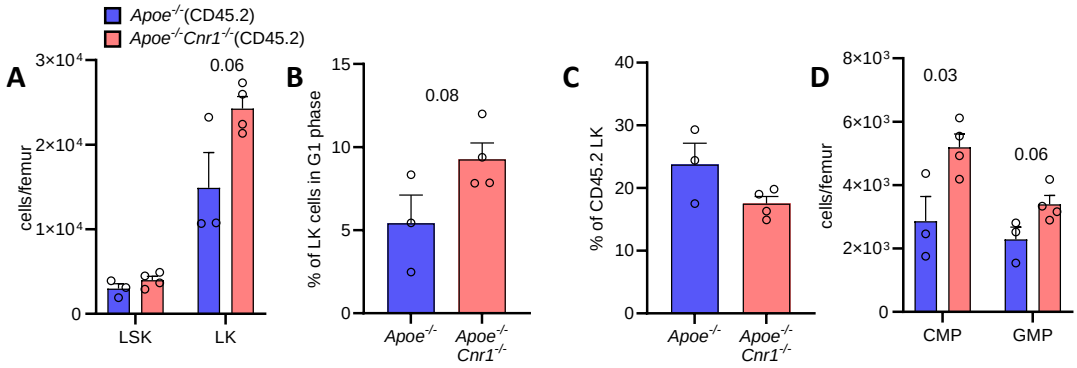

Figure 35. HSPC counts 6 weeks after competitive transplantation in femurs of *Apoe*$^{-/-}$ male mice. (**A**) Flow cytometric quantification of total LSKs and LKs. (**B**) Percentage of LKs in G1 cell cycle phase. (**C**) Proportion of CD45.2+ LKs out of total CD45+ LKs. (**D**) Flow cytometric quantification of total CMPs and GMPs. Each dot represents one mouse and all data are expressed as mean + s.e.m. Shapiro-Wilk normality test and ROUT method for outlier testing was performed. Student's unpaired t-test was used for graph **B**-**D** while the Mann-Whitney U test was used for graph **A**. The exact p-values are shown in the graph.

3.11 Effect of peripheral CB1 antagonism on hematopoiesis

Previous work from our lab has shown that blocking of peripheral CB1 signalling limits atherosclerotic plaque progression [135, 136]. To clarify if this beneficial effect is associated with changes in hematopoietic progenitors, bone marrow samples of a previously described experiment in *Ldlr*$^{-/-}$ mice fed with WD for 16 weeks and treated with the peripheral CB1 antagonist JD5037 during the last 8 weeks of the diet were analysed. In the context of this thesis, HSPC bone marrow counts were measured (Figure 36. A). The experimental details of this in *vivo* experiment and the effect on atherosclerotic plaques have already been reported by Chen et al. [135]. Chronic peripheral CB1 antagonism with JD5037 did not affect the total number of bone marrow LSKs in male hypercholesterolemic mice, but significantly increased the LK population compared to the vehicle group (Figure 36. B, C). Furthermore, chronic JD5037 injection significantly increased the number of ST-HSC, CMP, and GMP (Figure 36. D, E). In female mice, injection of JD5037 significantly increased the number of LSK without affecting other populations (Figure 36. B, C, F, G).

Measurement of CXCL12 and SCF in bone marrow lavage and bone marrow gene expression of *Cxcr4*, *Icam-1* and *V-cam1* showed no significant differences between the vehicle and

JD5037 groups in either sex (Figure 37). However, due to the small sample size and high variability of the CXCL12 and SCF ELISA results, the findings are not conclusive.

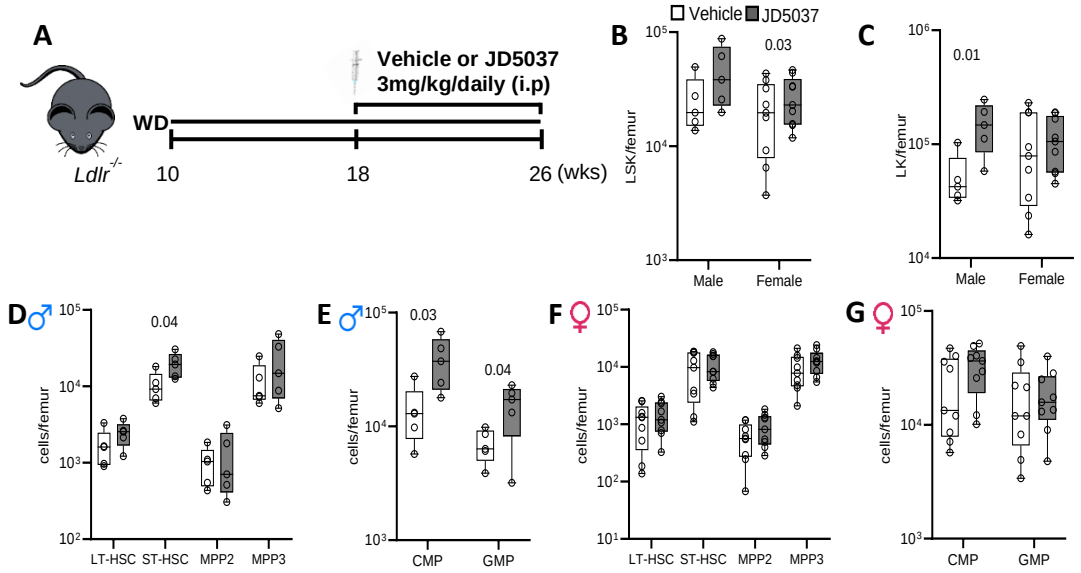

Figure 36. Peripheral CB1 antagonism in hypercholesterolemic *Ldlr*$^{-/-}$ mice increases myeloid progenitors. (**A**) Experimental design (JD5037, peripheral CB1 antagonist). (**B**-**G**) Flow cytometric quantification of LSK cells (**B**), LK cells (**C**), different hematopoietic primitive stem cells (**D**, **F**) and CMP and GMP cells (**E**, **G**). Each dot represents one mouse. Box plots show medians with 25th and 75th percentiles as boundaries and whiskers indicate the range. Shapiro-Wilk normality test and ROUT method for outlier testing was performed. Student's unpaired t-test was used for graph **B**, **D**, **E**, **F**, **G** while the Mann-Whitney U test was used for graph **C**. The exact p-values are shown in the graph.

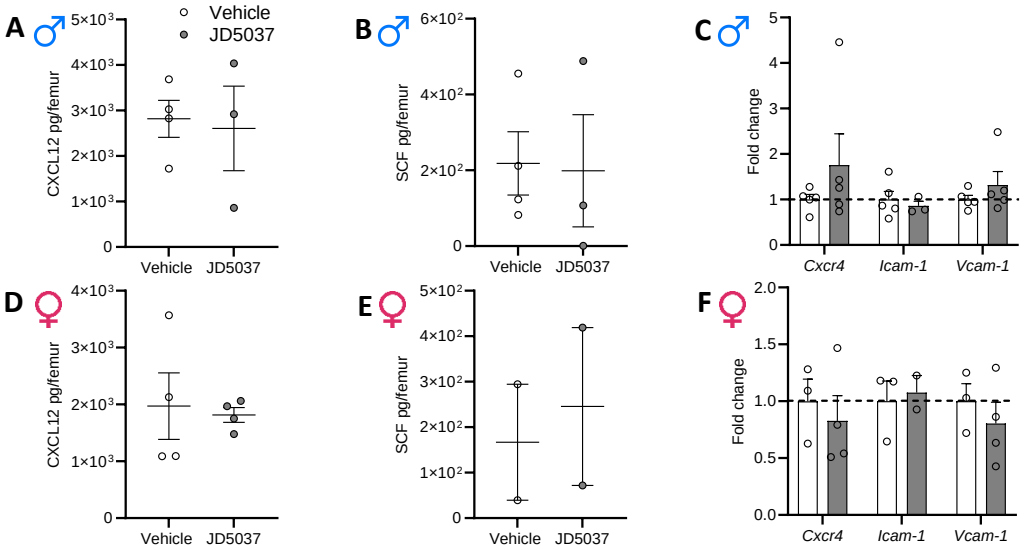

Figure 37. Effect of peripheral inhibition of CB1 on key proteins and genes in the bone marrow niche of sex-matched *Ldlr*$^{-/-}$ mice under WD. (**A**-**B**) CXCL12 and SCF levels in bone marrow lavage of male mice, determined by ELISA. (**C**) Gene expression in bone marrow cells of male mice, determined by RT-qPCR. (**D**-**E**) CXCL12 and SCF levels in bone marrow lavage of female mice. (**F**) Gene expression in bone marrow cells of female mice. Each dot represents one mouse and all data are expressed as mean + s.e.m. Shapiro-Wilk normality test and ROUT method for outlier testing was performed. Student's unpaired t-test was used for graph **A**, **B**, **D**, while the Mann-Whitney U test was used for graph **C**, **F.** Statistical analysis was not applied to data shown in **E** due to insufficient sample size The exact p-values are shown in the graph.

3.12 Role of CB1 in regulating acute inflammatory HSPC response

The findings so far indicate that CB1 plays a role in chronic inflammation caused by atherogenic conditions. Deficiency of *Cnr1* increased the number of myeloid progenitors, leading to monocytosis, which in turn enhances the formation of larger plaques. The next experiment aimed to study the impact of *Cnr1* deficiency on HSPC expansion in response to acute stimulation with G-CSF (Figure 38. A). In male mice, injection of G-CSF for 5 consecutive days significantly increased the number of circulating LSKs and CD11b+ cells compared to vehicle, independent of the genotype (Figure 38. B, C). Unexpectedly, in female mice the injection of G-CSF did not increase the number of circulating LSKs (Figure 38. D). Interestingly, G-CSF injection resulted in significantly higher numbers of circulating CD11b+ cells only in *Cnr1*$^{-/-}$ females, while no effect was seen in WT females compared to the corresponding vehicle group (Figure 38. E).

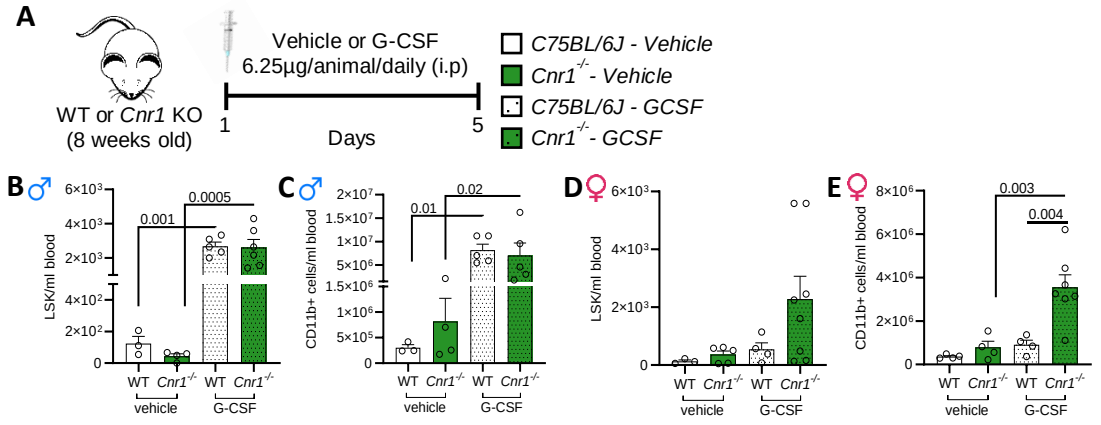

Figure 38. G-CSF induced mobilization of LSKs and CD11b+ cells in sex-matched *Cnr1*$^{-/-}$ and WT mice. (**A**) Experimental design. Flow cytometric analysis of circulating LSKs and CD11b+ cells in male (**B**, **C**) and female (**D**, **E**) *Cnr1*$^{-/-}$ and WT mice. Data are presented as mean + s.e.m. Each dot represents one mouse. Shapiro-Wilk normality test and ROUT method for outlier testing was performed. One-way ANOVA followed by post hoc Newman–Keuls multiple comparison test was used to determine the significant differences. The exact p-values are shown in the graph.

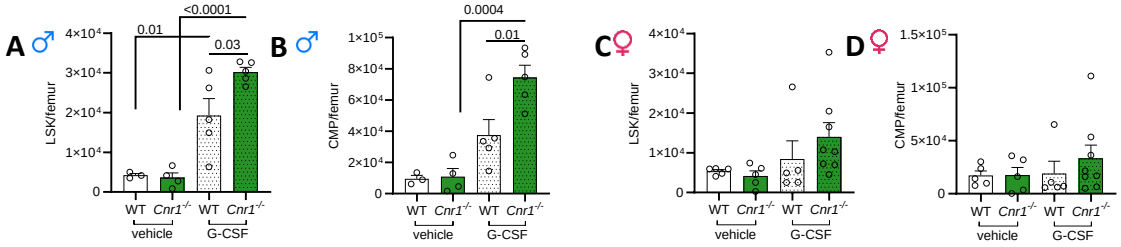

Figure 39. Impact of G-CSF injection on bone marrow progenitors in sex-matched WT and *Cnr1*$^{-/-}$ mice. Flow cytometric analysis of LSK and CMP counts per femur in male (**A**, **B**) or female (**C**, **D**) mice. Data are presented as mean + s.e.m. Each dot represents one mouse. Shapiro-Wilk normality test and ROUT method for outlier testing was performed. One-way ANOVA followed by post hoc Newman–Keuls multiple comparison test was used to determine the significant differences. The exact p-values are shown in the graph.

In addition the bone marrow counts of HSPC subsets in response to G-CSF stimulation were measured. In male mice, G-CSF injection resulted in significantly higher numbers of bone marrow LSKs and CMPs in *Cnr1* deficient compared to WT mice (Figure 39. A, B). In female mice, the injection of G-CSF did not cause any significant changes compared to vehicle or between genotypes (Figure 39. C, D).

3.13 Transcriptomic changes in *Cnr1* deficient HSPCs and stromal cells

To gain a global insight into the transcriptomic changes of *Cnr1* deficiency on the bone marrow hematopoietic system, scRNA-seq was performed with HSPCs (Lin^- $cKit^{+/-}$) and bone marrow stromal cells (Lin^- $CD45^-$) from WT and *Cnr1*$^{-/-}$ male mice at the age of 9 weeks. Figure 40 shows the experimental design. In brief, from each mouse two cellular fractions were isolated: fraction 1 contained bone marrow cells and fraction 2 contained cells isolated from digested bone tissue. After flow cytometric sorting, HSPCs and stromal cells from the same genotype were pooled and used to generate a library. From each mouse 35´000 HSPCs and 1´650 stromal cells were combined. Prior to analysis of differential gene expression, common filtering and quality control steps were performed as detailed in the methods. After filtering, HSPCs and stromal cells were processed separately for downstream analysis. For HSPCs, a total of 48´500 cells passed quality control and represent cells from 6 animals. The median UMI count and median genes per cell were 5´000 and 1´971, respectively. The cells separated into 13 clusters and despite lineage-negative sorting of HSPCs for sequencing, our clusters contained a substantial amount of mature leukocytes (clusters 0, 1, 2, 4, 5, 6, 7, 10, 11) while hematopoietic progenitors were represented in cluster 3 beside some clusters representing endothelial cells (cluster 8 and 9) and stromal cells (clusters 12 and 13) (Figure 40. B). To focus on the myeloid progenitor clusters, a myeloid score of expression markers from a previously published dataset was used (Figure 40. C) [133]. This allowed the extraction of cells with high myeloid marker score for downstream analysis. Three main myeloid progenitor clusters were identified: CMPs, GMPs and differentiated myeloid progenitors (Figure 40. D, E). These three clusters were detected in both genotypes, but the percentage of CMPs was significantly lower in the *Cnr1*$^{-/-}$ compared to the WT group, while the frequency of more differentiated progenitors was higher (Figure 40. F).

Downstream analysis was applied on gene expression matrix from the three combined myeloid clusters. *Cnr1* deficiency significantly affected 300 genes of which 190 were upregulated and 110 were downregulated (Figure 41. A). Most of the DEGs were mitochondrial, histone or ribosomal genes. Three of the downregulated genes were myeloperoxidase (MPO), S100 calcium binding protein A8 and A9 (S100A8/9). These genes are important during myeloid differentiation and neutrophil maturation. S100A8 and S100A9 are involved in inflammation response and regulate diverse processes such as leukocyte recruitment and cytokine

production and are associated with different types of leukaemia [137, 138]. GO enrichment analysis showed that DEGs were associated with oxidative phosphorylation, neutrophil aggregation, response to oxidative stress and regulation of apoptotic process (Figure 41. B). To relate the DEGs to pre-defined phenotypes, the gene set enrichment analysis (GSEA) was subsequently used. The analysis showed a positive correlation with granulocytopoetic cell and hematopoietic precursor cell aging gene sets, albeit with a low FDR value (Figure 41. C). Furthermore, transcription factor prediction analysis suggested that the transcriptomic signature of *Cnr1* deficient HSPCs is controlled by transcription factors important for myeloid differentiation and inflammatory response, including SPI1 (Spi-1 Proto-Oncogene also known as PU.1), CCAAT Enhancer Binding Protein Beta (CEBPB) and Interferon Regulatory Factor 1 and 8 (IRF1 and 8; Figure 41. D).

For stromal cell sequencing, Lin^-CD45^- cells were sorted. A major technical problem for the isolation of stromal cells is the required tissue digestion, which affected the yield of viable cells for analysis. Similar pre-processing and quality control steps were applied as described above. A total of 1´392 cells passed quality control and represent cells from 6 animals. The median UMI count and median genes per cell were 1´355 and 744, respectively. *Lepr* and *Cxcl12* expression were used as markers to identify stromal cells, which resulted in 75 cells from WT and 61 from *Cnr1* KO mice that separated into four clusters (Figure 42. A). Further analysis was based on other known markers for mesenchymal stem cells (*Cxcl12* and *LepR*), endothelial cells (*Cdh5*, *Pecam1*, *Emcn* and *Tie1*) and osteolineage cells (*Alpl* and *Spp1*) (Figure 42. B). *Cnr1* deficiency affected the expression of 36 genes, of which 16 were upregulated and 20 downregulated (Figure 42. C). These genes were associated with biological processes that are related to bone and bio-mineral tissue development (Figure 42. D). GSEA analysis showed an enrichment of transcriptomic signatures related to TNF alpha signalling and epithelial to mesenchymal transition in $Cnr1^{-/-}$ cells (Figure 42. E). Transcription factor prediction indicated that the DEGs are regulated by transcription factors SNAI2 and TEAD4, which play a role in cellular development and mesenchymal differentiation to osteolineage or adipolineage (Figure 42. F). These results support the finding that *Cnr1* deficiency regulates osteoblast differentiation and extracellular matrix composition in the bone marrow, which are important processes for the fitness of the hematopoietic stem cell populations.

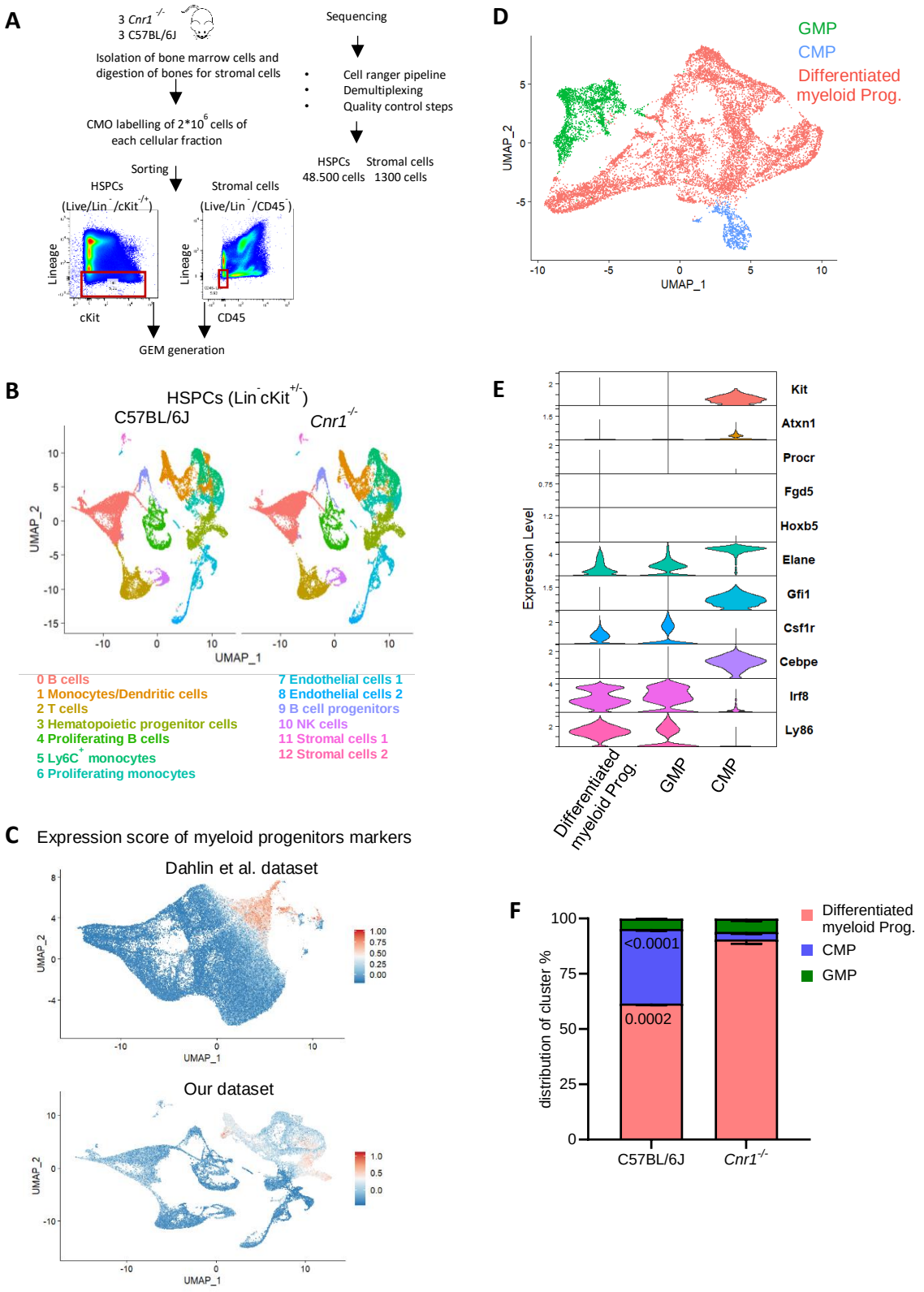

Figure 40. Single cell RNA sequencing of male WT and *Cnr1*$^{-/-}$ bone marrow HSPCs and stromal cells. (**A**) Experimental work flow of single cell transcriptomic analysis of HSPCs and stromal cells. Cells were sorted from male mice (n=3 per genotype). (**B**) UMAP plot of single-cell sequencing data showing 13 different clusters in the HSPC fraction. (**C**) UMAP plot of myeloid progenitor marker score expression across our dataset and the reference dataset. (**D**) UMAP plot of 3 myeloid progenitors clusters. (**E**) Violin plot showing the expression and distribution of markers used to annotate the myeloid progenitor clusters. (**F**) Distribution of cells per cluster.

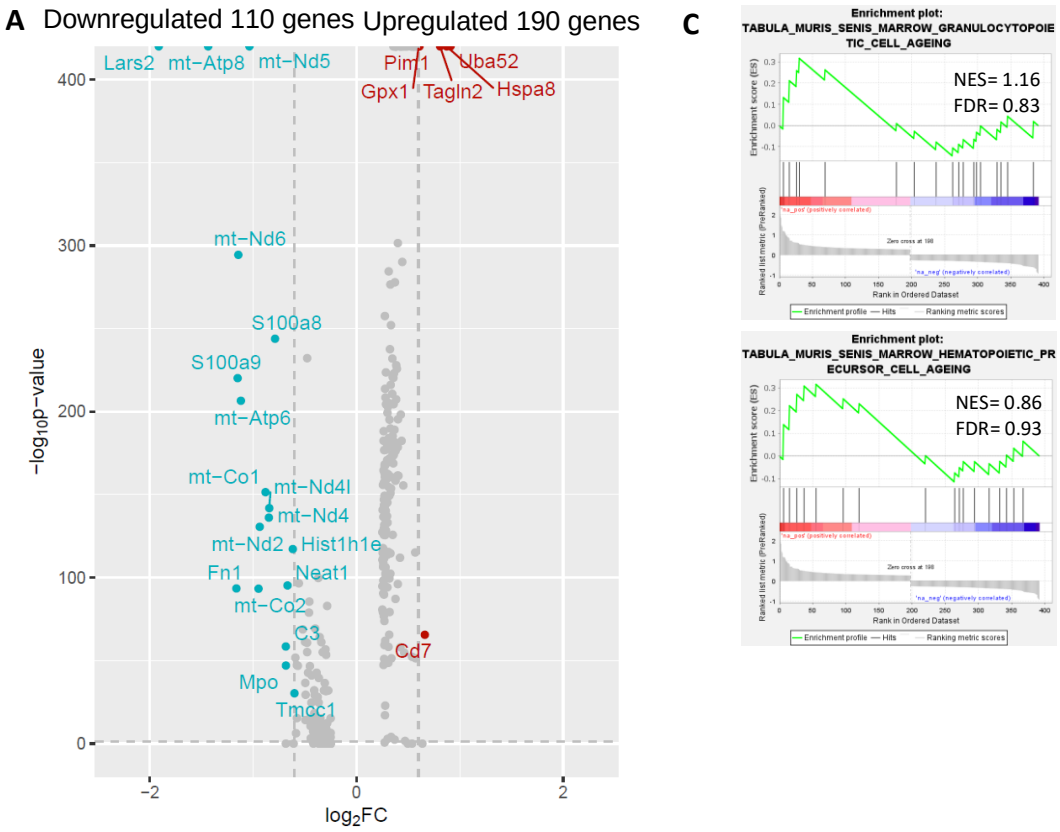

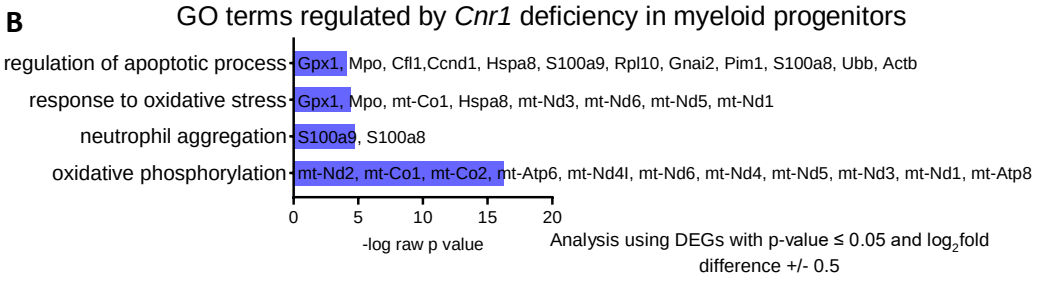

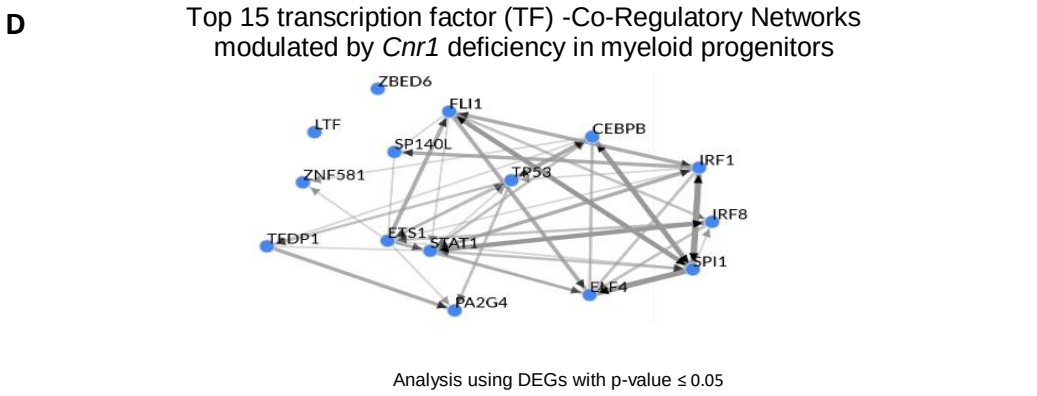

Figure 41. Transcriptomic pathway analysis of *Cnr1*$^{-/-}$ bone marrow myeloid progenitor clusters. (**A**) Volcano plot of all significant DEGs, the colored genes are with cut of +/-0.6 log_2FC between WT and *Cnr1*$^{-/-}$. (**B**) GO enrichment analysis of biological processes using all significant DEGs with fold difference of +/- 0.5 log_2FC in the three progenitors clusters. (**C**) Gene set enrichment analysis plots in the three progenitors clusters using all DEGs showing the normalized enrichment score (NES) and false discovery rate value (FDR). (**D**) Top 15 transcription factors associated with all significant DEGs as predicted by ChEA3.

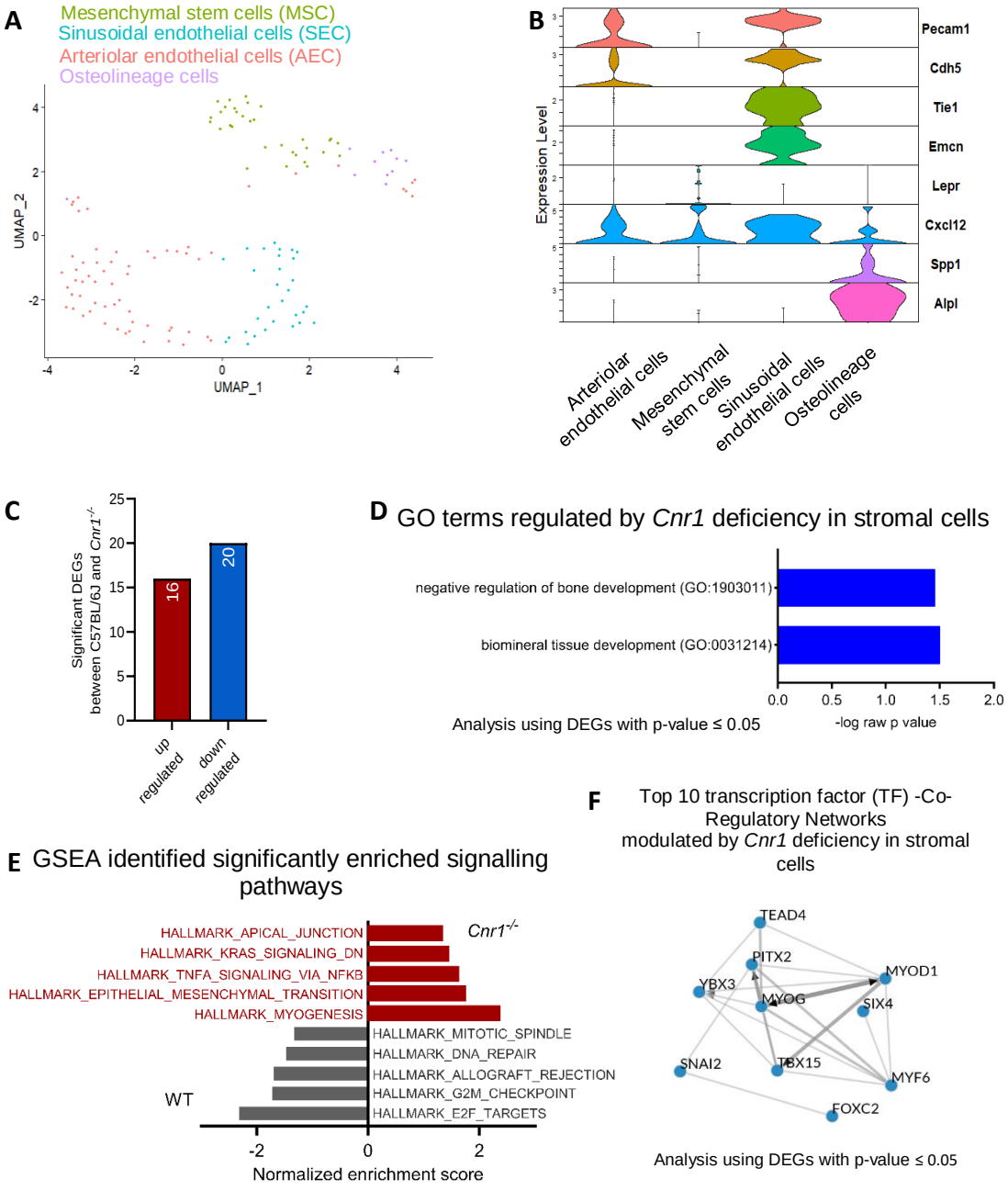

Figure 42. Single cell transcriptomic analysis of *Cnr1*$^{-/-}$ stromal bone marrow cells. (**A**) UMAP plot of single-cell sequencing data shows four different clusters in the stromal fraction, these clusters are arteriolar endothelial cells (AEC), sinusoid endothelial cells (SEC), mesenchymal stem cells (MSC) and osteolineage cells. (**B**) Violin plot showing the expression and distribution of markers used to identify the different clusters. (**C**) Number of differentially expressed genes by *Cnr1* deficiency. (**D**) Gene ontology terms analysis of biological processes using significant DEGs. (**E**) GSEA analysis showing significantly enriched pathways in *Cnr1* deficient stromal cells compared to WT. (**F**) Top 10 transcription factors associated with DEGs as predicted by ChEA3.

3.14 *In vitro* inhibition of CB1 decreases LSK quiescence and increases proliferation

To further understand the role of CB1 signalling in LSK and LK proliferation, sorted bone marrow cells were treated in vitro with CB1 antagonist AM281 (1µm) or the corresponding vehicle. After each time point (30 min, 4 and 8 hours) an aliquot of cells was used for flow cytometric cell cycle analysis in LSKs and LKs (Figure 43. A-F). In addition, CFU assay was performed with the cells after 8h of treatment (Figure 43. G-H). After 8 hours, LSK cells treated with AM281 were more proliferative as indicated by a significant reduction in the percentage of cells at G0 and a significant increase in cells at the G2-S-M stage compared to the vehicle control (Figure 43. A, C). There was no difference in LK cells between the vehicle control and AM281. Due to high variability and small sample size, the CFU assay did not reveal significant differences in the number of colonies between control and AM281 treatment (Figure 43. G, H).

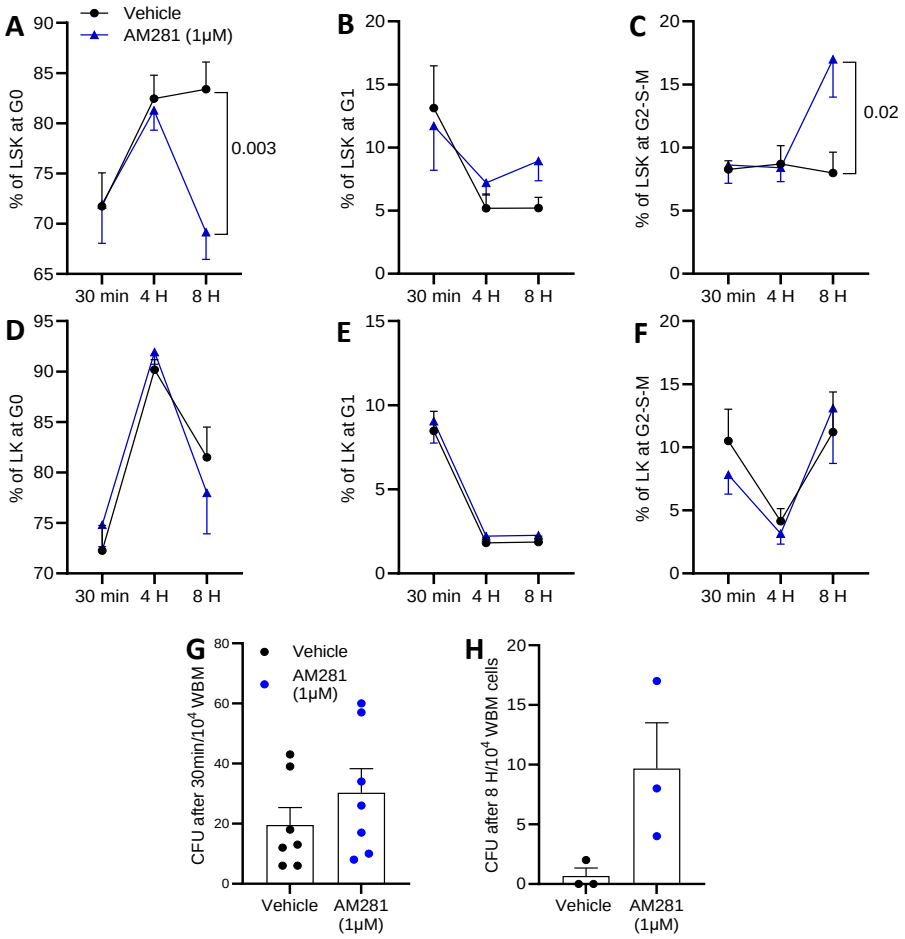

Figure 43. Effect of CB1 antagonist AM281 on cell cycle distribution in LSK and LK cells. (**A**-**C**) Cell cycle in LSK cells treated with AM281. (**D**-**F**) Cell cycle in LK cells treated with AM281. (**G**-**H**) CFU assay after 7 days of 10^4 whole bone marrow cells treated with AM281. (**A**-**F**) n = 6-8 mice for each treatment. Data are expressed as mean + s.e.m. Normality and outliers check was done by using the Shapiro-Wilk normality test and ROUT method for outlier testing was performed. Student's unpaired t-test was used for all graphs. The exact p-values are shown in the graph.

4 Discussion

CB1 belongs to the endocannabinoid system that is important for many biological processes in different organs [139]. The main research focus in the past focused on the role of the endocannabinoid system the central nervous system [99]. With the increasing knowledge of the beneficial effects of modulating the endocannabinoid system, understanding the function of the system in various organs in health and disease has become an important research focus in the biomedical field. Recent studies have shown the involvement of CB1 in cardiovascular pathologies and that inhibition of CB1 may be beneficial and reduce the burden of atherosclerosis by reducing plaque formation [136, 140]. In addition, CB1 is known to have anti-inflammatory and anti-stress properties, making CB1 targeting a potential approach to control inflammation and reduce the incidence of cardiovascular disease [141, 142].

The aim of this thesis was to study the function of CB1 in hematopoiesis, which is a lifelong, highly regulated process that is responsible for the production of leukocytes [32]. It is directly related to atherosclerosis as activated hematopoietic progenitors produce more inflammatory leukocytes that accumulate within growing plaques [143]. In this context, the aim was to explore the role of CB1 in the regulation of hematopoiesis and the changes associated with CB1 deficiency during homeostasis and inflammation.

The key findings of this thesis are that CB1 regulates hematopoiesis under chronic and acute inflammatory conditions through effects on the bone marrow niche. CB1 deficiency was associated with a reduction in SCF and increased expression of CXCR4 on myeloid progenitors. After bone marrow transplantation, stromal CB1 was dispensable for hematopoietic reconstitution but had an effect myeloid progenitors. In the *Ldlr*$^{-/-}$ mouse model, peripheral CB1 antagonism increased the myeloid bias, indicating the peripheral involvement of CB1 expression in regulating hematopoiesis. Transcriptomic data show that CB1 is involved in the metabolism and oxidative phosphorylation of myeloid progenitors and that it affects a set of genes that are expressed under myeloid related transcription factors. *In vitro* inhibition of CB1 increased proliferation and decreased quiescence of LSK cells.

4.1 Role of CB1 in homeostatic hematopoiesis

HSCs reside inside the bone marrow niche, where various cells contribute to maintaining the homeostatic state of the hematopoietic system through signalling molecules and direct interactions. During homeostasis, HSCs are quiescent with a balanced self-renewal and differentiation between myeloid and lymphoid lineages. These characteristics ensure that the pool of HSCs is not depleted and can renew itself. To understand the role of CB1 in the regulation of hematopoiesis, a global *Cnr1* KO mouse model on a WT background was used. CB1 deficiency had minimal effect on mature myeloid cells in the blood or in the bone marrow.

Furthermore, at the level of hematopoietic stem and progenitor cells, we did not find any difference between *Cnr1* KO and WT control. However, blocking CB1 *in vitro* increased LSK proliferation by reducing quiescence and activating cells into the G2/M/S cell cycle phase. In line with these findings, cannabinoids and cannabinoid receptors have been linked to regulation of cell proliferation and apoptosis, mainly in studies focusing on neuronal development and cancer metastasis [144, 145].

HSPCs can be found at very low numbers in the blood, and their egress from the bone marrow into the circulation follows a circadian rhythm [146, 147]. Mobilization of HSPCs into the blood is of particular importance in the context of bone marrow transplantation and treatment of blood disorders. Various compounds have been developed to mobilize HSPCs into the blood, these molecules differ in the efficacy and also in the subpopulations of HSPCs mobilized [148, 149]. CB1 deficient males had more circulating LSK cells in the blood, while females had less functional LSK mobilized into the blood. This suggests a link between CB1 expression and the homing or retention of LSK cells in the niche. In addition, the effect of CB1 signalling on HSPCs appears to differ by sex. HSC mobilization has previously been reported in response to cannabinoids and in mice lacking the other cannabinoid receptor, *Cnr2*$^{-/-}$ [150].

GO ontology analysis of DEGs in stromal cells showed that *Cnr1* is associated with bone development and ossification, which is in agreement with previous findings [120-122]. CB1 is known to be important for bone homeostasis and remodelling as it is expressed on osteoblasts and osteoclasts, making it an indirect factor for the niche fitness and homeostasis that is important for maintenance of HSCs [122, 151]. Transcriptomic analysis of HSPCs revealed that CB1 regulates apoptosis, response to oxidative stress and oxidative phosphorylation, and is associated with myeloid differentiation, emergency granulopoiesis and inflammatory response transcription factors such as IRF1/8 or SPI1 and CEBPB [152-155]. It is known that metabolism and energy state of the HSCs control their quiescence and fate decisions [156]. Most HSCs are in a quiescent state where they have low ROS, more dependent on glycolysis and have low energy production. Activation of HSCs alters the metabolic state and may lead to epigenetic changes and lineage commitment [157, 158]. In summary, our transcriptomic data suggest that *Cnr1* deficiency disrupts the molecular homeostasis of the niche cells and alters the metabolism of HSPCs to a state that favors a bias toward the myeloid lineage, similar to the phenotype observed during aging, which is also supported by the GSEA results. However, given that only moderate effects were observed on mature myeloid cells in the blood or in the bone marrow, but not on HSPC counts, it can be speculated that the contribution of CB1 signaling in the regulation of homeostatic hematopoiesis is of minor importance and may be more relevant in inflammatory conditions.

4.2 Role of CB1 in hematopoiesis in diet-induced atherogenic inflammation

It has been reported that blocking CB1 signalling improves metabolic parameters and reduces the burden of atherosclerosis [136]. In global *Cnr1* KO mice on *Apoe*$^{-/-}$ background, we found conflicting results with an in increased plaque size compared to *Apoe*$^{-/-}$ controls. A more pronounced increase in circulating myeloid cells, mainly monocytes was detected after 4 weeks WD. This was accompanied by an increase in myeloid progenitors, particularly GMPs, suggesting that CB1 negatively regulates hypercholesterolemia-driven myelopoiesis. Under these conditions, CB1 deficiency also reduced the viability of LSKs and LKs and increased apoptosis. The effect on HSPC maintenance was associated with decreased levels of SCF in the niche and increased expression of *Icam-1*. This suggests that CB1 regulates HSPC responses to chronic inflammation by altering the expression of key factors in bone marrow niche cells.

4.3 Role of CB1 in hematopoiesis in low grade atherogenic inflammation under normal diet

Hematopoiesis in the absence of atherogenic diet was also studied in *Apoe*$^{-/-}$*Cnr1*$^{-/-}$ mice. Mice on *Apoe*$^{-/-}$ background exhibit elevated plasma cholesterol levels even without WD, although less pronounced [123], thereby triggering a chronic low grade inflammatory state. *Apoe*$^{-/-}$*Cnr1*$^{-/-}$ mice under normal diet had elevated myeloid cell counts and changes in HSPCs, mainly LT-HSCs. Under these conditions, no effect on viability or cell cycle distribution was evident. Differences between males and females were obvious, especially at the level of HSPCs, while mature cell counts were comparable. As observed under WD, the reduction in SCF levels in males was also evident without WD feeding. Mobilization of HSPCs into the blood is mainly controlled by the CXCL12/CXCR4 axis and the expression of adhesion molecules [159]. Gene expression of *Cxcr4* was higher in *Apoe*$^{-/-}$*Cnr1*$^{-/-}$ male bone marrow compared to sex-matched *Apoe*$^{-/-}$ control samples, while *Icam-1* was lower. CXCR4 belongs to the chemokine receptor family and regulates the maturation and egress of myeloid progenitors and mature myeloid cells from the bone marrow into the blood [160]. CB1 has previously been shown to regulate chemokine receptor expression in mature myeloid cells [136]. Our flow cytometry data demonstrated increased CXCR4 surface expression on myeloid and more committed granulocytic progenitors. Taken together, these findings suggest a regulation of myeloid lineage progenitor maturation and retention by CB1 signalling in this low grade inflammatory state, at least in male mice.

Cnr1 deficiency in females reduced the expression of *Lepr* and *Adipoq* genes without reaching significance, hinting to an effect on MSCs and adipocytes. Both cell types are important for the regulation of bone marrow hematopoiesis [161-163]. Despite some similarities between male

and female mice, regulation of hematopoiesis by CB1 appears to be partially sex specific. Sex differences were also observed in the analysis of neuronal innervation in the bone marrow. Female *Apoe*$^{-/-}$*Cnr1*$^{-/-}$ tended to have less TH+ and CGRP+ nerves, while no differences in the concentration of NE or CGRP levels in the bone marrow lavage were observed. However, the small sample size and variability render these results inconclusive. Previous studies have highlighted the involvement of neuronal cues in the regulation of hematopoiesis under stress and pathological conditions [64, 164], and it is possible that neuronal CB1 receptors negatively control these neuronal signals [165-167].

4.4 Lack of *Cnr1* in the bone marrow niche induces myeloid differentiation

Since hematopoiesis is influenced by both hematopoietic cells and cells forming the bone marrow niche, bone marrow transplantation experiments are useful to clarify the specific contribution of a genetic deficiency in hematopoietic versus stromal cells to hematopoiesis. *Cnr1* deficiency in stromal cells resulted in an increase in myeloid progenitors and mature myeloid cells in the femurs, when transplanted with *Cnr1*-expressing *Apoe*$^{-/-}$ bone marrow cells. However, circulating myeloid cells and plaque size were not different regardless of stromal *Cnr1* deficiency or not. It is conceivable that the 4 weeks WD time point was too short to observe monocytosis and changes in plaque size by sole stromal *Cnr1* deficiency, as observed in global *Apoe*$^{-/-}$*Cnr1*$^{-/-}$ mice at this time point.

Conversely, when transplanting *Cnr1*$^{-/-}$ deficient bone marrow cells into *Apoe*$^{-/-}$ mice with WT *Cnr1* expression in the stromal bone marrow niche, a more pronounced increase in circulating myeloid cells after 2 and 6 weeks compared to the corresponding control was observed. This indicates a crucial role for CB1 in HSPC expansion after lethal irradiation and bone marrow reconstitution. As mentioned above, inflammation increases myeloid progenitor differentiation to fulfil the demand of mobilized leukocytes into the circulation [168, 169]. After 4 weeks of WD, animals transplanted with *Cnr1*$^{-/-}$ bone marrow cells accumulated fewer myeloid progenitors compared to animals transplanted with *Cnr1*-expressing bone marrow cells. This suggests that *Cnr1* deficiency in HSPCs reduces the myeloid differentiation, which might indicate that blocking CB1 signalling in the hematopoietic compartment might be protective under certain chronic inflammatory conditions such as atherosclerosis, which are associated with an excessive production of monocytes.

4.5 *Cnr1* deficient HSPCs have competitive reconstitution disadvantage

Competitive bone marrow transplantation is useful to check if a genetic deficiency affects the ability of HSPCs to reconstitute the mature hematopoietic system after irradiation. Cells from different donors are mixed in similar proportions and injected into recipients where they

compete to reconstitute the hematopoietic system [170]. Despite the small sample size, our data show that recipients of *Cnr1*$^{-/-}$ HSPCs had less circulating monocytes with an accumulation of more monocytes in the femur. Besides, LK cells were more activated and this was associated with more GMP and CMP numbers in femurs. On the other hand, no differences in reconstitution proportions between *Apoe*$^{-/-}$ and *Apoe*$^{-/-}$*Cnr1*$^{-/-}$ cells were detected. These findings support our hypothesis that CB1 is important for hematopoiesis and the reconstitution of the hematopoietic system during inflammation, which can be triggered by infection, metabolic disease, or exposure to irradiation [171].

4.6 CB1 deficiency regulates myeloid progenitors under G-CSF stimulation

Inflammation can be sensed by the hematopoietic stem cell system through several molecular pathways [172, 173]. To study hematopoiesis in *Cnr1* KO mice in response to acute inflammation, G-CSF was injected for five constitutive days. Levels of G-CSF are normally low during homeostasis, but rapidly increase upon bacterial or fungal infection to induce neutrophil production [174-176]. The mobilization of HSPCs and mature myeloid cells into the blood in response to G-CSF was not affected by CB1 deficiency in males. WT females did not show a mobilization response to G-CSF, which was only observed in *Cnr1* KO females. Similarly, G-CSF-induced expansion of HSCPs was observed only in males, but not in females, with significantly stronger responses in *Cnr1*$^{-/-}$ males compared to WT males. Sexual dimorphism in response to G-CSF is not well understood, but sex hormones have been shown to regulate innate immune cells, with many genes involved in innate immune response located on the X chromosome [177]. Our findings suggest that acute bacterial or viral infections or other conditions that cause an acute increase in circulating G-CSF may accelerate myelopoiesis when CB1 is blocked.

4.7 Peripheral CB1 inhibition promotes myelopoiesis in hypercholesterolemia

Peripheral CB1 antagonists are currently being investigated in preclinical studies for their therapeutic benefits in metabolic disorders and atherosclerosis [142]. Therefore, it is important to understand whether chronic peripheral antagonism affects hematopoiesis. Peripheral blocking of CB1 increased the number of ST- HSCs and myeloid progenitors without affecting CXCL12 or SCF levels in the bone marrow niche. This suggests that peripheral CB1 antagonism is sufficient to induce hematopoietic progenitor expansion and highlights the importance of peripheral CB1 signalling in bone marrow hematopoiesis.

4.8 Limitations of the study

A major limitation of the study is that only global *Cnr1* mice were used, so specific cell types responsible for the effects remain unknown. To define the function of CB1 in each cell type,

Cnr1-floxed mice with cell-specific Cre promoter lines have to be used, for example, B6.129(Cg)-*Lepr*tm2(cre)Rck/J [178, 179] or B6.Cg-Tg(*Prrx1*-cre)1Cjt/J [180] to target MSCs, B6.Cg-Tg(*Col1a1*-creERT2)1Crm to target osteolineage cells [179, 181], B6.FVB-Tg(*Cdh5*-cre)7Mlia/J [179, 182] to target endothelial cells and B6.Cg-7630403G23RikTg(*Th*-cre)1Tmd/J [183] to target sympathetic neurons. Another limitation is that sex differences in the phenotype of *Cnr1* deficient mice have not been studied in detail. Although the effect of *Cnr1* deficiency on atherosclerosis development and mature myeloid cells under WD was comparable in both male and female mice, the effect on HSPCs and stromal niche factors was partially sex-dependent. In addition, the response to peripheral CB1 antagonism and bone marrow transplantation showed some differences between males and females, as well as the response to G-CSF injection.

There is also a technical limitation as there are only few *in vitro* assays that can be used to study HSCs, and the *in vitro* maturation differs from *in vivo* models as HSCs differentiate faster due to the higher oxygen concentration that induces differentiation. This makes bone marrow transplantation experiments the gold standard for studying the functionality of HSCs, but requires longer time periods for experiments.

Finally, a major limitation is that several data sets have small sample sizes or high variability, which makes data interpretation difficult. The limited sample size was due in part to delays in the breeding of the transgenic mouse lines.

4.9 Conclusion

This thesis explored the role of CB1 signalling in the regulation of bone marrow hematopoiesis. The main conclusion is that CB1 is involved in the regulation of the metabolic state of myeloid progenitors which affects myeloid differentiation and transcription factors linked to inflammatory responses. A more prominent effect of *Cnr1* deficiency on hematopoiesis was noticed under acute and chronic inflammatory conditions compared to homeostatic hematopoiesis. Myeloid bias with enhanced production of myeloid progenitors were due to the lack of *Cnr1* in the stromal bone marrow niche. *Cnr1* deficiency decreased stem cell factor levels which is an important cytokine that is important for HSC maintenance. CB1 also affected CXCR4 chemokine receptor expression. In competitive transplantation experiments, recipients of CB1 deficient bone marrow cells tended to accumulate more monocyte, CMP and GMP in the femur. Further studies are needed to dissect which cells of the hematopoietic bone marrow compartment require CB1 expression. In addition, more studies in the inflammatory context are warranted to specify which molecular pathways underlie the observed phenotype of enhanced myelopoiesis in the absence of *Cnr1*.

References

1. Poller, W.C., M. Nahrendorf, and F.K. Swirski, *Hematopoiesis and Cardiovascular Disease.* Circ Res, 2020. **126**(8): p. 1061-1085.10.1161/CIRCRESAHA.120.315895
2. Alves-Silva, J.M., et al., *The Role of Essential Oils and Their Main Compounds in the Management of Cardiovascular Disease Risk Factors.* Molecules, 2021. **26**(12).10.3390/molecules26123506
3. Schloss, M.J., F.K. Swirski, and M. Nahrendorf, *Modifiable Cardiovascular Risk, Hematopoiesis, and Innate Immunity.* Circ Res, 2020. **126**(9): p. 1242-1259.10.1161/CIRCRESAHA.120.315936
4. Henein, M.Y., et al., *The Role of Inflammation in Cardiovascular Disease.* Int J Mol Sci, 2022. **23**(21).10.3390/ijms232112906
5. Thakkar, A., A. Agarwala, and E.D. Michos, *Secondary Prevention of Cardiovascular Disease in Women: Closing the Gap.* Eur Cardiol, 2021. **16**: p. e41.10.15420/ecr.2021.24
6. Herrington, W., et al., *Epidemiology of Atherosclerosis and the Potential to Reduce the Global Burden of Atherothrombotic Disease.* Circ Res, 2016. **118**(4): p. 535-46.10.1161/CIRCRESAHA.115.307611
7. Boyalla, V., E. Gallego-Colon, and M. Spartalis, *Immunity and inflammation in cardiovascular disorders.* BMC Cardiovasc Disord, 2023. **23**(1): p. 148.10.1186/s12872-023-03185-z
8. Pothineni, N.V.K., et al., *Infections, atherosclerosis, and coronary heart disease.* Eur Heart J, 2017. **38**(43): p. 3195-3201.10.1093/eurheartj/ehx362
9. Rollins, B.J., et al., *Cytokine-activated human endothelial cells synthesize and secrete a monocyte chemoattractant, MCP-1/JE.* Am J Pathol, 1990. **136**(6): p. 1229-33. PMID: 2113354
10. Theofilis, P., et al., *Inflammatory Mechanisms Contributing to Endothelial Dysfunction.* Biomedicines, 2021. **9**(7): p. 781.10.3390/biomedicines9070781
11. Flynn, M.C., et al., *Monocytes, Macrophages, and Metabolic Disease in Atherosclerosis.* Front Pharmacol, 2019. **10**: p. 666.10.3389/fphar.2019.00666
12. Puylaert, P., et al., *Regulated Necrosis in Atherosclerosis.* Arterioscler Thromb Vasc Biol, 2022. **42**(11): p. 1283-1306.10.1161/ATVBAHA.122.318177
13. Beck-Joseph, J., M. Tabrizian, and S. Lehoux, *Molecular Interactions Between Vascular Smooth Muscle Cells and Macrophages in Atherosclerosis.* Front Cardiovasc Med, 2021. **8**: p. 737934.10.3389/fcvm.2021.737934
14. Wang, S., et al., *Advances in Atherosclerosis Theranostics Harnessing Iron Oxide-Based Nanoparticles.* Adv Sci (Weinh), 2024. **11**(17): p. e2308298.10.1002/advs.202308298
15. Hansson, G.K. and A. Hermansson, *The immune system in atherosclerosis.* Nat Immunol, 2011. **12**(3): p. 204-12.10.1038/ni.2001
16. Drechsler, M., J. Duchene, and O. Soehnlein, *Chemokines control mobilization, recruitment, and fate of monocytes in atherosclerosis.* Arterioscler Thromb Vasc Biol, 2015. **35**(5): p. 1050-5.10.1161/ATVBAHA.114.304649
17. van der Vorst, E.P., Y. Doring, and C. Weber, *Chemokines and their receptors in Atherosclerosis.* J Mol Med (Berl), 2015. **93**(9): p. 963-71.10.1007/s00109-015-1317-8
18. Boring, L., et al., *Decreased lesion formation in CCR2-/- mice reveals a role for chemokines in the initiation of atherosclerosis.* Nature, 1998. **394**(6696): p. 894-7.10.1038/29788
19. Saederup, N., et al., *Fractalkine deficiency markedly reduces macrophage accumulation and atherosclerotic lesion formation in CCR2-/- mice: evidence for independent chemokine functions in atherogenesis.* Circulation, 2008. **117**(13): p. 1642-8.10.1161/CIRCULATIONAHA.107.743872
20. Medrano-Bosch, M., et al., *Monocyte-endothelial cell interactions in vascular and tissue remodeling.* Front Immunol, 2023. **14**: p. 1196033.10.3389/fimmu.2023.1196033
21. Rahaman, S.O., et al., *A CD36-dependent signaling cascade is necessary for macrophage foam cell formation.* Cell Metab, 2006. **4**(3): p. 211-21.10.1016/j.cmet.2006.06.007

22. Febbraio, M., et al., *Targeted disruption of the class B scavenger receptor CD36 protects against atherosclerotic lesion development in mice.* J Clin Invest, 2000. **105**(8): p. 1049-56.10.1172/JCI9259
23. Brinkmann, V., et al., *Neutrophil extracellular traps kill bacteria.* Science, 2004. **303**(5663): p. 1532-5.10.1126/science.1092385
24. Zhang, X., et al., *Role of neutrophils in different stages of atherosclerosis.* Innate Immun, 2023. **29**(6): p. 97-109.10.1177/17534259231189195
25. Doring, Y., O. Soehnlein, and C. Weber, *Neutrophil Extracellular Traps in Atherosclerosis and Atherothrombosis.* Circ Res, 2017. **120**(4): p. 736-743.10.1161/CIRCRESAHA.116.309692
26. Ammirati, E., et al., *The role of T and B cells in human atherosclerosis and atherothrombosis.* Clin Exp Immunol, 2015. **179**(2): p. 173-87.10.1111/cei.12477
27. Wigren, M., et al., *Lack of Ability to Present Antigens on Major Histocompatibility Complex Class II Molecules Aggravates Atherosclerosis in ApoE(-/-) Mice.* Circulation, 2019. **139**(22): p. 2554-2566.10.1161/CIRCULATIONAHA.118.039288
28. Saigusa, R., H. Winkels, and K. Ley, *T cell subsets and functions in atherosclerosis.* Nat Rev Cardiol, 2020. **17**(7): p. 387-401.10.1038/s41569-020-0352-5
29. Robertson, A.K. and G.K. Hansson, *T cells in atherogenesis: for better or for worse?* Arterioscler Thromb Vasc Biol, 2006. **26**(11): p. 2421-32.10.1161/01.ATV.0000245830.29764.84
30. Taylor, J.A., et al., *Antibodies in action: the role of humoral immunity in the fight against atherosclerosis.* Immun Ageing, 2022. **19**(1): p. 59.10.1186/s12979-022-00316-6
31. Perry, H.M., T.P. Bender, and C.A. McNamara, *B cell subsets in atherosclerosis.* Front Immunol, 2012. **3**: p. 373.10.3389/fimmu.2012.00373
32. Chotinantakul, K. and W. Leeanansaksiri, *Hematopoietic stem cell development, niches, and signaling pathways.* Bone Marrow Res, 2012. **2012**: p. 270425.10.1155/2012/270425
33. Yin, T. and L. Li, *The stem cell niches in bone.* J Clin Invest, 2006. **116**(5): p. 1195-201.10.1172/JCI28568
34. Johns, J.L. and M.M. Christopher, *Extramedullary hematopoiesis: a new look at the underlying stem cell niche, theories of development, and occurrence in animals.* Vet Pathol, 2012. **49**(3): p. 508-23.10.1177/0300985811432344
35. Zhang, P., et al., *The physical microenvironment of hematopoietic stem cells and its emerging roles in engineering applications.* Stem Cell Res Ther, 2019. **10**(1): p. 327.10.1186/s13287-019-1422-7
36. Mayer, I.M., et al. *Isolation, Maintenance and Expansion of Adult Hematopoietic Stem/Progenitor Cells and Leukemic Stem Cells*. Cancers, 2022. **14**, DOI: 10.3390/cancers14071723.
37. Oguro, H., L. Ding, and S.J. Morrison, *SLAM family markers resolve functionally distinct subpopulations of hematopoietic stem cells and multipotent progenitors.* Cell Stem Cell, 2013. **13**(1): p. 102-16.10.1016/j.stem.2013.05.014
38. Pietras, E.M., et al., *Functionally Distinct Subsets of Lineage-Biased Multipotent Progenitors Control Blood Production in Normal and Regenerative Conditions.* Cell Stem Cell, 2015. **17**(1): p. 35-46.10.1016/j.stem.2015.05.003
39. Cabezas-Wallscheid, N., et al., *Identification of regulatory networks in HSCs and their immediate progeny via integrated proteome, transcriptome, and DNA methylome analysis.* Cell Stem Cell, 2014. **15**(4): p. 507-522.10.1016/j.stem.2014.07.005
40. Kang, Y.A., et al., *Secretory MPP3 reinforce myeloid differentiation trajectory and amplify myeloid cell production.* J Exp Med, 2023. **220**(8): p. e20230088.10.1084/jem.20230088
41. Paul, F., et al., *Transcriptional Heterogeneity and Lineage Commitment in Myeloid Progenitors.* Cell, 2015. **163**(7): p. 1663-77.10.1016/j.cell.2015.11.013
42. Akashi, K., et al., *A clonogenic common myeloid progenitor that gives rise to all myeloid lineages.* Nature, 2000. **404**(6774): p. 193-7.10.1038/35004599
43. Cheng, H., Z. Zheng, and T. Cheng, *New paradigms on hematopoietic stem cell differentiation.* Protein Cell, 2020. **11**(1): p. 34-44.10.1007/s13238-019-0633-0

44. Oh, I.H. and K.R. Kwon, *Concise review: multiple niches for hematopoietic stem cell regulations.* Stem Cells, 2010. **28**(7): p. 1243-9.10.1002/stem.453
45. Le, P.M., M. Andreeff, and V.L. Battula, *Osteogenic niche in the regulation of normal hematopoiesis and leukemogenesis.* Haematologica, 2018. **103**(12): p. 1945-1955.10.3324/haematol.2018.197004
46. Sendker, S., K. Waack, and D. Reinhardt, *Far from Health: The Bone Marrow Microenvironment in AML, A Leukemia Supportive Shelter.* Children (Basel), 2021. **8**(5).10.3390/children8050371
47. Lazzari, E. and J.M. Butler, *The Instructive Role of the Bone Marrow Niche in Aging and Leukemia.* Curr Stem Cell Rep, 2018. **4**(4): p. 291-298.10.1007/s40778-018-0143-7
48. Boulais, P.E. and P.S. Frenette, *Making sense of hematopoietic stem cell niches.* Blood, 2015. **125**(17): p. 2621-9.10.1182/blood-2014-09-570192
49. Kulkarni, R. and V. Kale, *Physiological Cues Involved in the Regulation of Adhesion Mechanisms in Hematopoietic Stem Cell Fate Decision.* Front Cell Dev Biol, 2020. **8**: p. 611.10.3389/fcell.2020.00611
50. Karpova, D. and H. Bonig, *Concise Review: CXCR4/CXCL12 Signaling in Immature Hematopoiesis--Lessons From Pharmacological and Genetic Models.* Stem Cells, 2015. **33**(8): p. 2391-9.10.1002/stem.2054
51. Maryanovich, M., S. Takeishi, and P.S. Frenette, *Neural Regulation of Bone and Bone Marrow.* Cold Spring Harb Perspect Med, 2018. **8**(9): p. a031344.10.1101/cshperspect.a031344
52. Gao, X., et al., *Nociceptive nerves regulate haematopoietic stem cell mobilization.* Nature, 2021. **589**(7843): p. 591-596.10.1038/s41586-020-03057-y
53. Peci, F., et al., *The cellular composition and function of the bone marrow niche after allogeneic hematopoietic cell transplantation.* Bone Marrow Transplant, 2022. **57**(9): p. 1357-1364.10.1038/s41409-022-01728-0
54. Poulos, M.G., et al., *Endothelial Jagged-1 is necessary for homeostatic and regenerative hematopoiesis.* Cell Rep, 2013. **4**(5): p. 1022-34.10.1016/j.celrep.2013.07.048
55. Guo, P., et al., *Endothelial jagged-2 sustains hematopoietic stem and progenitor reconstitution after myelosuppression.* J Clin Invest, 2017. **127**(12): p. 4242-4256.10.1172/JCI92309
56. Morrison, S.J. and D.T. Scadden, *The bone marrow niche for haematopoietic stem cells.* Nature, 2014. **505**(7483): p. 327-34.10.1038/nature12984
57. Aprile, A., et al., *Targeting the Hematopoietic Stem Cell Niche in beta-Thalassemia and Sickle Cell Disease.* Pharmaceuticals (Basel), 2022. **15**(5): p. 592.10.3390/ph15050592
58. Fielding, C. and S. Mendez-Ferrer, *Neuronal regulation of bone marrow stem cell niches.* F1000Res, 2020. **9**.10.12688/f1000research.22554.1
59. Mendez-Ferrer, S., et al., *Haematopoietic stem cell release is regulated by circadian oscillations.* Nature, 2008. **452**(7186): p. 442-7.10.1038/nature06685
60. Kim, E.J. and J.J. Kim, *Neurocognitive effects of stress: a metaparadigm perspective.* Mol Psychiatry, 2023. **28**(7): p. 2750-2763.10.1038/s41380-023-01986-4
61. Hollins, S.L. and D.M. Hodgson, *Stress, microbiota, and immunity.* Current Opinion in Behavioral Sciences, 2019. **28**: p. 66-71.10.1016/j.cobeha.2019.01.015
62. Vignjevic Petrinovic, S., et al., *Interplay between stress and cancer-A focus on inflammation.* Front Physiol, 2023. **14**: p. 1119095.10.3389/fphys.2023.1119095
63. Popovic, D., et al., *Defining the importance of stress reduction in managing cardiovascular disease - the role of exercise.* Prog Cardiovasc Dis, 2022. **70**: p. 84-93.10.1016/j.pcad.2022.01.008
64. Heidt, T., et al., *Chronic variable stress activates hematopoietic stem cells.* Nat Med, 2014. **20**(7): p. 754-758.10.1038/nm.3589
65. McKim, D.B., et al., *Social Stress Mobilizes Hematopoietic Stem Cells to Establish Persistent Splenic Myelopoiesis.* Cell Rep, 2018. **25**(9): p. 2552-2562 e3.10.1016/j.celrep.2018.10.102
66. Nahrendorf, M. and F.K. Swirski, *Lifestyle effects on hematopoiesis and atherosclerosis.* Circ Res, 2015. **116**(5): p. 884-94.10.1161/CIRCRESAHA.116.303550

67. Stein, A., et al., *Clonal hematopoiesis and cardiovascular disease: deciphering interconnections.* Basic Res Cardiol, 2022. **117**(1): p. 55.10.1007/s00395-022-00969-w
68. Jaiswal, S., et al., *Age-related clonal hematopoiesis associated with adverse outcomes.* N Engl J Med, 2014. **371**(26): p. 2488-98.10.1056/NEJMoa1408617
69. Solary, E., et al., *The Ten-Eleven Translocation-2 (TET2) gene in hematopoiesis and hematopoietic diseases.* Leukemia, 2014. **28**(3): p. 485-96.10.1038/leu.2013.337
70. Fuster, J.J., et al., *Clonal hematopoiesis associated with TET2 deficiency accelerates atherosclerosis development in mice.* Science, 2017. **355**(6327): p. 842-847.10.1126/science.aag1381
71. Heyde, A., et al., *Increased stem cell proliferation in atherosclerosis accelerates clonal hematopoiesis.* Cell, 2021. **184**(5): p. 1348-1361 e22.10.1016/j.cell.2021.01.049
72. Haring, B., S. Wissel, and J.E. Manson, *Somatic Mutations and Clonal Hematopoiesis as Drivers of Age-Related Cardiovascular Risk.* Curr Cardiol Rep, 2022. **24**(8): p. 1049-1058.10.1007/s11886-022-01724-2
73. McAlpine, C.S., et al., *Sleep modulates haematopoiesis and protects against atherosclerosis.* Nature, 2019. **566**(7744): p. 383-387.10.1038/s41586-019-0948-2
74. Frodermann, V., et al., *Exercise reduces inflammatory cell production and cardiovascular inflammation via instruction of hematopoietic progenitor cells.* Nat Med, 2019. **25**(11): p. 1761-1771.10.1038/s41591-019-0633-x
75. Morgan, P.K., et al., *Hematopoiesis is regulated by cholesterol efflux pathways and lipid rafts: connections with cardiovascular diseases.* J Lipid Res, 2020. **61**(5): p. 667-675.10.1194/jlr.TR119000267
76. Yvan-Charvet, L., et al., *ATP-binding cassette transporters and HDL suppress hematopoietic stem cell proliferation.* Science, 2010. **328**(5986): p. 1689-93.10.1126/science.1189731
77. Westerterp, M., et al., *Regulation of hematopoietic stem and progenitor cell mobilization by cholesterol efflux pathways.* Cell Stem Cell, 2012. **11**(2): p. 195-206.10.1016/j.stem.2012.04.024
78. Dutta, P., et al., *Myocardial infarction accelerates atherosclerosis.* Nature, 2012. **487**(7407): p. 325-9.10.1038/nature11260
79. Rohde, D., et al., *Bone marrow endothelial dysfunction promotes myeloid cell expansion in cardiovascular disease.* Nat Cardiovasc Res, 2022. **1**(1): p. 28-44.10.1038/s44161-021-00002-8
80. Pietras, E.M., *Inflammation: a key regulator of hematopoietic stem cell fate in health and disease.* Blood, 2017. **130**(15): p. 1693-1698.10.1182/blood-2017-06-780882
81. Hormaechea-Agulla, D., D.T. Le, and K.Y. King, *Common Sources of Inflammation and Their Impact on Hematopoietic Stem Cell Biology.* Curr Stem Cell Rep, 2020. **6**(3): p. 96-107.10.1007/s40778-020-00177-z
82. Baldridge, M.T., et al., *Quiescent haematopoietic stem cells are activated by IFN-gamma in response to chronic infection.* Nature, 2010. **465**(7299): p. 793-7.10.1038/nature09135
83. Wang, J., M. Erlacher, and J. Fernandez-Orth, *The role of inflammation in hematopoiesis and bone marrow failure: What can we learn from mouse models?* Front Immunol, 2022. **13**: p. 951937.10.3389/fimmu.2022.951937
84. Schultze, J.L., E. Mass, and A. Schlitzer, *Emerging Principles in Myelopoiesis at Homeostasis and during Infection and Inflammation.* Immunity, 2019. **50**(2): p. 288-301.10.1016/j.immuni.2019.01.019
85. Xu, Y., A.J. Murphy, and A.J. Fleetwood, *Hematopoietic Progenitors and the Bone Marrow Niche Shape the Inflammatory Response and Contribute to Chronic Disease.* Int J Mol Sci, 2022. **23**(4): p. 2234.10.3390/ijms23042234
86. Bowers, E. and K. Singer, *Obesity-induced inflammation: The impact of the hematopoietic stem cell niche.* JCI Insight, 2021. **6**(3): p. e145295.10.1172/jci.insight.145295

87. Griffin, C., et al., *TLR4, TRIF, and MyD88 are essential for myelopoiesis and CD11c(+) adipose tissue macrophage production in obese mice.* J Biol Chem, 2018. **293**(23): p. 8775-8786.10.1074/jbc.RA117.001526
88. Saberi, M., et al., *Hematopoietic cell-specific deletion of toll-like receptor 4 ameliorates hepatic and adipose tissue insulin resistance in high-fat-fed mice.* Cell Metab, 2009. **10**(5): p. 419-29.10.1016/j.cmet.2009.09.006
89. Benova, A. and M. Tencerova, *Obesity-Induced Changes in Bone Marrow Homeostasis.* Front Endocrinol (Lausanne), 2020. **11**: p. 294.10.3389/fendo.2020.00294
90. Tie, G., et al., *Hypercholesterolemia induces oxidant stress that accelerates the ageing of hematopoietic stem cells.* J Am Heart Assoc, 2014. **3**(1): p. e000241.10.1161/JAHA.113.000241
91. Alfulaij, N., et al., *Cannabinoids, the Heart of the Matter.* J Am Heart Assoc, 2018. **7**(14): p. e009099.10.1161/JAHA.118.009099
92. Matsuda, L.A., et al., *Structure of a cannabinoid receptor and functional expression of the cloned cDNA.* Nature, 1990. **346**(6284): p. 561-4.10.1038/346561a0
93. Rinaldi-Carmona, M., et al., *Characterization of two cloned human CB1 cannabinoid receptor isoforms.* J Pharmacol Exp Ther, 1996. **278**(2): p. 871-8. PMID: 8768742
94. Kendall, D.A. and G.A. Yudowski, *Cannabinoid Receptors in the Central Nervous System: Their Signaling and Roles in Disease.* Front Cell Neurosci, 2016. **10**(294): p. 294.10.3389/fncel.2016.00294
95. Walsh, K.B. and H.K. Andersen, *Molecular Pharmacology of Synthetic Cannabinoids: Delineating CB1 Receptor-Mediated Cell Signaling.* Int J Mol Sci, 2020. **21**(17): p. 6115.10.3390/ijms21176115
96. Garcia-Arencibia, M., E. Molina-Holgado, and F. Molina-Holgado, *Effect of endocannabinoid signalling on cell fate: life, death, differentiation and proliferation of brain cells.* Br J Pharmacol, 2019. **176**(10): p. 1361-1369.10.1111/bph.14369
97. Bernard, C., et al., *Altering cannabinoid signaling during development disrupts neuronal activity.* Proc Natl Acad Sci U S A, 2005. **102**(26): p. 9388-93.10.1073/pnas.0409641102
98. Begbie, J., P. Doherty, and A. Graham, *Cannabinoid receptor, CB1, expression follows neuronal differentiation in the early chick embryo.* J Anat, 2004. **205**(3): p. 213-8.10.1111/j.0021-8782.2004.00325.x
99. Fernandez-Moncada, I., et al., *An enquiry to the role of CB1 receptors in neurodegeneration.* Neurobiol Dis, 2023. **184**: p. 106235.10.1016/j.nbd.2023.106235
100. Berry, A.J., et al., *Endocannabinoid system alterations in Alzheimer's disease: A systematic review of human studies.* Brain Res, 2020. **1749**: p. 147135.10.1016/j.brainres.2020.147135
101. Tibirica, E., *The multiple functions of the endocannabinoid system: a focus on the regulation of food intake.* Diabetol Metab Syndr, 2010. **2**(1): p. 5.10.1186/1758-5996-2-5
102. Osei-Hyiaman, D., et al., *Endocannabinoid activation at hepatic CB1 receptors stimulates fatty acid synthesis and contributes to diet-induced obesity.* J Clin Invest, 2005. **115**(5): p. 1298-305.10.1172/JCI23057
103. Senin, L.L., et al., *The gastric CB1 receptor modulates ghrelin production through the mTOR pathway to regulate food intake.* PLoS One, 2013. **8**(11): p. e80339.10.1371/journal.pone.0080339
104. Ruiz de Azua, I., et al., *Adipocyte cannabinoid receptor CB1 regulates energy homeostasis and alternatively activated macrophages.* J Clin Invest, 2017. **127**(11): p. 4148-4162.10.1172/JCI83626
105. Osei-Hyiaman, D., et al., *The role of the endocannabinoid system in the control of energy homeostasis.* Int J Obes (Lond), 2006. **30 Suppl 1**(1): p. S33-8.10.1038/sj.ijo.0803276
106. Tam, J., et al., *Peripheral cannabinoid-1 receptor blockade restores hypothalamic leptin signaling.* Mol Metab, 2017. **6**(10): p. 1113-1125.10.1016/j.molmet.2017.06.010
107. Chakravarti, B., J. Ravi, and R.K. Ganju, *Cannabinoids as therapeutic agents in cancer: current status and future implications.* Oncotarget, 2014. **5**(15): p. 5852-72.10.18632/oncotarget.2233

108. Wiley, J.L., et al., *CB1 cannabinoid receptor-mediated modulation of food intake in mice.* Br J Pharmacol, 2005. **145**(3): p. 293-300.10.1038/sj.bjp.0706157
109. Tam, J., et al., *Peripheral CB1 cannabinoid receptor blockade improves cardiometabolic risk in mouse models of obesity.* J Clin Invest, 2010. **120**(8): p. 2953-66.10.1172/JCI42551
110. Pacher, P. and S. Steffens, *The emerging role of the endocannabinoid system in cardiovascular disease.* Semin Immunopathol, 2009. **31**(1): p. 63-77.10.1007/s00281-009-0145-8
111. Gatta-Cherifi, B. and D. Cota, *New insights on the role of the endocannabinoid system in the regulation of energy balance.* Int J Obes (Lond), 2016. **40**(2): p. 210-9.10.1038/ijo.2015.179
112. Hourani, W. and S.P.H. Alexander, *Cannabinoid ligands, receptors and enzymes: Pharmacological tools and therapeutic potential.* Brain Neurosci Adv, 2018. **2**: p. 2398212818783908.10.1177/2398212818783908
113. Forsythe, M.L. and A.J. Boileau, *Use of cannabinoids for the treatment of patients with post-traumatic stress disorder.* J Basic Clin Physiol Pharmacol, 2021. **33**(2): p. 121-132.10.1515/jbcpp-2020-0279
114. Gelfand, E.V. and C.P. Cannon, *Rimonabant: a selective blocker of the cannabinoid CB1 receptors for the management of obesity, smoking cessation and cardiometabolic risk factors.* Expert Opin Investig Drugs, 2006. **15**(3): p. 307-15.10.1517/13543784.15.3.307
115. Dol-Gleizes, F., et al., *Rimonabant, a selective cannabinoid CB1 receptor antagonist, inhibits atherosclerosis in LDL receptor-deficient mice.* Arterioscler Thromb Vasc Biol, 2009. **29**(1): p. 12-8.10.1161/ATVBAHA.108.168757
116. Guillamat-Prats, R., et al., *Endocannabinoid Signalling in Atherosclerosis and Related Metabolic Complications.* Thromb Haemost, 2019. **119**(4): p. 567-575.10.1055/s-0039-1678738
117. Jiang, S., Y. Fu, and H.K. Avraham, *Regulation of hematopoietic stem cell trafficking and mobilization by the endocannabinoid system.* Transfusion, 2011. **51 Suppl 4**: p. 65S-71S.10.1111/j.1537-2995.2011.03368.x
118. Patinkin, D., et al., *Endocannabinoids as positive or negative factors in hematopoietic cell migration and differentiation.* Eur J Pharmacol, 2008. **595**(1-3): p. 1-6.10.1016/j.ejphar.2008.05.002
119. Hoggatt, J. and L.M. Pelus, *Eicosanoid regulation of hematopoiesis and hematopoietic stem and progenitor trafficking.* Leukemia, 2010. **24**(12): p. 1993-2002.10.1038/leu.2010.216
120. Tam, J., et al., *The cannabinoid CB1 receptor regulates bone formation by modulating adrenergic signaling.* FASEB J, 2008. **22**(1): p. 285-94.10.1096/fj.06-7957com
121. Bab, I. and A. Zimmer, *Cannabinoid receptors and the regulation of bone mass.* Br J Pharmacol, 2008. **153**(2): p. 182-8.10.1038/sj.bjp.0707593
122. Idris, A.I., et al., *Cannabinoid receptor type 1 protects against age-related osteoporosis by regulating osteoblast and adipocyte differentiation in marrow stromal cells.* Cell Metab, 2009. **10**(2): p. 139-47.10.1016/j.cmet.2009.07.006
123. Zhang, S.H., et al., *Spontaneous hypercholesterolemia and arterial lesions in mice lacking apolipoprotein E.* Science, 1992. **258**(5081): p. 468-71.10.1126/science.1411543
124. Gistera, A., et al., *Animal Models of Atherosclerosis-Supportive Notes and Tricks of the Trade.* Circ Res, 2022. **130**(12): p. 1869-1887.10.1161/CIRCRESAHA.122.320263
125. Ali, K., et al., *Apolipoprotein E suppresses the type I inflammatory response in vivo.* Circ Res, 2005. **97**(9): p. 922-7.10.1161/01.RES.0000187467.67684.43
126. Murphy, A.J., et al., *ApoE regulates hematopoietic stem cell proliferation, monocytosis, and monocyte accumulation in atherosclerotic lesions in mice.* J Clin Invest, 2011. **121**(10): p. 4138-49.10.1172/JCI57559
127. Ishibashi, S., et al., *Massive xanthomatosis and atherosclerosis in cholesterol-fed low density lipoprotein receptor-negative mice.* J Clin Invest, 1994. **93**(5): p. 1885-93.10.1172/JCI117179
128. Oppi, S., T.F. Luscher, and S. Stein, *Mouse Models for Atherosclerosis Research-Which Is My Line?* Front Cardiovasc Med, 2019. **6**: p. 46.10.3389/fcvm.2019.00046

129. Zimmer, A., et al., *Increased mortality, hypoactivity, and hypoalgesia in cannabinoid CB1 receptor knockout mice.* Proc Natl Acad Sci U S A, 1999. **96**(10): p. 5780-5.10.1073/pnas.96.10.5780
130. Percie du Sert, N., et al., *The ARRIVE guidelines 2.0: Updated guidelines for reporting animal research.* PLoS Biol, 2020. **18**(7): p. e3000410.10.1371/journal.pbio.3000410
131. Zheng, G.X., et al., *Massively parallel digital transcriptional profiling of single cells.* Nat Commun, 2017. **8**(1): p. 14049.10.1038/ncomms14049
132. Hao, Y., et al., *Integrated analysis of multimodal single-cell data.* Cell, 2021. **184**(13): p. 3573-3587 e29.10.1016/j.cell.2021.04.048
133. Dahlin, J.S., et al., *A single-cell hematopoietic landscape resolves 8 lineage trajectories and defects in Kit mutant mice.* Blood, 2018. **131**(21): p. e1-e11.10.1182/blood-2017-12-821413
134. Hétu-Arbour, R., S. Bouali, and K.M. Heinonen, *Experimental Competitive Bone Marrow Transplant Assays*, in *Leukemia Stem Cells: Methods and Protocols*, C. Cobaleda and I. Sánchez-García, Editors. 2021, Springer US: New York, NY. p. 195-214.10.1007/978-1-0716-0810-4_12
135. Chen, B., et al., *Endothelial cannabinoid CB1 receptor deficiency reduces arterial inflammation and lipid uptake in response to atheroprone shear stress.* bioRxiv, 2024: p. 2024.05.15.594375.10.1101/2024.05.15.594375
136. Wang, Y., et al., *Myeloid cannabinoid CB1 receptor deletion confers atheroprotection in male mice by reducing macrophage proliferation in a sex-dependent manner.* Cardiovasc Res, 2024. **120**(12): p. 1411-1426.10.1093/cvr/cvae125
137. Singh, P. and S.A. Ali, *Multifunctional Role of S100 Protein Family in the Immune System: An Update.* Cells, 2022. **11**(15): p. 2274.10.3390/cells11152274
138. Lockhart, J.S. and R. Sumagin, *Non-Canonical Functions of Myeloperoxidase in Immune Regulation, Tissue Inflammation and Cancer.* Int J Mol Sci, 2022. **23**(20): p. 12250.10.3390/ijms232012250
139. Zou, S. and U. Kumar *Cannabinoid Receptors and the Endocannabinoid System: Signaling and Function in the Central Nervous System*. International Journal of Molecular Sciences, 2018. **19**, DOI: 10.3390/ijms19030833.
140. Sugamura, K., et al., *Cannabinoid 1 receptor blockade reduces atherosclerosis with enhances reverse cholesterol transport.* J Atheroscler Thromb, 2010. **17**(2): p. 141-7.10.5551/jat.2865
141. Crowe, M.S., et al., *The endocannabinoid system modulates stress, emotionality, and inflammation.* Brain Behav Immun, 2014. **42**: p. 1-5.10.1016/j.bbi.2014.06.007
142. Eid, B.G., *Cannabinoids for Treating Cardiovascular Disorders: Putting Together a Complex Puzzle.* J Microsc Ultrastruct, 2018. **6**(4): p. 171-176.10.4103/JMAU.JMAU_42_18
143. Kong, P., et al., *Inflammation and atherosclerosis: signaling pathways and therapeutic intervention.* Signal Transduct Target Ther, 2022. **7**(1): p. 131.10.1038/s41392-022-00955-7
144. Bockmann, E.C., et al., *The Role of Cannabinoids in CNS Development: Focus on Proliferation and Cell Death.* Cell Mol Neurobiol, 2023. **43**(4): p. 1469-1485.10.1007/s10571-022-01263-y
145. Pennant, N.M. and C.V. Hinton, *The evolution of cannabinoid receptors in cancer.* WIREs Mech Dis, 2023. **15**(4): p. e1602.10.1002/wsbm.1602
146. Mende, N. and E. Laurenti, *Hematopoietic stem and progenitor cells outside the bone marrow: where, when, and why.* Exp Hematol, 2021. **104**: p. 9-16.10.1016/j.exphem.2021.10.002
147. Mendez-Ferrer, S., et al., *Circadian rhythms influence hematopoietic stem cells.* Curr Opin Hematol, 2009. **16**(4): p. 235-42.10.1097/MOH.0b013e32832bd0f5
148. Domingues, M.J., S.K. Nilsson, and B. Cao, *New agents in HSC mobilization.* Int J Hematol, 2017. **105**(2): p. 141-152.10.1007/s12185-016-2156-2
149. Luo, C., et al., *Comparison of the efficacy of hematopoietic stem cell mobilization regimens: a systematic review and network meta-analysis of preclinical studies.* Stem Cell Res Ther, 2021. **12**(1): p. 310.10.1186/s13287-021-02379-6
150. Jiang, S., et al., *Cannabinoid receptor 2 and its agonists mediate hematopoiesis and hematopoietic stem and progenitor cell mobilization.* Blood, 2011. **117**(3): p. 827-38.10.1182/blood-2010-01-265082

151. Xiao, Y., et al., *Interoceptive regulation of skeletal tissue homeostasis and repair.* Bone Res, 2023. **11**(1): p. 48.10.1038/s41413-023-00285-6
152. Hirai, H., et al., *Non-steady-state hematopoiesis regulated by the C/EBPbeta transcription factor.* Cancer Sci, 2015. **106**(7): p. 797-802.10.1111/cas.12690
153. Friedman, A.D., *Transcriptional control of granulocyte and monocyte development.* Oncogene, 2007. **26**(47): p. 6816-28.10.1038/sj.onc.1210764
154. Bonifer, C., et al., *How transcription factors program chromatin--lessons from studies of the regulation of myeloid-specific genes.* Semin Immunol, 2008. **20**(4): p. 257-63.10.1016/j.smim.2008.05.001
155. Wang, L., et al., *The multiple roles of interferon regulatory factor family in health and disease.* Signal Transduct Target Ther, 2024. **9**(1): p. 282.10.1038/s41392-024-01980-4
156. Karigane, D. and K. Takubo, *Metabolic regulation of hematopoietic and leukemic stem/progenitor cells under homeostatic and stress conditions.* Int J Hematol, 2017. **106**(1): p. 18-26.10.1007/s12185-017-2261-x
157. Ito, K. and T. Suda, *Metabolic requirements for the maintenance of self-renewing stem cells.* Nat Rev Mol Cell Biol, 2014. **15**(4): p. 243-56.10.1038/nrm3772
158. Chandel, N.S., et al., *Metabolic regulation of stem cell function in tissue homeostasis and organismal ageing.* Nat Cell Biol, 2016. **18**(8): p. 823-32.10.1038/ncb3385
159. Winkler, I.G. and J.P. Levesque, *Mechanisms of hematopoietic stem cell mobilization: when innate immunity assails the cells that make blood and bone.* Exp Hematol, 2006. **34**(8): p. 996-1009.10.1016/j.exphem.2006.04.005
160. Capucetti, A., F. Albano, and R. Bonecchi, *Multiple Roles for Chemokines in Neutrophil Biology.* Front Immunol, 2020. **11**: p. 1259.10.3389/fimmu.2020.01259
161. Wang, L., et al., *Bone Marrow Adipocytes: A Critical Player in the Bone Marrow Microenvironment.* Front Cell Dev Biol, 2021. **9**: p. 770705.10.3389/fcell.2021.770705
162. Anthony, B.A. and D.C. Link, *Regulation of hematopoietic stem cells by bone marrow stromal cells.* Trends Immunol, 2014. **35**(1): p. 32-7.10.1016/j.it.2013.10.002
163. Zhou, B.O., et al., *Leptin-receptor-expressing mesenchymal stromal cells represent the main source of bone formed by adult bone marrow.* Cell Stem Cell, 2014. **15**(2): p. 154-68.10.1016/j.stem.2014.06.008
164. Steidl, U., et al., *Primary human CD34+ hematopoietic stem and progenitor cells express functionally active receptors of neuromediators.* Blood, 2004. **104**(1): p. 81-8.10.1182/blood-2004-01-0373
165. Shen, M., et al., *Cannabinoid receptor agonists inhibit glutamatergic synaptic transmission in rat hippocampal cultures.* J Neurosci, 1996. **16**(14): p. 4322-34.10.1523/JNEUROSCI.16-14-04322.1996
166. Szabo, B., et al., *Inhibition of GABAergic inhibitory postsynaptic currents by cannabinoids in rat corpus striatum.* Neuroscience, 1998. **85**(2): p. 395-403.10.1016/s0306-4522(97)00597-6
167. Schlicker, E. and M. Kathmann, *Modulation of transmitter release via presynaptic cannabinoid receptors.* Trends Pharmacol Sci, 2001. **22**(11): p. 565-72.10.1016/s0165-6147(00)01805-8
168. Buechler, M.B., H.M. Akilesh, and J.A. Hamerman, *Cutting Edge: Direct Sensing of TLR7 Ligands and Type I IFN by the Common Myeloid Progenitor Promotes mTOR/PI3K-Dependent Emergency Myelopoiesis.* J Immunol, 2016. **197**(7): p. 2577-82.10.4049/jimmunol.1600813
169. Boettcher, S. and M.G. Manz, *Sensing and translation of pathogen signals into demand-adapted myelopoiesis.* Curr Opin Hematol, 2016. **23**(1): p. 5-10.10.1097/moh.0000000000000201
170. Kwarteng, E.O. and K.M. Heinonen, *Competitive Transplants to Evaluate Hematopoietic Stem Cell Fitness.* J Vis Exp, 2016(114).10.3791/54345
171. Elgazzar, A.H., *Inflammation*, in *Synopsis of Pathophysiology in Nuclear Medicine*, A.H. Elgazzar, Editor. 2023, Springer International Publishing: Cham. p. 51-72.10.1007/978-3-031-20646-7_4

172. Boettcher, S. and M.G. Manz, *Regulation of Inflammation- and Infection-Driven Hematopoiesis.* Trends Immunol, 2017. **38**(5): p. 345-357.10.1016/j.it.2017.01.004
173. Nagai, Y., et al., *Toll-like receptors on hematopoietic progenitor cells stimulate innate immune system replenishment.* Immunity, 2006. **24**(6): p. 801-812.10.1016/j.immuni.2006.04.008
174. Lieschke, G.J., et al., *Mice lacking granulocyte colony-stimulating factor have chronic neutropenia, granulocyte and macrophage progenitor cell deficiency, and impaired neutrophil mobilization.* Blood, 1994. **84**(6): p. 1737-1746.10.1182/blood.V84.6.1737.1737
175. Kawakami, M., et al., *Levels of serum granulocyte colony-stimulating factor in patients with infections.* Blood, 1990. **76**(10): p. 1962-4.10.1182/blood.V76.10.1962.1962
176. Mehta, H.M. and S.J. Corey, *G-CSF, the guardian of granulopoiesis.* Semin Immunol, 2021. **54**: p. 101515.10.1016/j.smim.2021.101515
177. Jaillon, S., K. Berthenet, and C. Garlanda, *Sexual Dimorphism in Innate Immunity.* Clin Rev Allergy Immunol, 2019. **56**(3): p. 308-321.10.1007/s12016-017-8648-x
178. DeFalco, J., et al., *Virus-assisted mapping of neural inputs to a feeding center in the hypothalamus.* Science, 2001. **291**(5513): p. 2608-13.10.1126/science.1056602
179. Tikhonova, A.N., et al., *The bone marrow microenvironment at single-cell resolution.* Nature, 2019. **569**(7755): p. 222-228.10.1038/s41586-019-1104-8
180. Logan, M., et al., *Expression of Cre Recombinase in the developing mouse limb bud driven by a Prxl enhancer.* Genesis, 2002. **33**(2): p. 77-80.10.1002/gene.10092
181. Kim, J.E., K. Nakashima, and B. de Crombrugghe, *Transgenic mice expressing a ligand-inducible cre recombinase in osteoblasts and odontoblasts: a new tool to examine physiology and disease of postnatal bone and tooth.* Am J Pathol, 2004. **165**(6): p. 1875-82.10.1016/S0002-9440(10)63240-3
182. Alva, J.A., et al., *VE-Cadherin-Cre-recombinase transgenic mouse: a tool for lineage analysis and gene deletion in endothelial cells.* Dev Dyn, 2006. **235**(3): p. 759-67.10.1002/dvdy.20643
183. Savitt, J.M., et al., *Bcl-x is required for proper development of the mouse substantia nigra.* J Neurosci, 2005. **25**(29): p. 6721-8.10.1523/JNEUROSCI.0760-05.2005

Affidavit

Affidavit

Shakir, George

_____

Surname, first name

_____

Street

I hereby declare, that the submitted thesis entitled:

Role of the cannabinoid receptor CB1 in the regulation of bone marrow hematopoiesis

is my own work. I have only used the sources indicated and have not made unauthorised use of services of a third party. Where the work of others has been quoted or reproduced, the source is always given.

I further declare that the dissertation presented here has not been submitted in the same or similar form to any other institution for the purpose of obtaining an academic degree.

Munich, 25.07.2025 George Shakir

_____ _____

place, date Signature doctoral candidate

Confirmation of congruency

LMU LUDWIG-MAXIMILIANS-UNIVERSITÄT MÜNCHEN

Promotionsbüro
Medizinische Fakultät

MMRS

Confirmation of congruency between printed and electronic version of the doctoral thesis

Doctoral candidate: George Shakir

Address:

I hereby declare, that the submitted thesis entitled:

Role of the cannabinoid receptor CB1 in the regulation of bone marrow hematopoiesis

is congruent with the printed version both in content and format.

Munich,25.07.2025 George Shakir

_____ _____

place, date Signature doctoral candidate

List of publication

1. Yong Wang, Guo Li, Bingni Chen, **George Shakir**, Mario Volz, Emiel P C van der Vorst, Sanne L Maas, Martina Geiger, Carolin Jethwa, Alexander Bartelt, Zhaolong Li, Justus Wettich, Nadja Sachs, Lars Maegdefessel, Maliheh Nazari Jahantigh, Michael Hristov, Michael Lacy, Beat Lutz, Christian Weber, Stephan Herzig, Raquel Guillamat Prats, Sabine Steffens, Myeloid cannabinoid CB1 receptor deletion confers atheroprotection in male mice by reducing macrophage proliferation in a sex-dependent manner, *Cardiovascular Research*, Volume 120, Issue 12, August 2024, Pages 1411–1426, https://doi.org/10.1093/cvr/cvae125

2. Bingni Chen, Aishvaryaa Prabhu, Guo Li, Anna Kaltenbach, Yong Wang, **George Shakir**, Lucia Natarelli, Remco Megens, Yvonne Jansen, Srishti Ramanathan, Martina Geiger, Alexander Faussner, Michael Hristov, Daniel Richter, Xinyu Di, Mario van der Stelt, Zhaolong Li, Nadja Sachs, Valentina Paloschi, Lars Maegdefessel, Susanna M. Hofmann, Christian Weber, Stephan Herzig, Raquel Guillamat Prats, Sabine Steffens, Endothelial cannabinoid CB1 receptor deficiency reduces arterial inflammation and lipid uptake in response to atheroprone shear stress (bioRxiv 2024.05.15.594375; doi: https://doi.org/10.1101/2024.05.15.594375)

3. Fahim SA, Abdullah MS, Espinoza-Sánchez NA, Hassan H, Ibrahim AM, Ahmed SH, **Shakir G**, Badawy MA, Zakhary NI, Greve B, El-Shinawi M, Götte M, Ibrahim SA. Inflammatory Breast Carcinoma: Elevated microRNA miR-181b-5p and Reduced miR-200b-3p, miR-200c-3p, and miR-203a-3p Expression as Potential Biomarkers with Diagnostic Value. Biomolecules. 2020 Jul 16;10(7):1059. doi: 10.3390/biom10071059. PMID: 32708601; PMCID: PMC7407124.